
**GEOLOGICAL SURVEY OF CANADA**
**OPEN FILE 6214**

# Near surface geology of the Halibut Channel region of the SW Newfoundland Slope from GSC data holdings

**D.C. Mosher, D.J.W. Piper, K. MacKillop and K. Jarrett**

**2010**

Natural Resources Canada Ressources naturelles Canada

Canada


**GEOLOGICAL SURVEY OF CANADA**
**OPEN FILE 6214**

# Near surface geology of the Halibut Channel region of the SW Newfoundland Slope from GSC data holdings

**D.C. Mosher, D.J.W. Piper, K. MacKillop and K. Jarrett**
Natural Resources Canada
Geological Survey of Canada − Atlantic
1 Challenger Drive (P.O. Box 1006)
Dartmouth, Nova Scotia B2Y 4A2
Telephone (902) 426-3149
Fax (902) 426-4104
dmosher@nrcan.gc.ca

## 2010



This publication is available from the Geological Survey of Canada Bookstore (http://gsc.nrcan.gc.ca/bookstore_e.php). It can also be downloaded free of charge from GeoPub (http://geopub.rncan.gc.ca/).

Mosher, D.C., Piper, D.J.W., MacKillop, K. and Jarrett, K. 2010. Near surface geology of the Halibut Channel region of the SW Newfoundland Slope from GSC data holdings. Geological Survey of Canada, Open File 6214, 72 p.

Open files are products that have not gone through the GSC formal publication process.

# 1. INTRODUCTION

This report represents a compilation of data holdings of the Geological Survey of Canada in the area of the eastern Laurentian Fan/Halibut Channel of the continental slope off the SW Grand Banks of Newfoundland, along with data interpretations. These data consist of multibeam sonar, seismic reflection and core sedimentologic and geotechnical information.

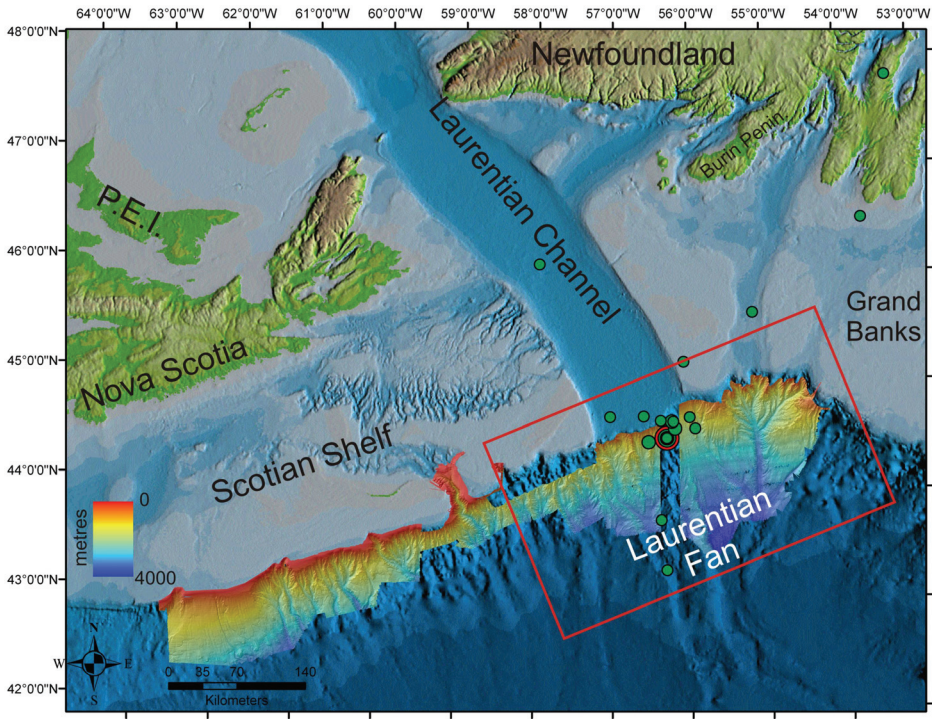


*Figure 1.1.1 Seafloor rendering using the entire deep water multibeam bathymetric data set for the Scotian and SE Newfoundland margins. The area in the red box represents the data acquired in 2006. Other data were acquired in 2000 . The dots represent historic seismicity epicentres over the past 100 years.*

The following three figures (Figs. 1.1.1 to 1.1.3) represent renderings of the multibeam data acquired in 2006.

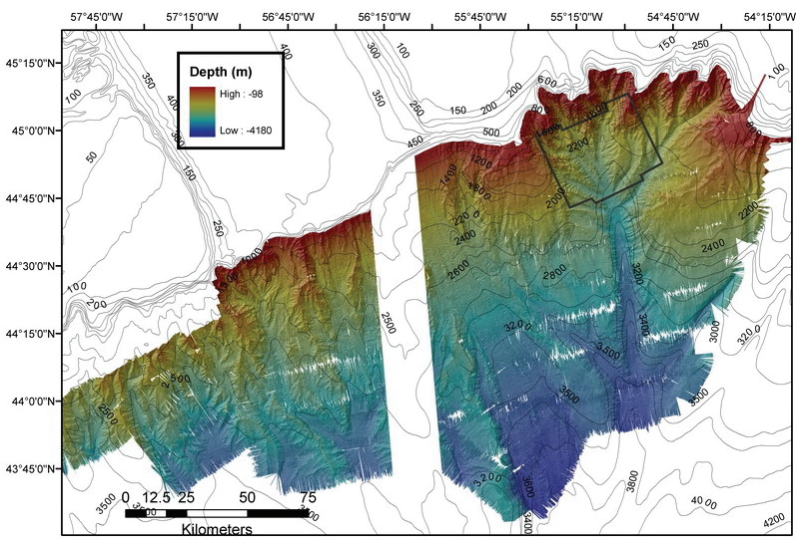


*Figure 1.1.2. Study area: seafloor render of data acquired in 2006 by the Kommandor Jack. The black box in the NE quadrant is the outline of the ConocoPhillips Laurentian East 3D seismic volume area.*

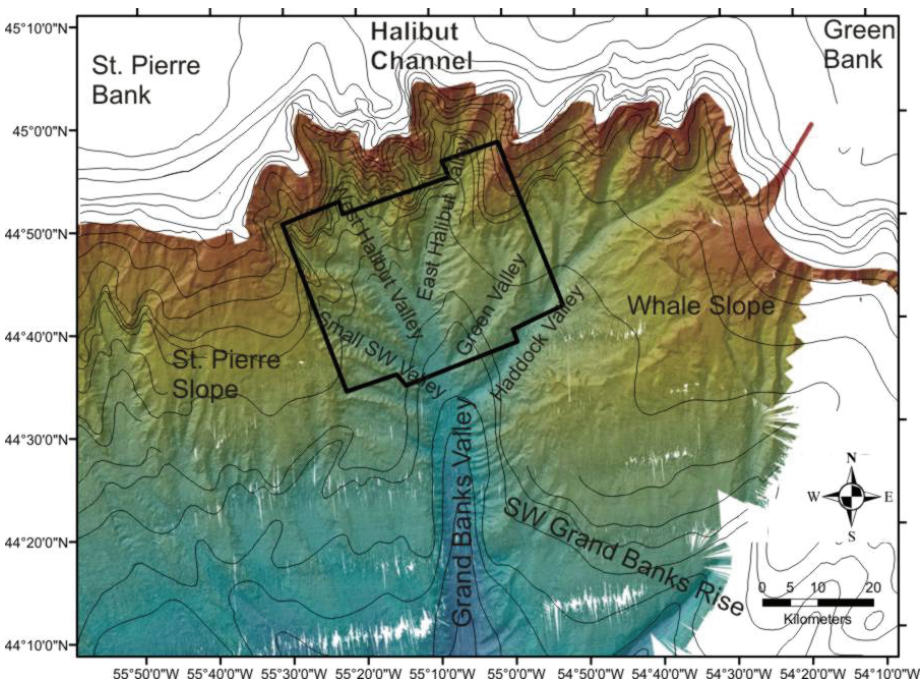


*Figure 1.1.3 Focused study area with geographic names for reference. The black polygon represents the area of the Laurentian East 3D volume.*

***1.2 Background Geology***

Miocene and Pliocene evolution of the eastern Canadian continental margin is not well known. Thick, predominantly muddy Miocene successions were developed on the Scotian Slope following widespread Oligocene canyon cutting (e.g. Wade et al. 1995; Brake et al. 2008a,b, 2009) and similar strata are present in places on the Grand Banks and Labrador margins (e.g. Wielens et al. 2004; Hinz et al. 1979). On the continental rise, there is considerable winnowing and reworking of sediment by bottom currents, starting in the Oligocene in the Labrador Sea and migrating southwards (Gradstein et al. 1990). In the Early to mid Pliocene on the Scotian margin, there is a pronounced change in sedimentation style that includes accumulation of turbidites on the upper Scotian Rise (Piper & Ingram, 2003) and on the Laurentian Fan (Uchupi & Austin, 1979; Piper & Normark, 1989) and the development of leveed turbidity current channels on St Pierre Slope (Piper et al. 2005). On the Grand Banks margin, significant progradation took place towards Flemish Pass and Orphan Basin (Deptuck 2003; Sonnichsen & King 2005). The onset of shelf-crossing glaciations off Nova Scotia and the southern Grand Banks of Newfoundland has been dated as mid Pleistocene, probably in MIS 12 (Piper et al. 1994, 2002, Piper & Campbell 2005).

Almost the entire continental shelf off eastern Canada was glaciated numerous times in the mid to Late Pleistocene. The resulting morphology consists of transverse troughs and intervening banks (Piper 1988). There is a zone of deep basins (marginal trough) at the landward edge of the Mesozoic-Cenozoic wedge. The mean depth of continental shelves increases from south to north, but the relative importance of various contributing factors is uncertain. These factors include subsidence related to the age of the adjacent ocean, other tectonic subsidence, glacio-isostatic loading, glacial erosion, and low rates of glacial sedimentation between ice streams on shelves with deep shelf breaks. Large areas of the Grand Banks and Scotian Shelf that are less than 100 m deep (Fig. 2) were emergent at lowstands of relative sea level during the mid to Late Pleistocene (Shaw et al., 2006).

The Laurentian Channel was a major Pleistocene ice outlet corridor that extended across the continental shelf from the Gulf of St. Lawrence (Shaw et al., 2006). The Channel is a U-shaped glacially excavated trough extending from the St. Lawrence estuary across the Gulf of St. Lawrence to the shelf edge SW of Newfoundland. It was fed by a series of tributary troughs draining ice originating in the Appalachian Ice Complex (Dyke and Prest, 1987). Erratics from the Canadian Shield are known only from the northern Gulf of St. Lawrence and it appears that most sediment glacially transported to the shelf edge was derived from the Appalachian orogen and its successor basins (Grant, 1989).

The Laurentian Fan is a major Quaternary sediment accumulation seaward of Laurentian Channel (Stow, 1981; Skene and Piper, 2003, 2006). Two main fan valleys, with high levees, extend southward to the lower fan and Sohm Abyssal Plain. Pliocene–Quaternary sediment is up to 3 km thick on the fan. Study of detrital sediments on the continental margin suggests that the Laurentian Channel was principally excavated during isotopic stage 12 (ca. 450 ka) and prior to stage 14, sediment transport to the Laurentian Fan was by a proto-St. Lawrence River (Piper et al., 1994). It is the largest deep-sea fan on the Atlantic margin of Canada and merges seaward with the Sohm Abyssal Plain. Shaw et al (2006) show major ice streams emanating from the Laurentian Channel and the SW Grand Banks out to the continental slope during the Wisconsinan glaciation as late as 16.8 ka (cal.) BP. Ice survived on the SW Grand Banks as late as 14 ka (cal.) BP, with sea level as low as 120 m below present at that time. The modern shelf break and edge of the channel lies in

about 400 m water depth and the transition to the abyssal plain is in about 5000 m water depth. The proximal position of these ice shelves and ice streams played a significant role in formation of the present canyon morphology of the adjacent continental slope.

### ***1.3 Seismicity***

In the immediate area of the Laurentian Fan, seismic activity is more common than elsewhere along the eastern seaboard, increasing its seismic hazard assessment (Adams and Halchuk, 2003) (See Fig. 1.1.1). A Mesozoic fault system (the Cobequid-Chedabucto fault) sweeps beneath the Laurentian Channel and extends to the southwestern edge of the Grand Banks. In addition, the Newfoundland transform is projected to extend beneath the Laurentian Channel and fan. It is possibly on these structures that ongoing low-grade seismicity occurs. Mazotti and Adams (2005) indicate glacial rebound tectonics still influences the measured strain rates in eastern Canada. They suggest a Mw=7 earthquake every 350-3500 years is possible, based on historical earthquake data. The 1929 Grand Banks earthquake in the middle of the Laurentian Fan was a Mw=7.2 event. Based on a regional model, calculated on measured strain rate and tectonic and geological structures such as the current and ancient passive margins, Mazotti and Adams (2005) suggest a frequency recurrence of a Mw=7 event at 1 in 50 years along the eastern continental margin. It should be noted that this is two orders of magnitude higher in frequency than that inferred from the paleoseismic record of sediment failure on the margin, summarized by Mosher et al. (2004), Piper (2005) and Jenner et al. (2006).

# 2. METHODS

As most data acquisition systems used in this compilation are reported elsewhere, details will not be discussed herein, but simply introduced and referenced.

## *2.1 Multibeam*

### Bathymetry

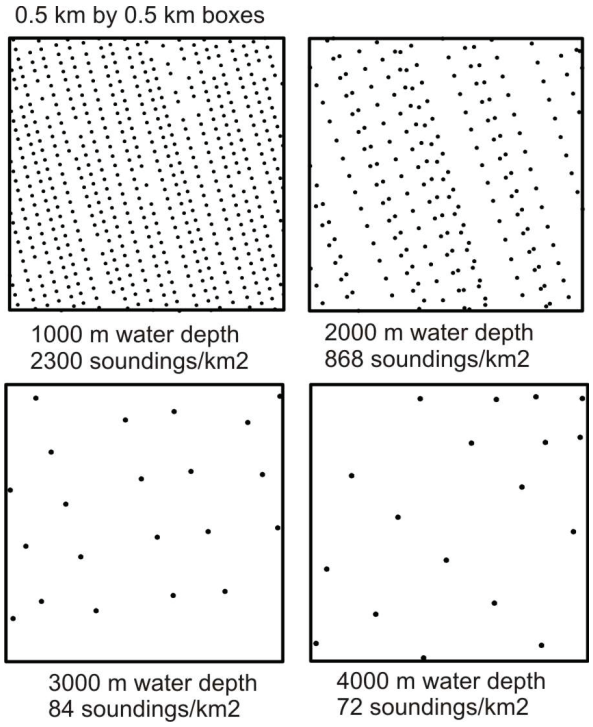


*Figure 2.1.1. Multibeam sounding density in four different water depths for the 2006 Kommandor Jack survey of the Laurentian Fan region.*

The multibeam bathymetric data set covering 32,150 km$^2$ of the upper Laurentian Fan was acquired in September, 2006 with the vessel Kommandor Jack. Data were collected by Fugro Jacques GeoSurveys Inc. of St. John's, Newfoundland. The vessel was equipped with a Kongsberg Simrad EM120 multibeam system that operates at a nominal frequency of 12 kHz, with 191 receive beams covering an ideal swath width of 150°. Maximum swath widths of about 10 km were achieved. Data density is the greatest restriction on multibeam sonar resolution in deep water (Mosher et al., 2006). In this study, data density is on the order of 2300 soundings per km$^2$ in 1000 m of water and 84 soundings per km$^2$ in 3000 m (Fig. 2.1.1). These values imply that horizontal resolution is nominally about 40 m at the shallower depth and 400 m in the deep.

In addition to this latest survey, to maximize data coverage, existing digital bathymetric data from a variety of sources were integrated before final grid production and seafloor rendering. These data sources include a 12 kHz Seabeam data set from 1986 over a portion of the study region (Hughes Clarke et al. 1990), single beam sounding data digitized from previous Geological Survey of Canada expeditions, bathymetric field sheet data from the Canadian Hydrographic Service, and first arrival picks from 2D and 3D seismic data in the region. A seafloor rendering of the resulting compilation is shown in Figure 2.1.2.

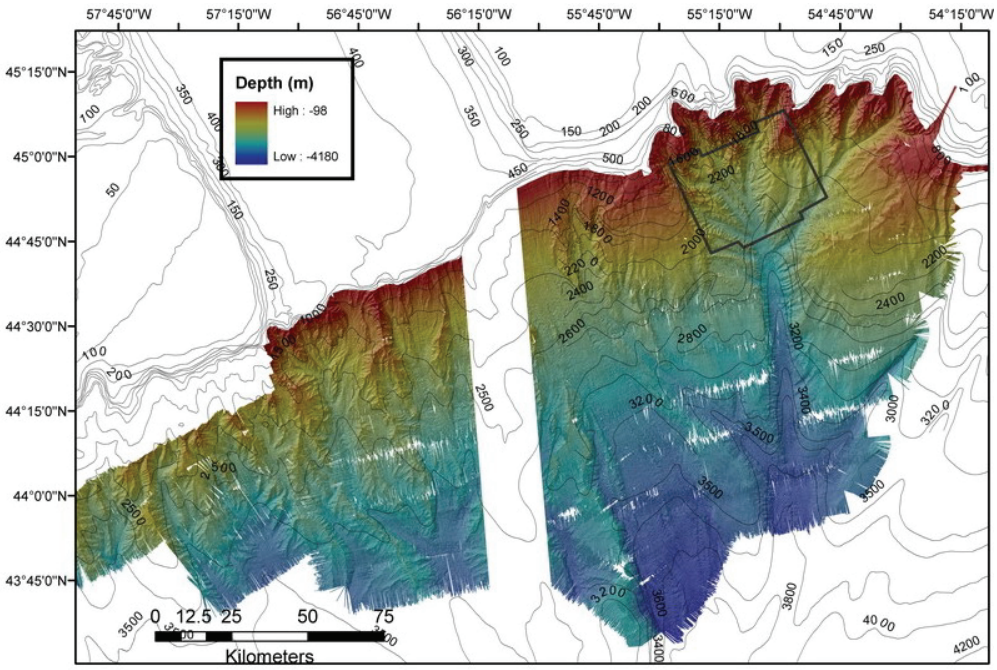


*Figure 2.1.2. Hillshade seafloor geomorphologic render of the bathymetric data compilation, Laurentian Fan region.*

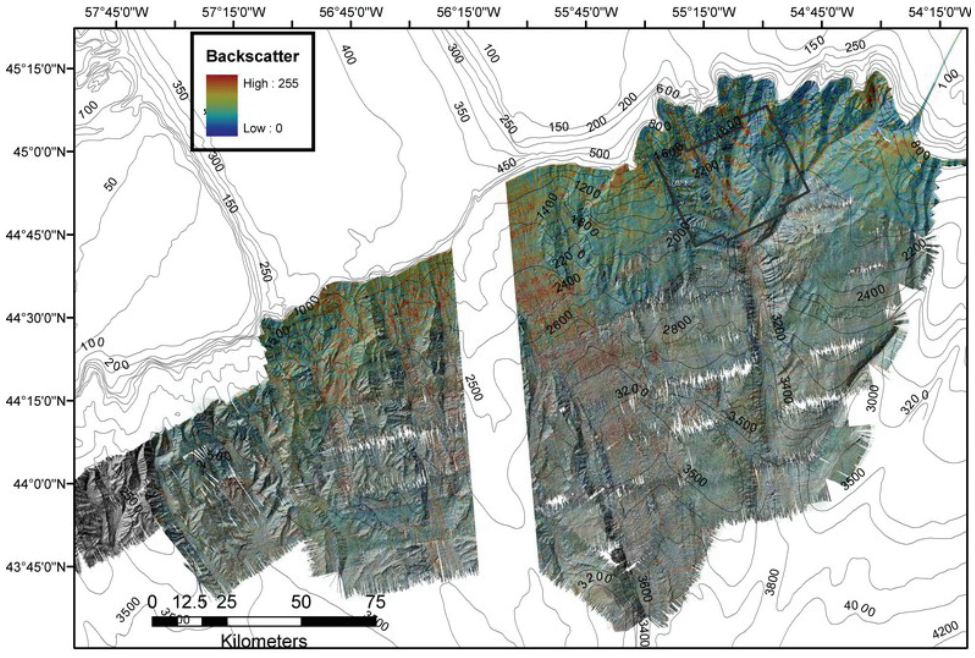


*Figure 2.1.3. Multibeam backscatter intensity draped over topographic data*

**Backscatter Intensity**

Backscatter intensity, derived from multibeam data (Fig. 2.1.3), was processed to gain compensate for angle of emission of the beam. Problems with backscatter at acquisition resulted in poor quality imaging of the data. As a result, general patterns of backscatter are notable, but details are lost. High backscatter in valley and canyon floors and walls, canyon heads and low areas suggests coarse (sand and gravel) or consolidated material forms the seafloor in these regions. Alternatively, low relative backscatter on the adjacent highs, canyon ridges and buttes suggests fine-grained sediment forms the surficial material.

**Slope Angle**

Slope angle maps were derived from the multibeam bathymetric data compilations at a grid interval of 100 m and displayed in variable slope angle categories to accentuate the critical slope angle intervals (e.g. Fig. 2.1.4).

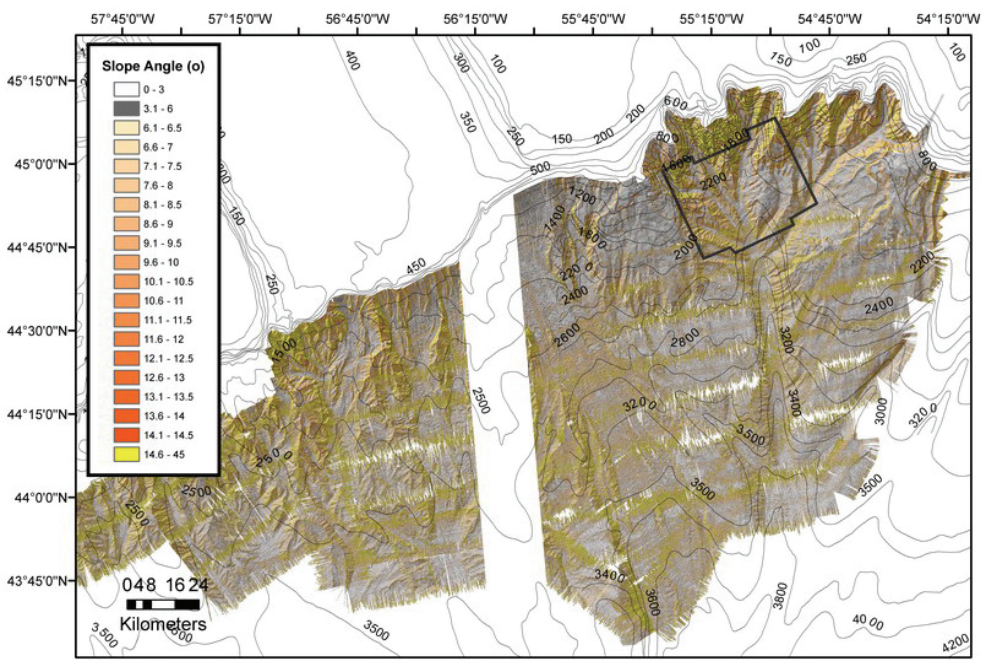


*Figure 2.1.4. Slope angle draped over bathymetry of the Laurentian Fan region.*

## ***2.2 Seismic reflection***

Seismic reflection data from several sources were used in this assessment: 1) The St. Pierre Slope (STP) 2D seismic data survey was shot in 1989-1990 for the Geological Survey of Canada – Atlantic (GSC-A), 2) 2D industry exploration data shot in 1999 and 2000, supplied on a confidential basis by TGS-Nopec, 3) 3D seismic exploration data of the Laurentian East volume supplied by ConocoPhillips, 4) high resolution seismic reflection data acquired during three missions of the GSCA (2004-030, 2006-048 and 2007-020), and 5) ultra high resolution Huntec sparker data acquired during these latter three missions. Details of the GSC systems can be found in the appropriate cruise reports (Mosher, 2005; Piper and King, 2006, and Mosher and West, 2007) and a regional track chart is shown in Figure 2.2.1. Examples of the high resolution seismic data are shown in Figure 2.2.2

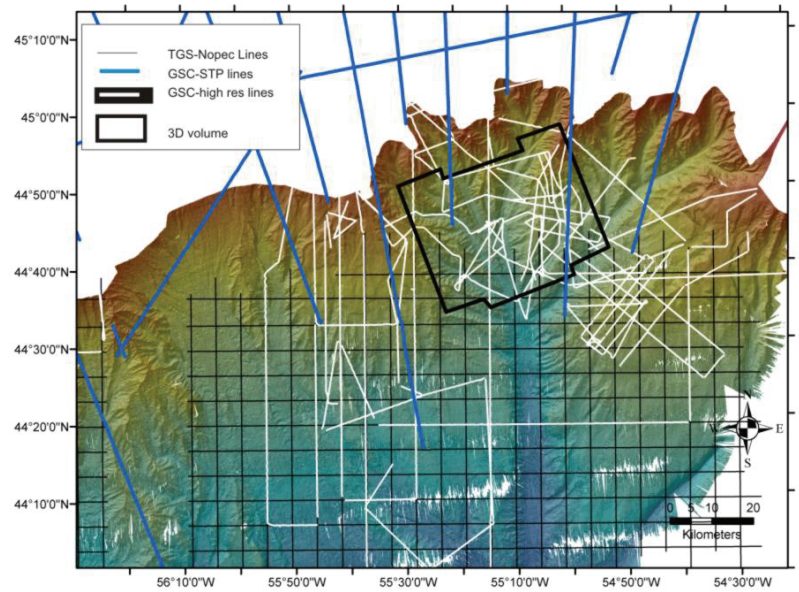


*Figure 2.2.1 Seismic reflection tracklines of data used in this investigation*

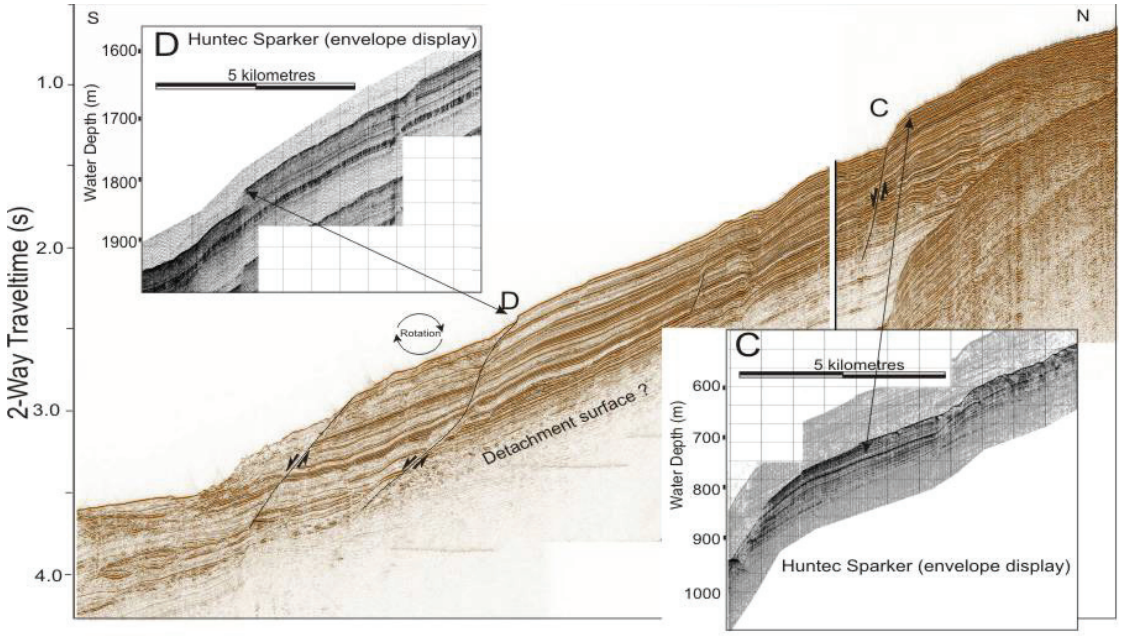


*Figure 2.2.2. High resolution (2 x 210 in$^3$ GI gun) and ultra-high resolution (C&D insets of Huntec sparker) seismic reflection data examples from the St. Pierre Slope.*

## ***2.3. Seismic refraction/wide angle reflection***

Ocean bottom seismometers were used to acquire wide angle reflection and refraction data at two sites proximal to the study area – St. Pierre Slope and Halibut Channel Slope. The Halibut Channel data set was acquired in 2004 (mission Hudson 2004-030) and analysis are reported in a Louden and

LeBlanc (2006) contract report. The St. Pierre data set was acquired during mission Hudson 2007-020 (Mosher and West, 2007) and analysed by Chian (2007). The four Haddock Channel deployments (HC) used DAL OBS with TT7 data logger and geophones contained within a separate package deployed onto the seafloor from the floatation frame. This was the first use of this external geophone arrangement. The Hudson 2007-020 data set was acquired with GSC instrument L and configured the same as in the previous deployment. All instruments were configured to sample at 558 Hz. The ship's Differential Global Positioning System (DGPS) was used for positioning and timing control. The seismic source for both of these experiments was a 2x210 $in^3$ GI gun array. All OBS's were equipped with a hydrophone and a three orthogonal component (vertical and two horizontal) 4.5 Hz geophone mounted in an external pressure case.

Processing of OBS data included parsing the data into seismic traces by correlating times with shot tables and assembling traces into CMP gathers. Navigation data were merged with the shot data into the Seg-Y headers. Data were then correlated and instruments relocated on the seafloor based upon the direct arrival signal. Little processing of the seismic data was required because of their high quality and high signal to noise ratio. Wide-angle reflection and refraction signals were picked to derived velocities and forward and inverse ray path models were run to confirm results. Details of OBS instrumentation, methodologies, analytic techniques and results are in Louden and LeBlanc (2006) and Chian (2007).

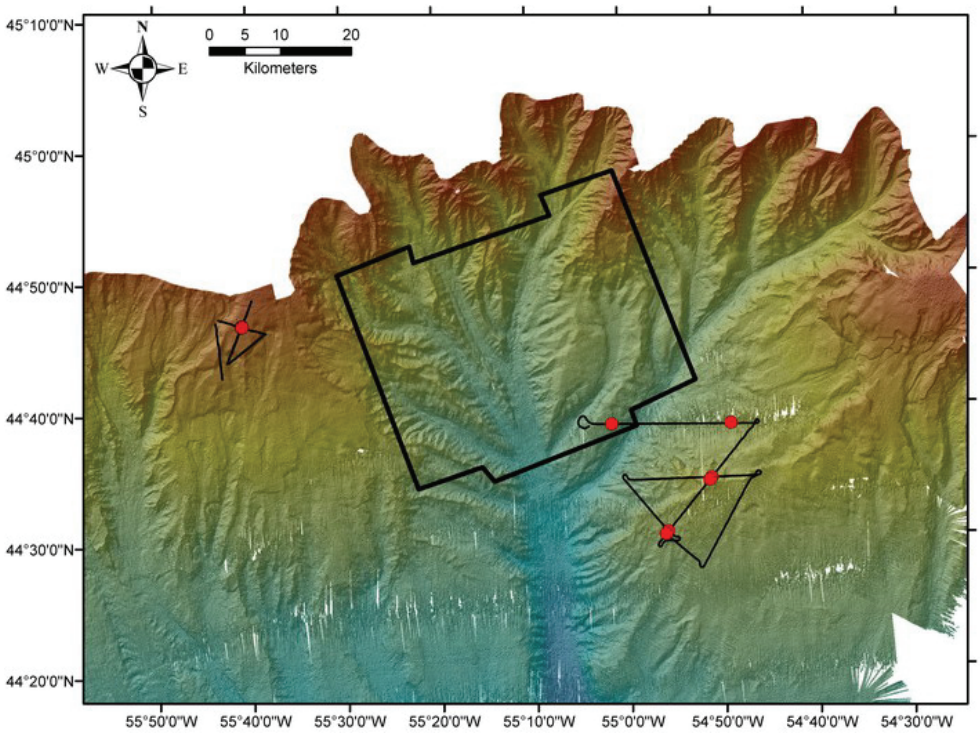


*Figure 2.3.1 Location of ocean bottom seismometer deployments (red dots) and associated seismic track lines. Location of the Laurentian East 3D volume is shown by the black polygon. The eastern locations are the Whale Slope deployments and the western is the St. Pierre Slope deployment (see Fig. 1.1.3 for geographic names).*

## *2.4 Sediment coring*

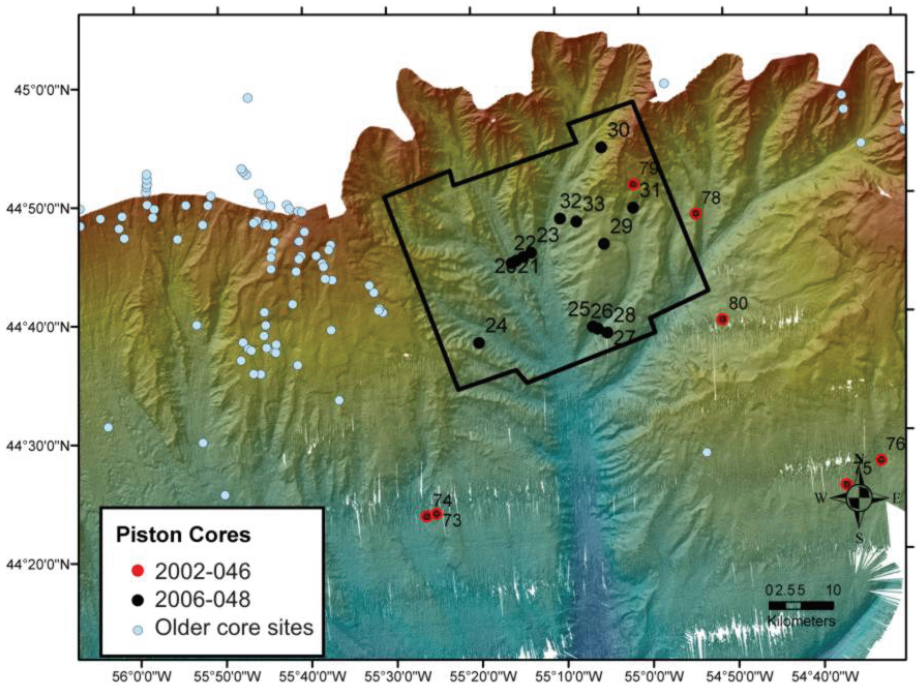


*Figure 2.4.1 Core locations.*

The piston coring system used was the AGC Long Corer. This device obtains a 10 cm diameter core sample. Barrel lengths are 10 ft (3.05 m), and typically the system was rigged with four or five barrels. The core head is 3 m long, 0.6 m diameter and weighs 2000 lb (900 kg). The core pipe has a 4.25" ID (10.8 cm), with 3/8" (9.5 mm) wall thickness, with exterior couplings secured by set screws. The liner was CAB plastic in 10 ft. (3.05 m) lengths. A split piston with two O-rings and variable orifice size was used. For most sites, a standard core catcher was used. The trip arm supported a 4.25" (10.8 cm) diameter gravity corer with a 6 ft (1.82 m) barrel and 300 lb (135 kg) head. The corer used 3/4" (19 mm) wire cable on the Pengo winch. The corer was operated using a handling system including a rotating core-head cradle, outboard support brackets, a monorail transport system, and a lifting winch. The system was broken down at the barrel joints and moved to a processing half-height container, where the cores were extracted from the barrels, split into 1.53 m (or less) section lengths and labeled. Figure 2.4.1 shows core site locations; relevant cores to this study were acquired during expeditions 2006-048 and 2002-046.

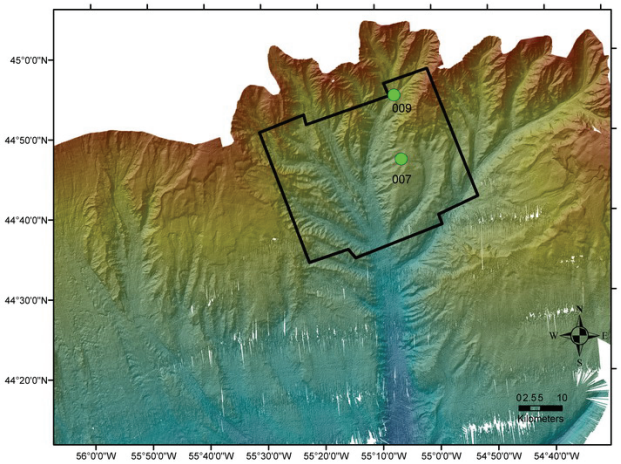


*Figure 2.5.1. Camera station locations for expedition 2007-020*

## *2.5 Bottom Photography*

The ADOC camera system is based on GSCA's Scorpio Insite TriTech underwater digital camera. The camera's flash photos are controlled by the ADOC microcontroller that senses bottom contact via a bottom contact switch and pinger arrangement. Photo location, daytime and station location information are entered into the header of the photographs. Two stations with 50 successful frames were acquired during mission 2007-020 (Fig. 2.5.1) stations 007 and 009); one in the East Halibut Valley and the other on the adjacent ridge to the east. Results can be viewed on the Cruise Report DVD (Mosher and West, 2007).

## *2.6 Core Physical Properties*

### Index Properties

Sediment core physical property data were derived from discrete measurement of core material and from whole core logging instrumentation (multi-sensor track (MST)). MST data include magnetic susceptibility, ultra-sonic acoustic compression velocity and bulk density derived by gamma-ray attenuation techniques (Compton scattering), measured at 1 cm intervals. Split-core photographs were taken of the entire core with a digital camera system and images spliced together. Discrete core measurements included colour photospectrometry at 10 cm intervals, bulk density by constant volume (including derived index properties of water content, dry density, porosity, and grain density) at 25 cm intervals, acoustic compressional velocity at 10 cm intervals, and peak shear strength at 10 cm intervals (according to procedures: ASTM 468-94). Whole round samples were removed from core sections prior to splitting but after MST analysis for geomechanical testing.

### Atterberg Limits

Atterberg limit testing (ASM D-4318) was performed on trimmings from consolidation and triaxial samples. Atterberg limits provide the liquid and plastic limits of the sediments and are used for the classification of fine grained soils. The liquidity index ($L_i$) can be used to aid in the evaluation of stress history (Skempton, 1970). The Atterberg tests results are presented in Table 2.6.1.

**Table 2.6.1. Summary of consolidation test results for Laurentian Slope samples.**

| Station | Depth (cm) | Void Ratio | W (%) | LL (%) | PL (%) | $L_i$ | $C_c$ | $C_r$ | OCR | Classification |
|---|---|---|---|---|---|---|---|---|---|---|
| 2006048029 | 463 | 1.18 | 42.0 | 27.3 | 17.6 | 2.50 | 0.23 | 0.020 | 0.34 | CL |
| 2006048029 | 476 | 1.10 | 38.4 | 27.3 | 17.6 | 2.10 | 0.26 | 0.020 | 0.47 | CL |
| 2006048030 | 315 | 3.59 | 125.1 | 117.2 | 56.7 | 1.13 | 0.99 | 0.097 | 1.40 | MH&OH |
| 2006048030 | 460 | 2.26 | 81.1 | 70.4 | 33.5 | 1.29 | 0.73 | 0.046 | 1.30 | CH |
| 2006048031 | 712 | 1.35 | 48.6 | 35.2 | 19.8 | 1.87 | 0.41 | 0.041 | 1.36 | CL |
| 2006048036 | 248 | 0.98 | 32.16 | 33.75 | 15.92 | 0.90 | 0.29 | 0.039 | 1.67 | CL |
| 2006048037 | 306 | 1.05 | 39.27 | 34.15 | 19.09 | 1.34 | 0.23 | 0.038 | 0.87 | CL |

## *2.7 Geomechanical Testing*

### Consolidation Testing

The compressibility of the sediments was measured in standard incremental loading tests with a load increment ratio of 0.5. The testing of 6 samples from 4 piston cores (2006048 029,031,036,037) and one fixed reference core (2006048 30) was preformed using a GeoTest back-pressured consolidometer. A duplicate sample from piston core 2006048029 (474cm) was tested using a GDS system consisting of pressure/volume controllers and a Rowe and Barden consolidation cell. The preconsolidation stress ($\sigma'_c$) was taken as the average value determined using the Cassagrande, work (Becker 1987) and Silvia (Silva 1970) methods. The effective overburden stress ($\sigma'_{vo}$) was calculated integrating MST bulk density with depth. The overconsolidation ratio (OCR), defined as $\sigma'_c/\sigma'_{vo}$ was also determined. A summary of the consolidation tests results is presented in Table 2.6.1. Consolidation plots are presented in Appendix A.

### Triaxial Testing

Isotropically consolidated undrained (CIU) triaxial tests were conducted on 3 samples from 3 piston cores (2006048 29, 30, 31). A continuous profile of undrained shear strength was calculated using the Mohr-Coulomb relationship (Bradshaw et al 2004):

$$\frac{S_u}{\sigma'_{v0}} = \frac{[K_0 + A_f(1-K_0)]\sin\phi' + \dfrac{c'}{\sigma'_{v0}\cos\phi'}}{1 + (2A_f - 1)\sin\phi'} \qquad \text{Eq 1}$$

where
$\sigma_{vo}$ = the effective vertical overburden stress (kPa)
$K_o \approx 1-\sin\phi'$
$A_f = \frac{\Delta \text{pore pressure}}{\Delta \text{deviator stress}}$ (at failure)
$\phi'$ = friction angle
$C'$ = cohesion

The normalized strengths from the CIU triaxial tests were used to obtain profiles of undrained shear strength (Roberts and Camp, 1996) using :

$$\frac{S_u}{\sigma'_{v0}} = A_c A_r S(OCR)^m \qquad \text{Eq 2}$$

where $A_c$ = correction for anisotropic consolidation, Ar = correction for cyclic loading, S = the ratio of the measured $S_u$ to triaxial consolidation stress, OCR = 1 and $m$ = a soil constant. The parameters Ac, Ar and m have been assumed to be 0.8, 1 and 0.8 respectively. A summary of the triaxial test results is presented in Table 2.7.1. Failure envelopes for the triaxial tests are presented in Appendix B.

**Table 2.7.1. Summary of triaxial test results.**

| Station | Depth (cm) | Void Ratio | W (%) | LL (%) | PL (%) | $L_i$ | $\phi'$ | $C'$ | $Su/\sigma'_c$ | $A_f$ | Classification |
|---|---|---|---|---|---|---|---|---|---|---|---|
| 2006048029 | 463 | 1.14 | 42.0 | 27.3 | 17.6 | 2.50 | 32.3 | 2.7 | 0.40 | 0.52 | CL |
| 2006048030 | 443 | 2.31 | 81.1 | 70.4 | 33.5 | 1.29 | 32.3 | 2.7 | 0.40 | 0.41 | CH |
| 2006048031 | 718 | 1.13 | 41.5 | 35.2 | 19.8 | 1.41 | 32.2 | 0.3 | 0.44 | 0.58 | CL |

## Bender Element Tests

The purpose of the bender element test was to calculate the shear modulus from the measured shear wave velocity. S-wave and P-wave tests were performed on the sample after each consolidation and shear stage of the CIU triaxial test, at 25kPa, 50kPa and 100kPa. The shear wave velocity through the sample was determined as:

$$v_s = \frac{d}{t} \qquad \text{Eq 3}$$

where d = distance from tip to tip of the piezoelectric elements extruding from the top cap and base pedestal and t = travel time. The shear modulus was calculated using:

$$G_{max} = v_s^2 \qquad \text{Eq 4}$$

where $\rho$ = bulk density of the soil sample and $v_s$ = shear velocity.The bender element test results are summarized in Table 2.7.2. Plots of shear wave velocity and shear modulus vs. confining pressures are presented in Appendix C

**Table 2.7.2. Summary of bender element test results.**

| Confining Pressure (kPa) | Void Ratio | Bulk Density (g/cm3) | S Wave Velocity (m/s) | Shear Modulus (MPa) |
|---|---|---|---|---|
| Intial | 1.10 | 1.83 | 32.6 | 1.95 |
| 24.9 | 0.97 | 1.89 | 82.6 | 12.89 |
| 49.4 | 0.91 | 1.92 | 101.3 | 19.72 |
| 99.0 | 0.85 | 1.95 | 129.1 | 32.50 |

# 3. DISCUSSION

## *3.1 Seafloor Geomorphology*

The recently acquired multibeam data in the Laurentian Fan region, merged with other bathymetric data of the area (Fig. 2.1.2) reveal that area is heavily incised by canyon and valley systems. These systems have complex upslope tributary systems and merge downslope into several major canyons. Average slope angles are between three and six degrees (sub-critical static slope stability), but exceed 15° in the canyon heads and walls (Fig. 2.1.4). On the Laurentian Fan, these erosional systems include the Eastern, Western and Central Valleys (Fig. 2.1.2). The largest, Eastern Valley is about 20 km-wide at its upslope limit, but reaches over 30 km width by the 4000 m isobath. It is locally as much as 800 m deeper than adjacent levees. Western Valley forms at 3400 m water depth at the confluence of four valleys emanating from the western portion of the mouth of Laurentian Channel. At this point of confluence, its valley floor is 11 km wide, nearly 30 km-wide from levee to levee and 590 m deep from levee crest to valley floor (Fig. 2.1.2). Central Valley appears as a narrow (<8 km wide) corridor branching from Eastern Valley at about the 2800 m isobath and merging with Western Valley at about the 3800 m contour. St. Pierre Valley cuts the western part of St. Pierre Slope and enters Eastern Valley near the 2600 m isobath. Farther east, significant canyon systems seaward of Halibut and Haddock Channels (Figs. 2.1.2 and 3.1.1) converge to form the Grand Banks Valley that enters Eastern Valley near the 4200 m isobath. The upper reaches of Grand Banks Valley are 10-15 km wide and 300 m deep (Fig. 3.1.1).

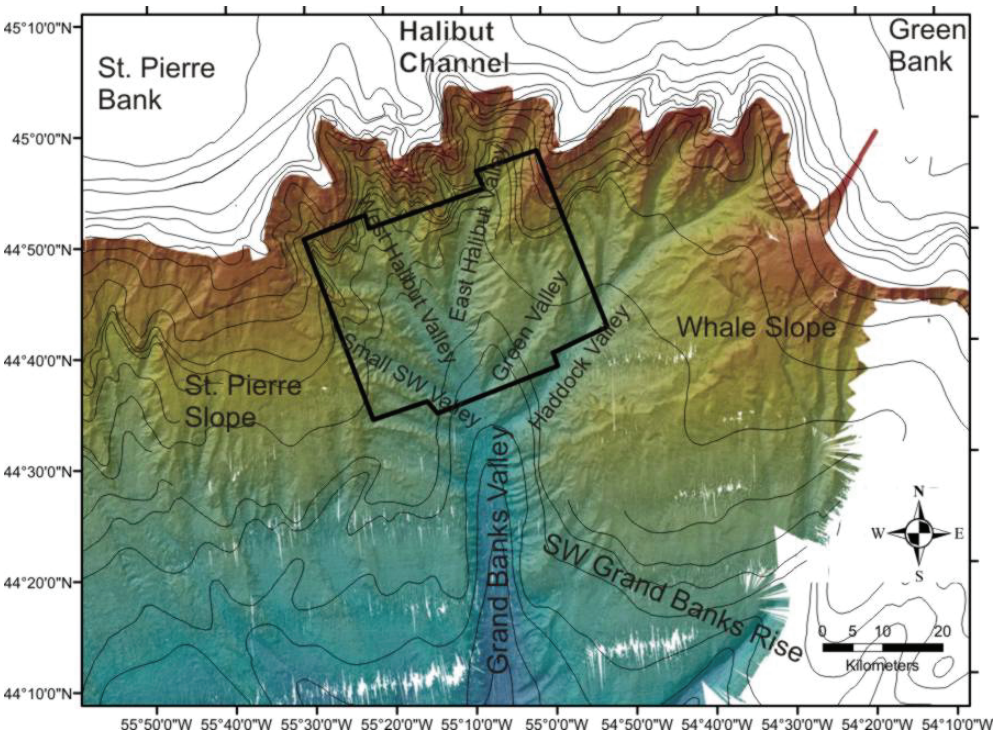


*Figure 3.1.1 Laurentian east study area with geographic names referenced in this report. The Laurentian East 3D seismic volume is indicated with the black polygon.*

The canyons and valleys consist of pinnate ridges, gullies, terraces, and escarpments (Figs. 2.1.2 and 3.1.1). Slope angles of the walls of these canyons are typically 10-20° but can reach 40° (Figs. 2.1.4 and 3.1.2). The floors of these valleys and tributaries are broadly flat at coarse scale, but on close inspection their features are numerous. Many small channels and talwegs are apparent, particularly in the upper slope portion of Eastern Valley (Fig. 3.1.1). Sediment waves and scours (flute marks) are apparent on valley floors, well-known from previous sidescan sonar investigations (Hughes Clarke et al., 1990; Shor et al. 1990; Piper et al., 2007). These features as well as other anomalous pits, scours, buttes, channels and talwegs are notable on the valley floor. Debris lobes are also apparent on the valley floors, such as within Central Valley (Hughes Clarke, 1990). Acoustic backscatter values from multibeam data show stronger reflectivity within channels and tributaries than on adjacent ridges; particularly notable within the Eastern Valley (Fig. 2.1.3).
The eastern St. Pierre Slope is a broad flat area of relatively low gradients (3-6°) seaward of the

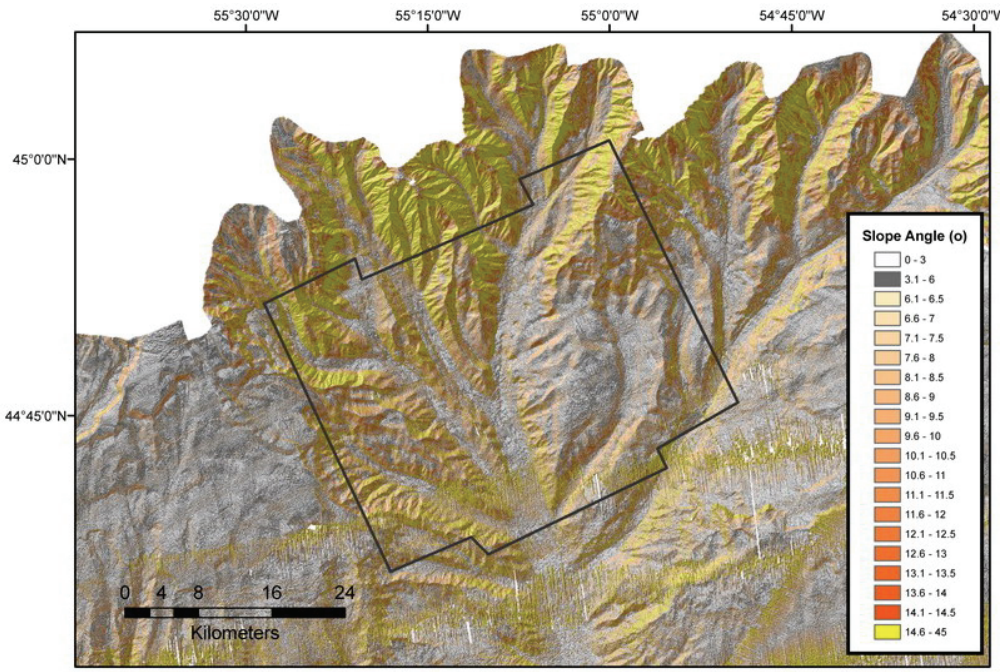


*Figure 3.1.2. Slope angles for the Laurentian East area*

eastern part of St. Pierre Bank (Fig. 3.1.2). It broadens seaward with a regional increase in gradient between the 2000 and 2500 m isobaths. Between 500 and 2000 m water depth, the predominant morphological features are sinuous escarpments presumably formed by retrogressive failure (see Figs. 2.2.2 and 3.1.1). Escarpment may have slope angles in excess of $10^{o}$ and 100 m relief. The steeper area between the 2000 and 2500 m isobaths is incised by a series of 100-150 m deep sub-parallel gullies interpreted as retrogressive headwall failure. Failure in this area is interpreted to have been widespread. It is estimated that the total amount of failed sediment in the area of St. Pierre Valley and St. Pierre Slope, between the 500 and 2000 m isobaths, was about 93.5 $km^3$, of which about half was evacuated and half remained in place (McCall, 2006).

A dendritic series of slope canyons is developed seaward of Halibut Channel, Green Bank and Haddock Channel, which merge down slope to become the Grand Banks Valley (Fig. 3.1.1). Very little of the seafloor in this area is unaffected by canyon incision and escarpments presumably represent mass-failure scars. Seismic profiles and cores indicate widespread failure in 1929 at the western edge of this drainage system (McCall, 2006). Several sites on the ridges show a muted morphology, without intense gullying, that is interpreted as evidence for recent sediment mass-failure. Elsewhere, cores suggest that there were local failures on canyon walls and a turbidity current flow in 1929 was confirmed by the distribution of cable breaks (Mosher and Piper, 2007a). Backscatter intensity is most prominent on the floor of West Halibut Valley (Fig. 3.1.3), suggesting transport of sand down the valley axis is recent probably as a result of the 1929 event, but is possibly ongoing.

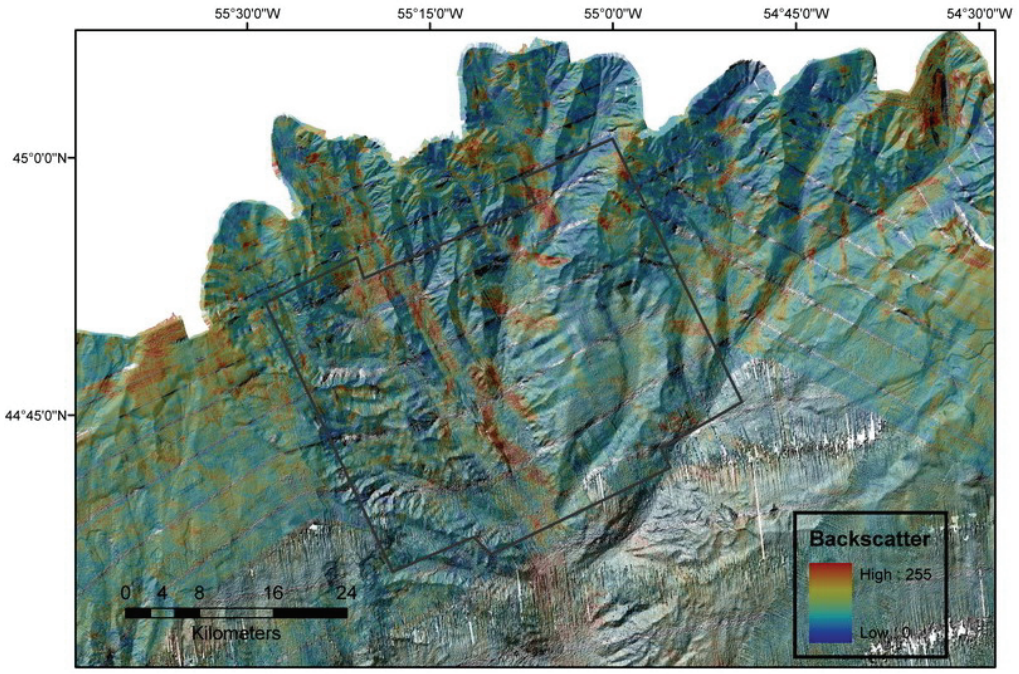


*Figure 3.1.3. Multibeam backscatter intensity of the Laurentian east area.*

## ***3.2 Shallow stratigraphy***

### Description, correlation and interpretation of cores

Piston cores (Fig. 2.4.1) were collected in 2002 and 2006 to characterise sediment type and sedimentation processes in the upper ten metres of sediment in the Laurentian east area. They are also used in a later section to draw conclusions on geotechnical properties. Cores were split, laboratory measurements were made, and the cores were described following procedures outlined in Tripsanas et al. (2007).

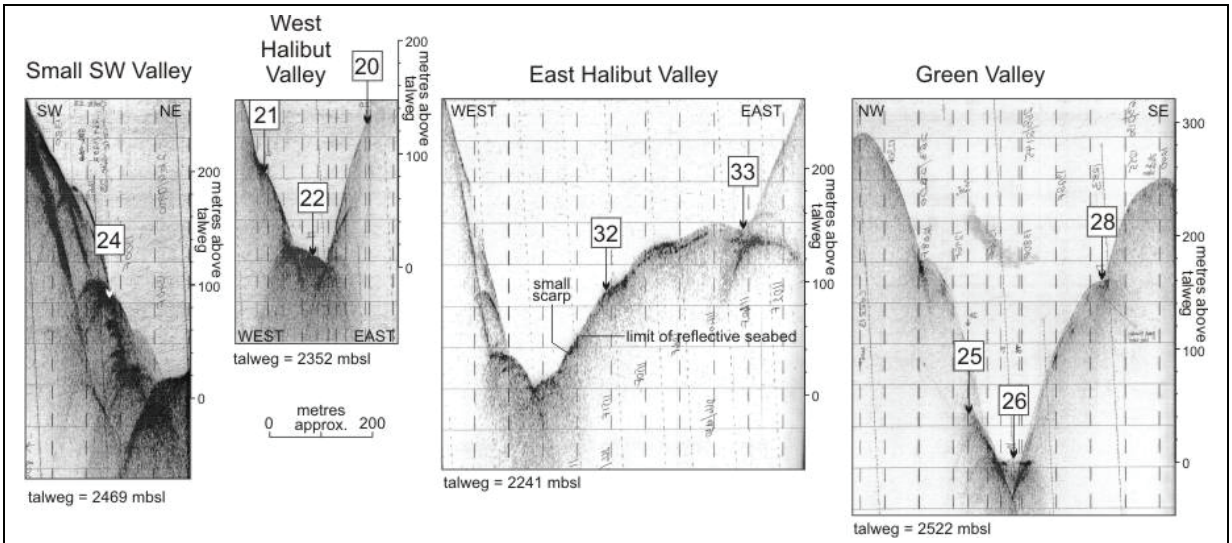


*Figure 3.2.1. Bathymetric setting of cores from valley floors and terraces from cruise 2006-048.*

Most cores were taken from submarine valleys and terraces on their walls (Fig. 3.2.1) to assess geohazards related to turbidity currents and local failures. Core 26 from the floor of Green Valley penetrated 3 m of very uniform mud (Fig. 3.2.2). Compared with other cores, there is no down-core increase in shear strength, which may indicate that the core penetrated a slurry-like debris flow deposit. A Huntec profile (Fig. 3.2.3) shows a highly reflective valley floor overlain by two or three transparent incoherent packets up to 10 ms thick, with a small reflective talweg channel beside the uppermost packet. Sediment recovered in core 26 is probably from the upper packet beside this channel and further penetration was prevented by something hard at the top of the underlying packet.

In contrast, core 22 was taken from the floor of West Halibut Valley, about 15 m above the talweg. There was a 5 cm thick veneer of olive-grey mud, overlying a stiff grey mud with small pebbles and one cobble. The shear strength of the mud was measured at 45 kPa, suggesting original burial to at least 35 m depth (cf. Mulder et al. 1997). The most probable interpretation of the grey mud is that it was a pebbly debris flow deposit, buried to 35 m, and then re-exposed by erosion. However, the possibility of an outcropping mudstone layer mixed with channel floor pebbles as a result of coring disturbance cannot be ruled out.

In East Halibut Valley, cores 32 and 33 were taken from a post-glacial “inner levee” within the valley (Fig. 3.2.4). A hard reflective 4 km-wide valley floor is exposed on the west side of the valley in the talweg, but passes under a 50 m high inner levee on the east side of the valley, which provided the only sediment soft enough for coring. Core 32 is located 90 m above the talweg and core 33 at 155 m. The two cores can be correlated principally using the a* (red = hematite) colour variations, which show a prominent peak that drops off rapidly at a depth of 7–8 m. This pattern can be correlated to the ridge cores and more widely to other cores on the SW Grand Banks margin where the base corresponds to the H1 marker (e.g. cores 75 and 80 in Fig. 13 of Ledger-Piercey and Piper, 2007). The available dates from this study bracket the radiocarbon age to between 13.3 and 14.2 ka, consistent with the correlation with Heinrich layer

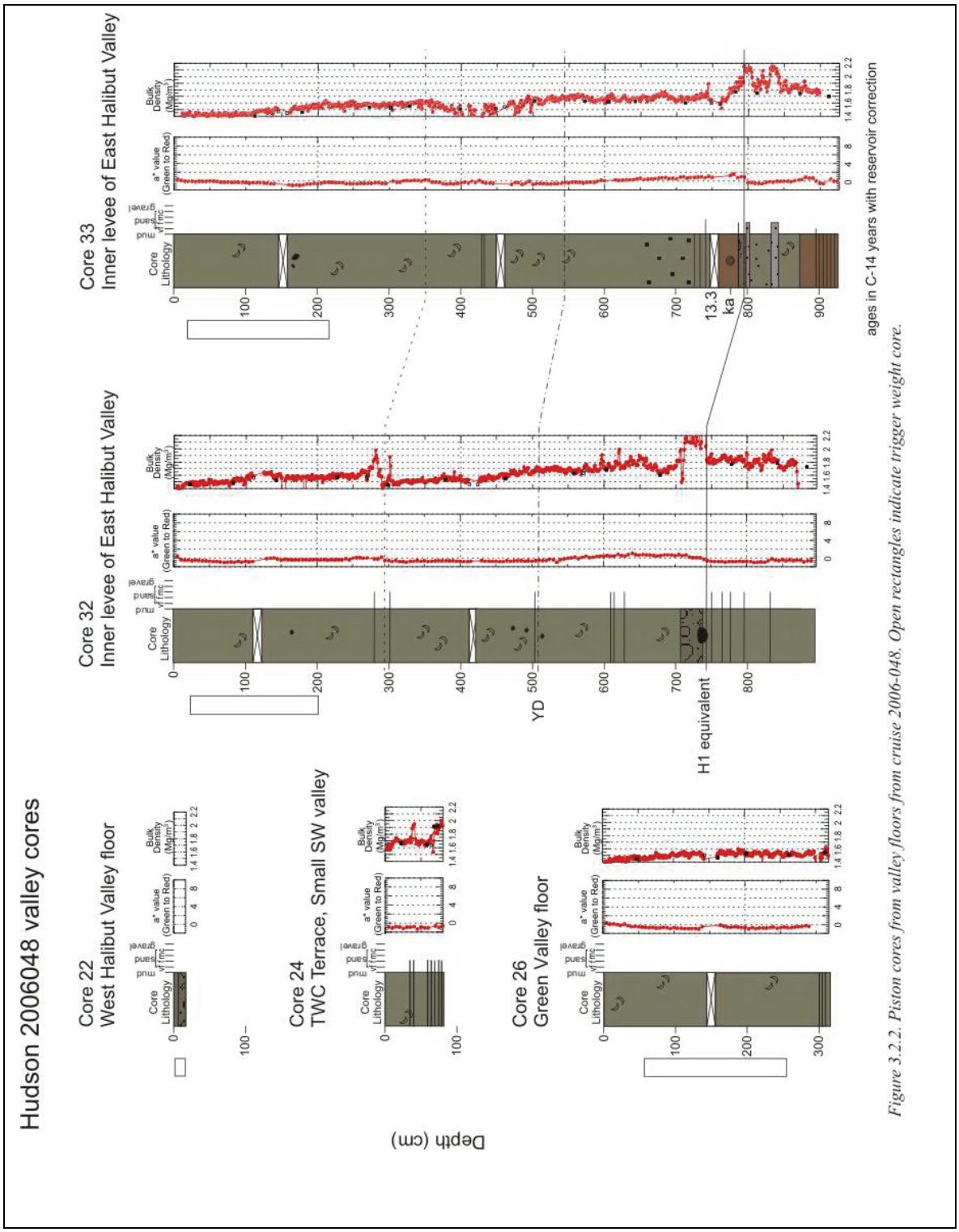


*Figure 3.2.2. Piston cores from valley floors from cruise 2006-048. Open rectangles indicate trigger weight core.*

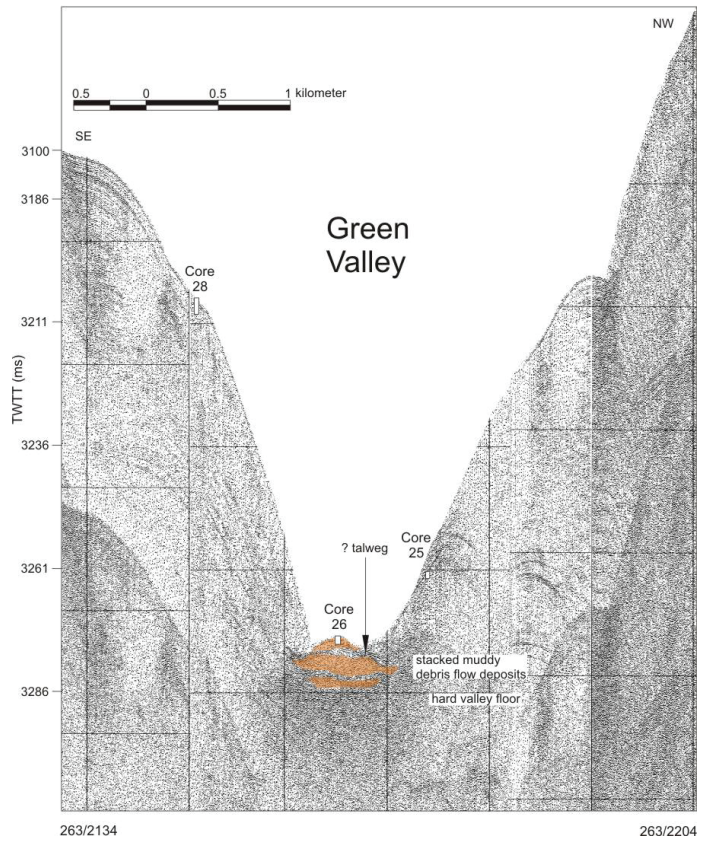


*Figure 3.2.3. Huntec sparker profile across Green Valley showing location of piston cores. Orange indicates interpreted mass-transport deposits.*

1. At this horizon there is also a prominent 20 cm thick sand bed, the only bed of such thickness in either core (Fig. 3.2.5). A second correlatable horizon at about 5 m, again based on the a* colour variations, can be correlated to a dated Younger Dryas horizon in core MD95-2031 on the SW Grand Banks slope (Piper and Gould, 2004). A third horizon, at about 3 m, is marked by an increase in bulk density due to higher sand or silt content and is of unknown age.

The flank of the inner levee, to 35 m above the talweg, appears to have been eroded in the Holocene and the seafloor appears reflective (likely sandy) to 55 m above the talweg (Fig. 3.2.4). Core 32, 90 m above the talweg, has more and thicker sand beds than core 33, 155 m above the talweg (Fig. 3.2.2) and the prominent sand bed at the H1 marker is a gravelly coarse sand in core 32, but a fine sand in core 33 (Fig. 3.2.5). This sand bed

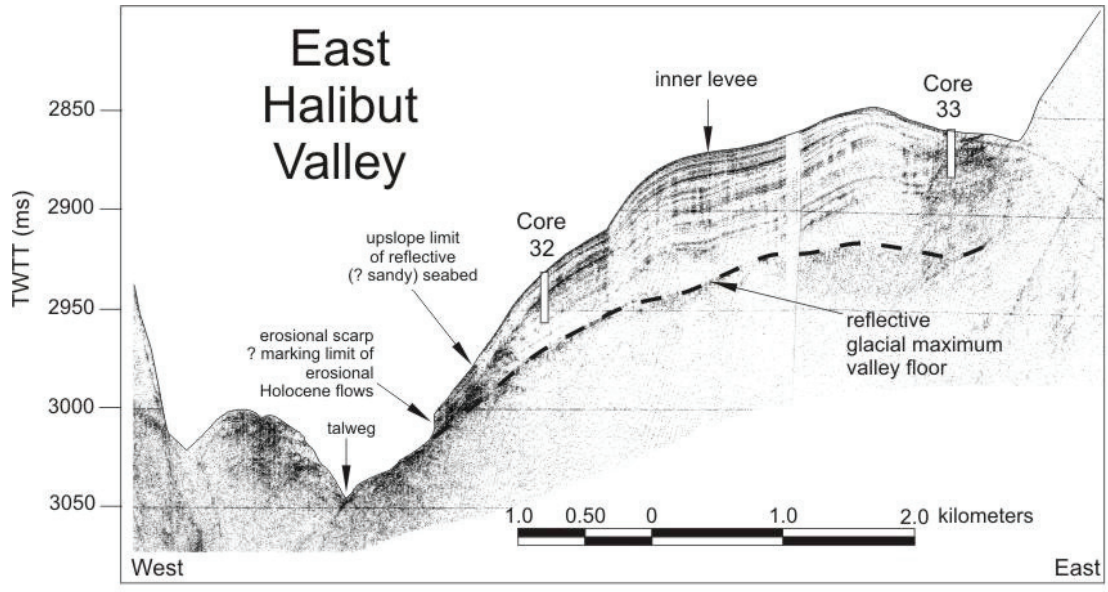


*Fig. 3.2.4. Huntec sparker profile across East Halibut Valley showing muddy inner levee and location of piston cores. Compare with Fig. 3.2.17b.*

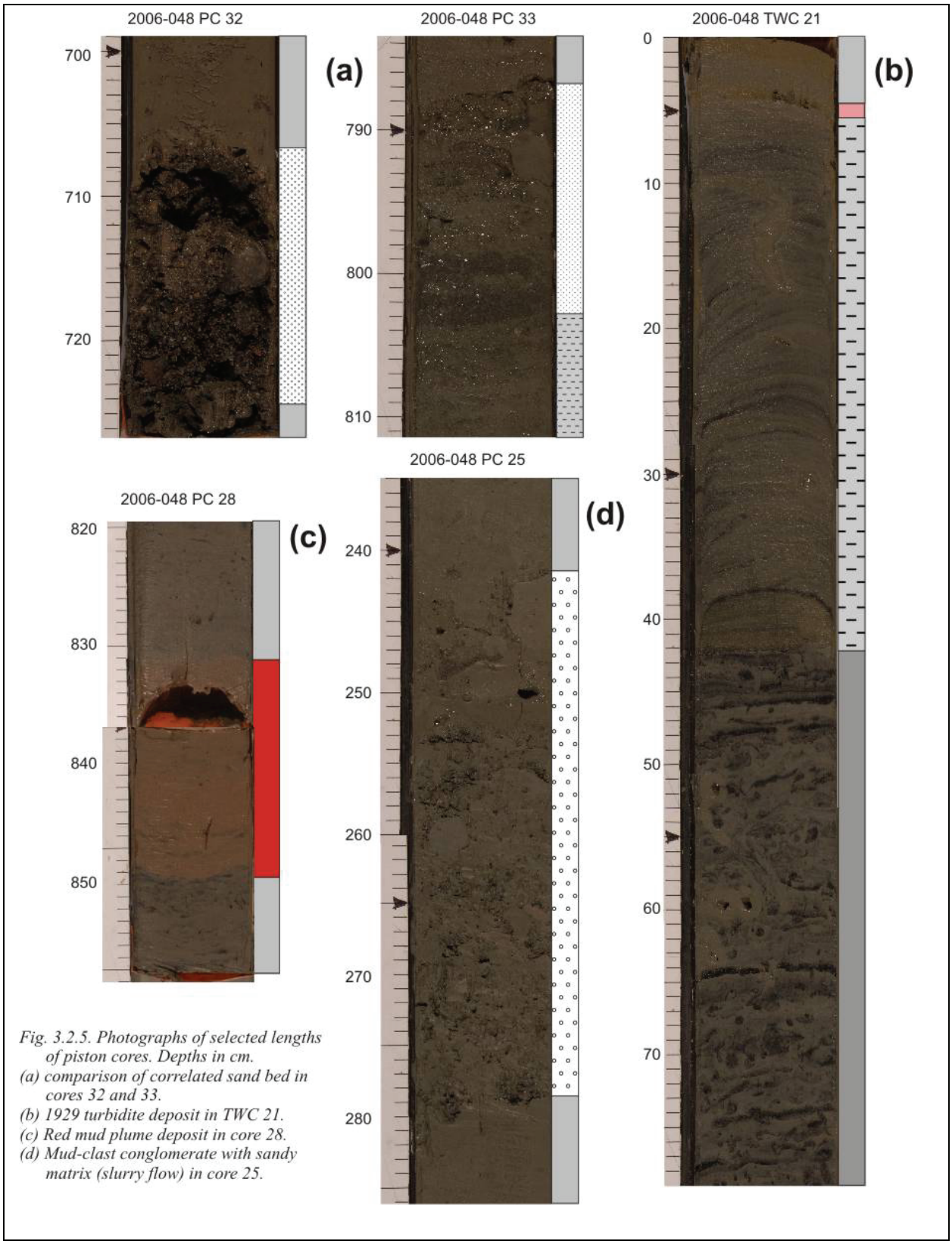


*Fig. 3.2.5. Photographs of selected lengths of piston cores. Depths in cm.*
*(a) comparison of correlated sand bed in cores 32 and 33.*
*(b) 1929 turbidite deposit in TWC 21.*
*(c) Red mud plume deposit in core 28.*
*(d) Mud-clast conglomerate with sandy matrix (slurry flow) in core 25.*

likely resulted from subglacial meltwater discharge, given the evidence for discharge at the same time from the eastern margin of the Newfoundland ice cap (Tripsanas and Piper, 2008). The sands at 3 m depth are the only evidence for a sizeable Holocene turbidity current and are likely of early Holocene age. The risk of turbidity currents in East Halibut Valley is thus difficult to evaluate with the present data. The evidence of Holocene erosion and the reflective seabed to 55 m above the talweg suggests one or more late Holocene turbidity currents (perhaps from local slumping in 1929), but the currents were not sufficiently large to deposit sand 90 m above the talweg at core site 32.

In West Halibut Valley, cores 20 and 21 were taken from terraces respectively 130 and 80 m above the talweg (Figs. 2.4.1 and 3.2.1). In core 20 (Fig. 3.2.6), the YD and H1 markers are recognised from the a* colour variations and confirmed by a radiocarbon date of 14.2 $^{14}$C ka. One thin sand bed is present at 1 m sub-bottom, indicating a thick mid-Holocene turbidity current, but there is no evidence of younger turbidites in either the piston or trigger-weight core. In contrast, the TWC of core 21 has at the top a 40 cm bed of laminated silt and mud, with an erosional base and capped by a 1 cm pink mud overlain by oxidised hemipelagic mud (Fig. 3.2.5b). This succession is interpreted as the deposit of the 1929 Grand Banks turbidity current. The underlying succession in both the PC and the TWC includes common thin silt laminae, indicating frequent turbidity currents, but there is no age control except for a radiocarbon date of 12.9 $^{14}$C ka at 3.3 m downcore. It is possible that the entire succession beneath the 1929 deposit is of late Pleistocene age. Thus the risk of turbidity currents in West Halibut Valley is difficult to assess with present data.

In Green Valley, cores 25 and 28 (Fig. 3.2.6) were taken from terraces respectively 45 m and 155 m above the talweg (Figs. 3.2.1 and 3.2.3). In core 28, the H1 equivalent marker is quite clear from the a* colour values at 7 m and the Younger Dryas (YD) is at approximately 2.5 m. Below H1 is a prominent 20 cm red mud bed (Fig. 3.2.5c), correlated with the topmost red mud bed found elsewhere on St Pierre Slope (e.g. cores 73, 74, Fig. 2.4.1) and the SW Grand Banks Rise off Whale Bank (e.g. core 80, Fig. 2.4.1; see also Ledger-Piercey and Piper, 2007, their Fig. 13), dated at 14.1 $^{14}$C ka by Skene and Piper (2003). Core 28 has numerous bioturbated thin fine-grained sand beds from the YD downwards, many more than on the inner levee of East Halibut Valley. Core 25 is only 3.5 m long and appears to reach the YD marker. It includes at this level a 35 cm thick mud-clast conglomerate with a sandy matrix (Fig. 3.2.5d), interpreted as a slurry flow deposit. No sand beds are recognised in the overlying Holocene section.

Three long cores (29–31) are available from the ridge between Green Valley and East Halibut Valley (Figs. 2.4.1 and 3.2.7). Two sedimentary units are recognised. The upper 4–6 m comprises bioturbated mud, locally with thin bioturbated sand beds. Below this, there is an abrupt increase in bulk density and numerous thin sand beds. Correlation with cores 20 and 33 using the a* colour plot suggests that the top of the sandy unit dates from about the H1 event at ca. 14 ka ($^{14}$C years). This in turn implies a very high mean sedimentation rate of 4 m/ka between 14 and 15 ka ($^{14}$C years). Within the upper unit, a tentative YD correlation is made on the basis of the a* colour values. No sand beds are present above the YD.

There are more sand beds between the YD and H1 markers in core 31 on the ridge and core 28 on the terrace in Green Valley than in the equivalent interval in cores 32 and 33 on the inner levee of East Halibut Valley. This suggests that reworking of sands took place in shallow water of Green Bank, upslope from core 31 and Green Valley, but not in the deeper water of Halibut Channel.

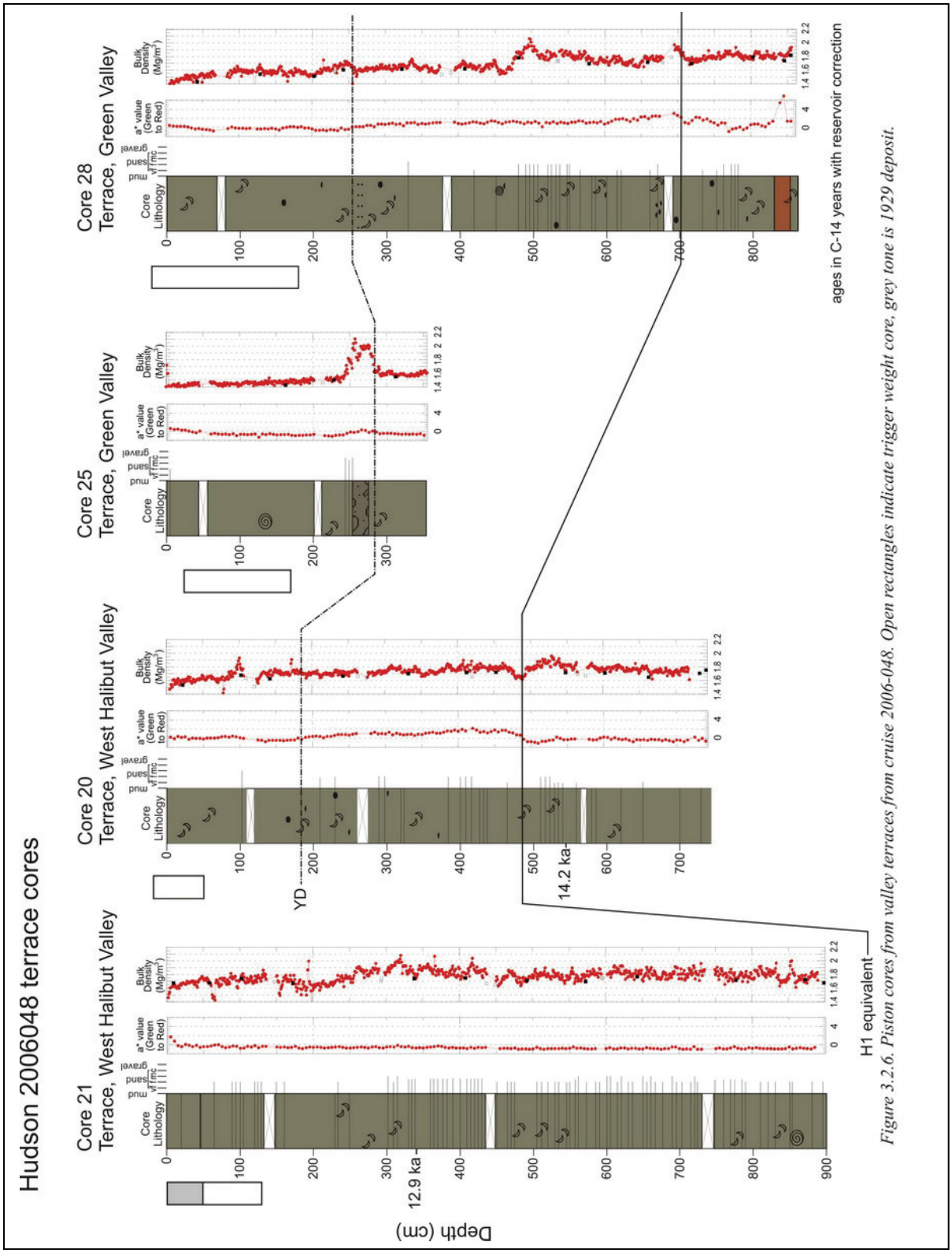


*Figure 3.2.6. Piston cores from valley terraces from cruise 2006-048. Open rectangles indicate trigger weight core, grey tone is 1929 deposit.*

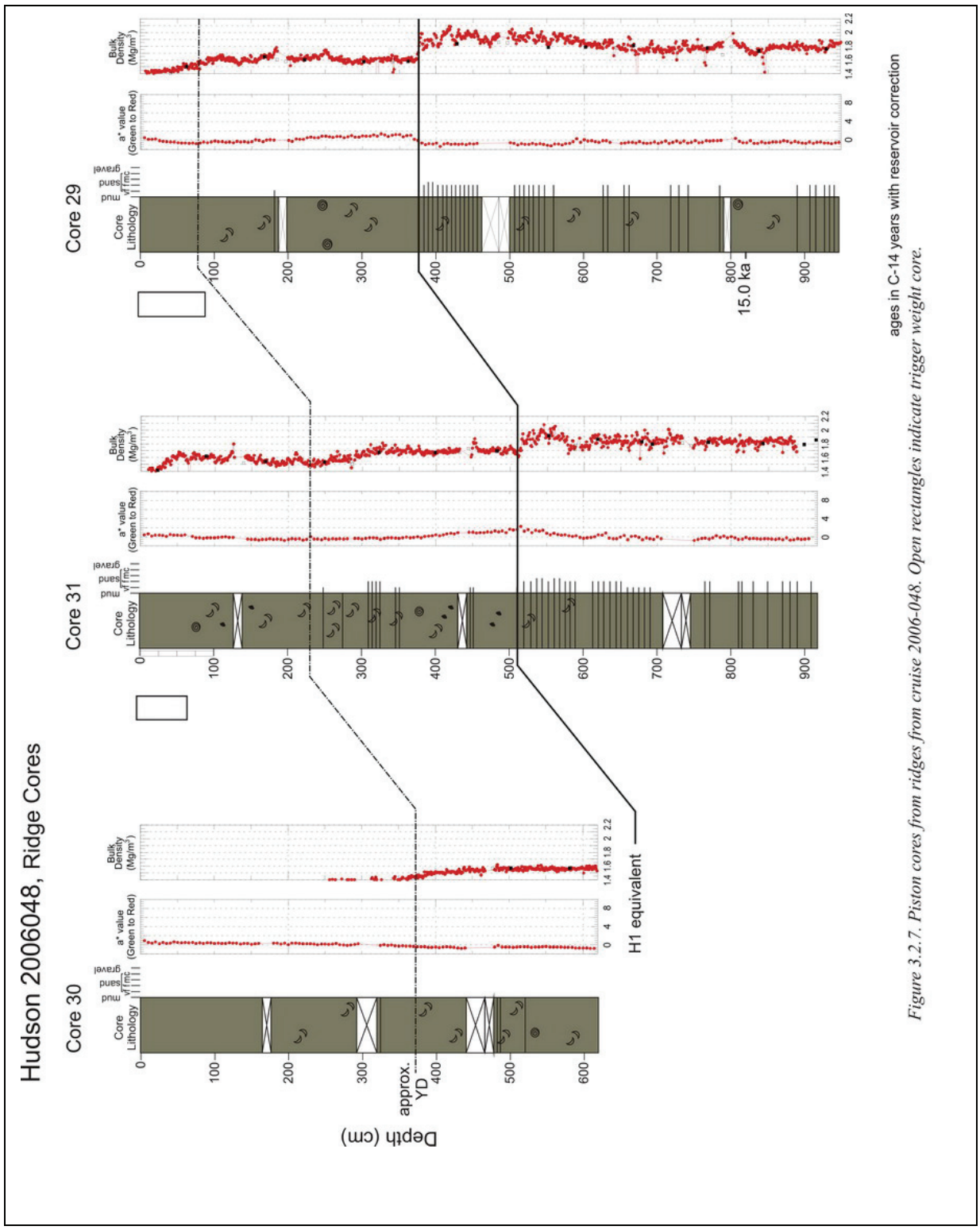


*Figure 3.2.7. Piston cores from ridges from cruise 2006-048. Open rectangles indicate trigger weight core.*

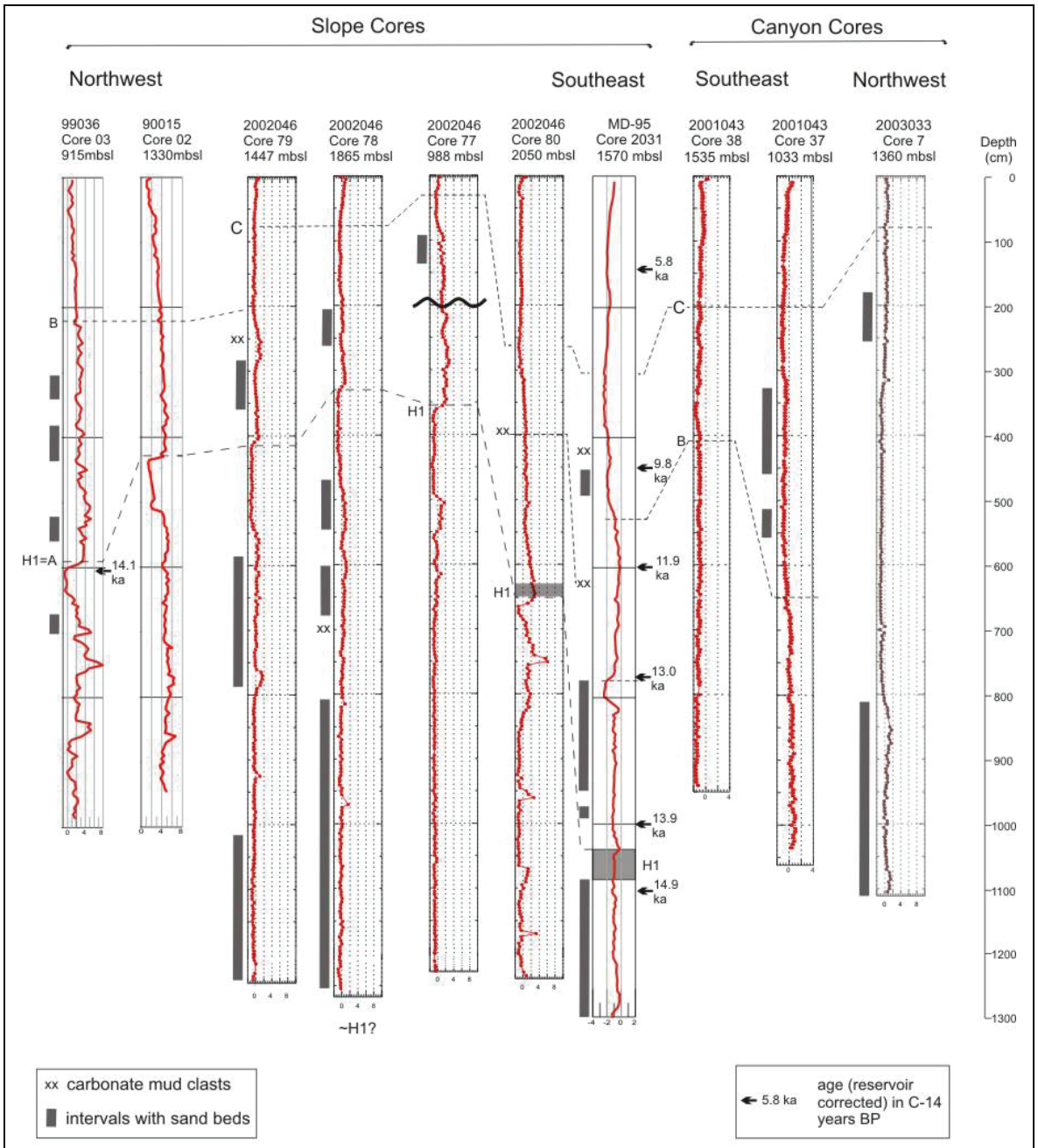


*Figure 3.2.8. Correlation of a* colour trace from piston cores from the SW Grand Banks slope. Modified from figure 14 of Ledger-Piercey and Piper (2007) with revised correlation of cores 78 and 79.*

In addition, two previous cores from the ridge between Green Valley and East Halibut Valley, 78 and 79 from 2002-046, are reported by Ledger-Piercey and Piper (2007). Data for these cores are included in this report. Comparison of thicknesses and the a* colour variations with dated core 29 suggests that the tentative correlation of Ledger-Piercey and Piper (2007) may be incorrect and the H1 equivalent is likely at a depth of 3–4 m in these cores (Fig. 3.2.8).

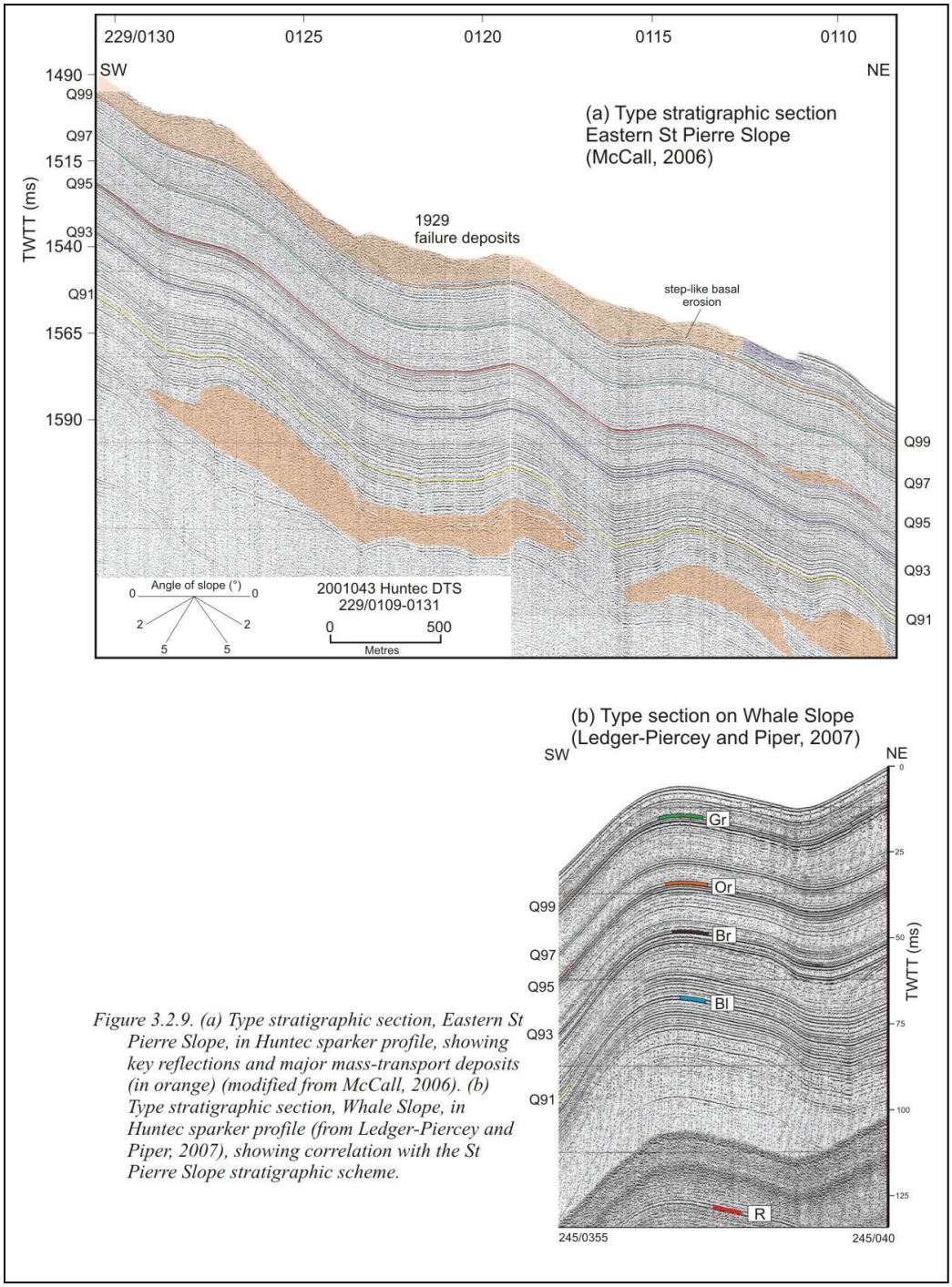


*Figure 3.2.9. (a) Type stratigraphic section, Eastern St Pierre Slope, in Huntec sparker profile, showing key reflections and major mass-transport deposits (in orange) (modified from McCall, 2006). (b) Type stratigraphic section, Whale Slope, in Huntec sparker profile (from Ledger-Piercey and Piper, 2007), showing correlation with the St Pierre Slope stratigraphic scheme.*

**Geohazard implications of core data**

The two major valleys, East Halibut and West Halibut valley, were the site of erosion and sediment bypass in the Holocene. Such erosion may have been restricted to the 1929 Grand Banks turbidity current and a significant early to mid Holocene current in both valleys, but the possibility of smaller currents cannot be ruled out. Both the 1929 and the mid-Holocene currents were at least 100 m thick and caused erosion at least 50 m above the talweg.

Prior to the 16.5 ka (cal.) H1 marker, at depths of 4–8 m in most cores, thin sand beds are abundant (and more common than in most settings on the Scotian Slope) and sedimentation rates were very high, on the order of several metres per thousand years (higher than most settings on the Scotian Slope). The risk of significant underconsolidation at depths beyond those penetrated by cores is thus high.

**Description, correlation and interpretation of Huntec profiles**

The Huntec sparker system profiles image the upper 50-100 m of seabed (see Fig. 2.2.2). The incised character of the Laurentian East block means that in many places Huntec data are discontinuous; broken up by valleys across which it is difficult to make stratigraphic correlation.

Reference stratigraphic sections (Fig. 3.2.9) are available in adjacent areas on St Pierre Slope (McCall, 2006) and on Whale Slope (Ledger-Piercey and Piper, 2007). On St Pierre Slope, key stratigraphic horizons have been dated by reference to till tongues and using radiocarbon dates (Piper et al., 2005; McCall, 2006) and are regarded as reasonably secure. There is likely some drift in correlating of a few cycles, which is a serious problem only for the youngest part of the section (Q99) that probably has an age of 13 ka (cal) corresponding to the shallowest till tongue on St Pierre Slope. On Whale Slope, age assignments are more speculative, except for the shallowest marker Gr, which is dated from cores as corresponding to Heinrich event 1 (16.5 ka [cal]). As part of this study, the St Pierre Slope stratigraphy was correlated to parts of the Laurentian East block (Figs. 3.2.10, 3.2.11, 3.2.12). Correlation is possible on ridges between valleys on which the predominant sedimentation is from proglacial plume fall-out. The amplitude and abundance of reflections is a consequence of variations in supply of sediment in the plumes, including the amounts of quartz and carbonate rock flour. As a result, similar patterns are visible over many tens of kilometres in similar water depths.

Mass-transport deposits (MTDs) are recognised from Huntec sparker profiles from their incoherent reflections and commonly irregular top, as shown by the 1929 failure deposits on St Pierre Slope (Fig. 3.2.10). In some cases, the base of the MTD is step-like, perhaps indicating failure by retrogressive rotational slumps (Fig. 3.2.10, 3.2.14). Adjacent to steep slopes, such as levees beside major channels, small MTDs are trapped at the foot of slope (e.g. in the middle of Fig. 3.2.11) and probably correlative headscarps are present on the adjacent levee (SW end of Fig. 3.2.11). Such failures can commonly be correlated over tens of kilometres and occur in multiple valley systems; such failures have been generally interpreted as triggered by earthquakes on the eastern Canadian margin (e.g. Mosher et al., 2004; Piper, 2005).

In some valleys, most clearly in the upper part of Green Valley (Figs. 3.2.11, 3.2.13b) but also in the area west of West Halibut Valley (Fig. 3.2.12b), MTDs are very abundant at some stratigraphic intervals and do not appear to correlate with failures in intervalley areas. This is seen most clearly in Figure 3.2.11, where valley MTDs are abundant between Q99 and Q97 and again below Q95, whereas slumps off the steep back-side of the levee to the southeast occur between Q97 and Q93 and on the ridge to the northwest (Fig. 3.2.13a) are only present between Q99 and Q97.

It is well established that glacial till was deposited on the outer shelf and upper slope off southeastern Canada, to present water depths of 500–700 m (e.g. Mosher et al., 1989; Piper and Brunt, 2006). The timing of till tongues, representing advance of ice across the outer shelf, is well established for St Pierre Slope (Piper et al., 2005; McCall, 2006) and is illustrated in Figure 3.2.15. Two ice advances dating at about 12 ka and younger than 41 ka were recognised from a borehole record in Halibut Channel (Miller et al., 2001). The distal ends of two till tongues were imaged by Huntec sparker at the head of West Halibut Valley (Fig. 3.2.16a), but the seafloor is too dissected to trace these horizons seawards into a known stratigraphy. Up-dip, the head of West Halibut Valley (Fig. 3.2.16b) is floored by a hard reflective till (probably overconsolidated), overlain by a less reflective till that is probably normally consolidated (cf. Piper and MacDonald, 2002, at the head of Laurentian Channel and the 2006-048 cores in Laurentian West block). The weakly reflective till in the valley floor appears to be the lateral
equivalent of the distal part of the till tongue (Fig. 3.2.16a). In the head of East Halibut Valley, the valley is relatively flat floored with steep walls, giving an overall U shape (Fig. 3.2.17a). The floor of the valley has large-scale furrows spaced on a kilometre scale, with a superimposed small-scale roughness due to iceberg scouring (Fig. 3.2.17b).

The internal structure of East and West Halibut valleys is quite different as imaged by our high-resolution seismic system (Fig. 3.2.18). West Halibut Valley appears to be erosional with at most a few metres of coarse-grained sediment or MTD on its floor (cf. core 22).

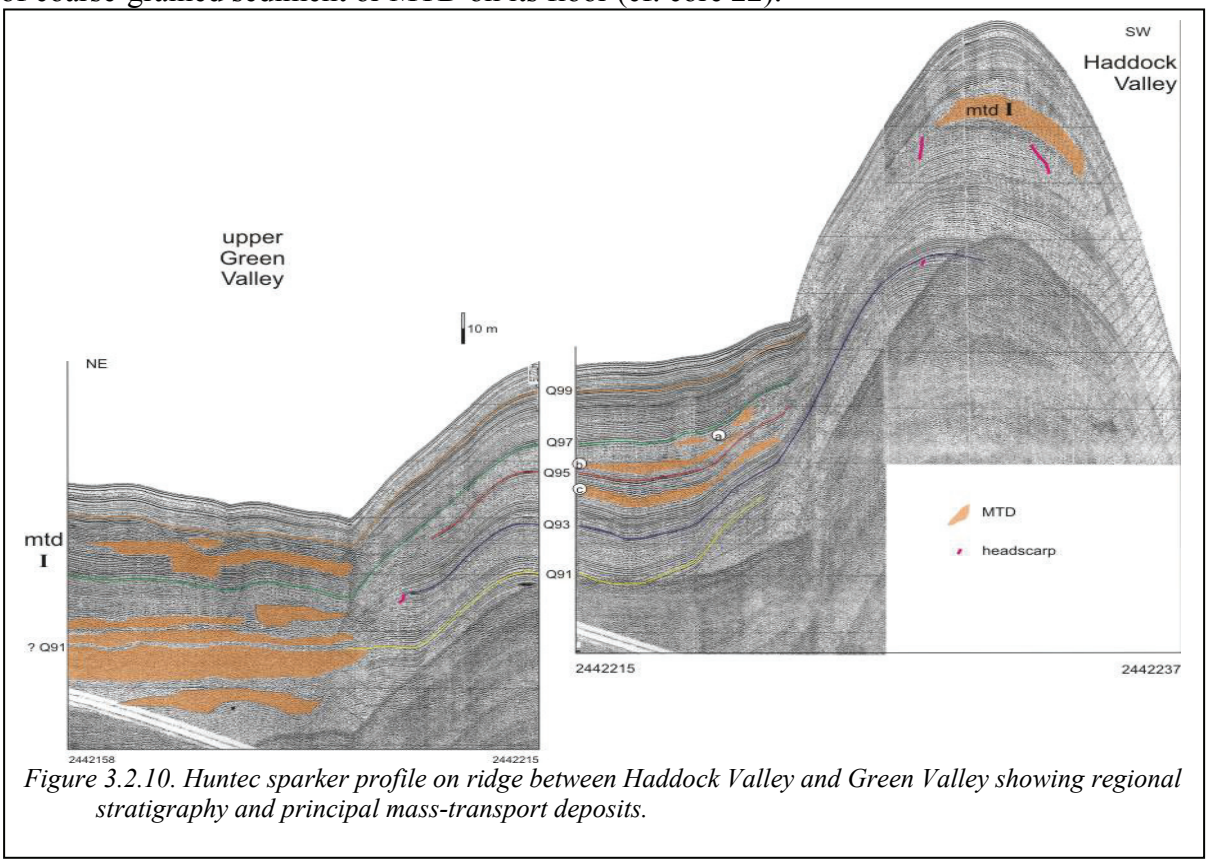


*Figure 3.2.10. Huntec sparker profile on ridge between Haddock Valley and Green Valley showing regional stratigraphy and principal mass-transport deposits.*

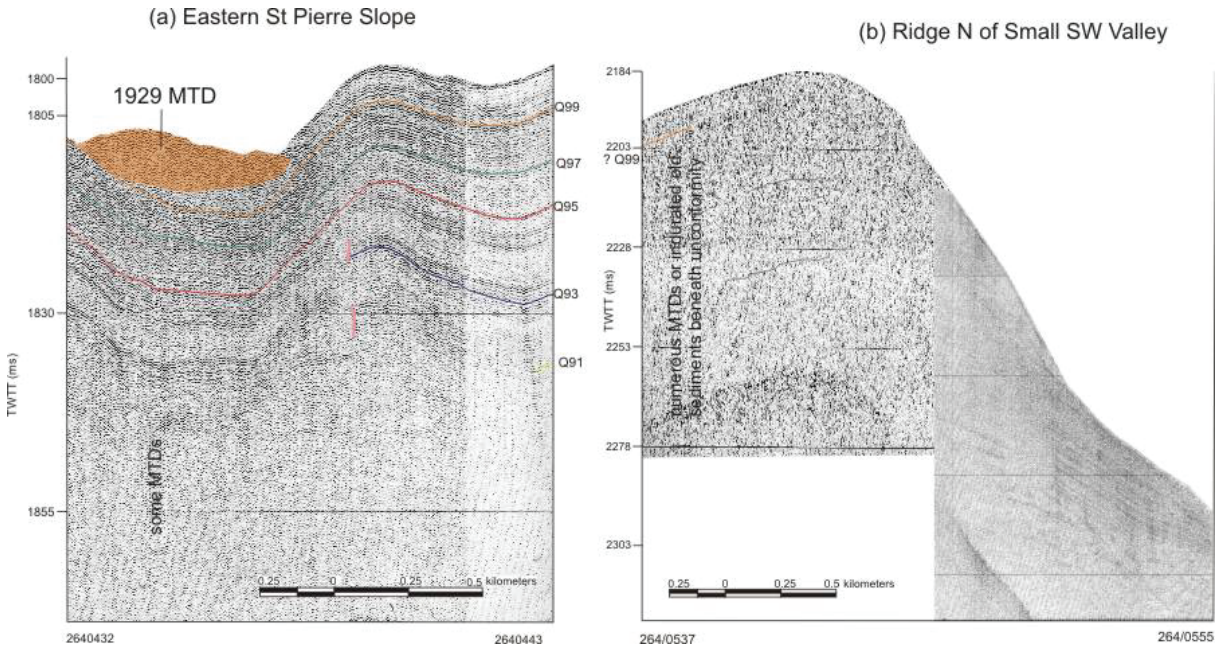


*Figure 3.2.11. Huntec sparker profile on ridges in western part of Laurentian East block showing stratigraphic markers and mass-transport deposits.*

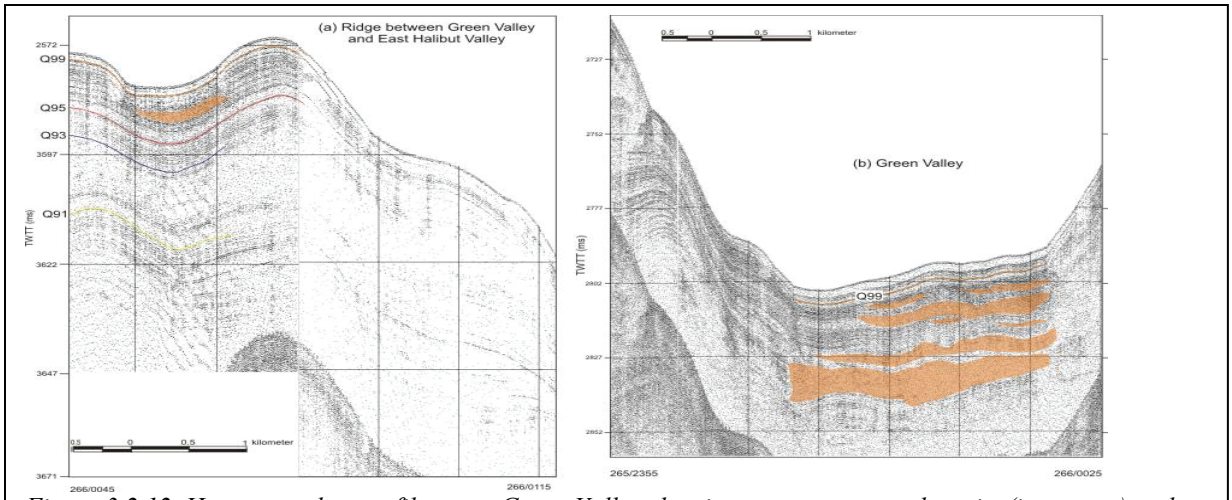


*Figure 3.2.12. Huntec sparker profiles near Green Valley showing mass-transport deposits (in orange) and key reflections.*

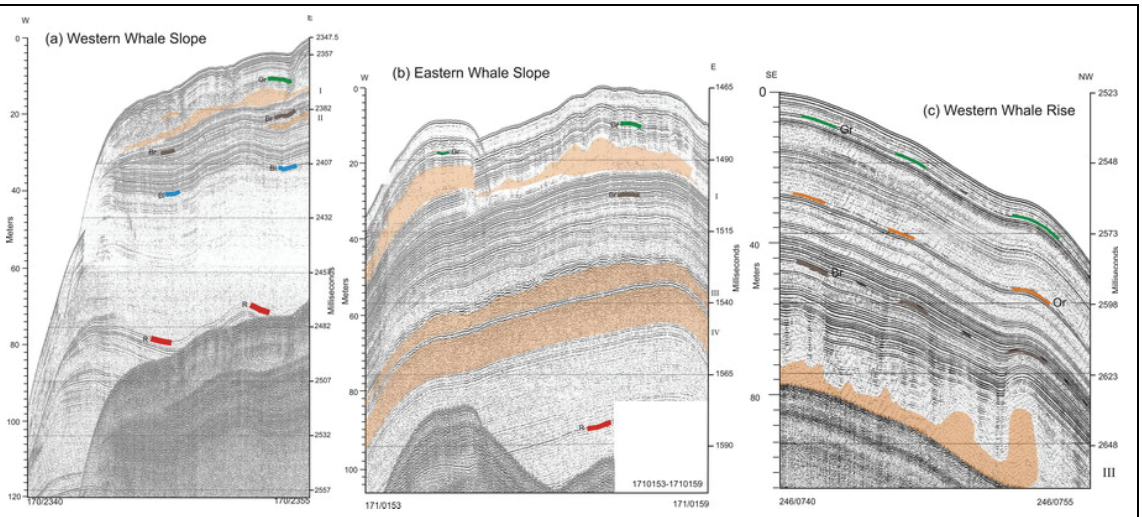


*Figure 3.2.13. Correlated stratigraphic sections from the SW Grand Banks Slope and Rise showing key reflections and major mass transport deposits (in orange) (modified from Ledger-Piercy and Piper, 2007).*

In contrast, East Halibut Valley is wider (4 km cf. 1.5 km) and has an aggradational package of highly reflective facies that is overlain by a muddy inner levee (Fig. 3.2.5). A third type of valley is represented by Green Valley, which is floored by stacked MTDs (Fig. 3.2.4).

We suggest that the style of valleys and the distribution of MTDs were controlled to a great extent by a complex glacial history because:

(a) The ages of till tongues correspond to the abundant mass-transport deposits in the floor of upper Green Valley, for which there is no correlative extensive failure on the adjacent ridges. (Figs. 3.2.11, 3.2.13). They may represent the result of either direct supply of till to the upper slope or overloading and failure of upper slope sediment. None of our cores penetrated this type of MTD, so that their drilling character is unknown.

(b) The U-shaped cross-section of East Halibut Valley is characteristic of catastrophic meltwater discharge from an ice-margin (Piper et al. 2007; Tripsanas and Piper, 2008). The aggradational character of the valley floor suggests direct flow of hyper-concentrated sand and gravel bedload into the upper valley, analogous to Eastern Valley of Laurentian Fan (Piper et al. 2007). The age of the discharge is unknown, but the principal meltwater discharge from the northeastern side of the Newfoundland ice-sheet was at 23 ka (cal) (Tripsanas and Piper, in revision) and a similar age may be likely for Halibut Channel.

(c) West Halibut Valley may also have been sculpted by hyperpycnal flows from subglacial meltwater, but such flows were smaller than those in East Halibut Valley and were probably fully turbulent, accelerating downslope and transporting sediment to the Sohm Abyssal Plain.

(d) Glacial meltwater discharge also transported large quantities of muddy sediment in surface plumes, from the Grand Banks ice margin and through Haddock and Halibut channels. It was fluctuations in this supply that led to the correlatable Huntec sparker seismic stratigraphy. It also resulted in very high rates of sedimentation, estimated at several metres per thousand years during the last glacial maximum (Q91–Q97).

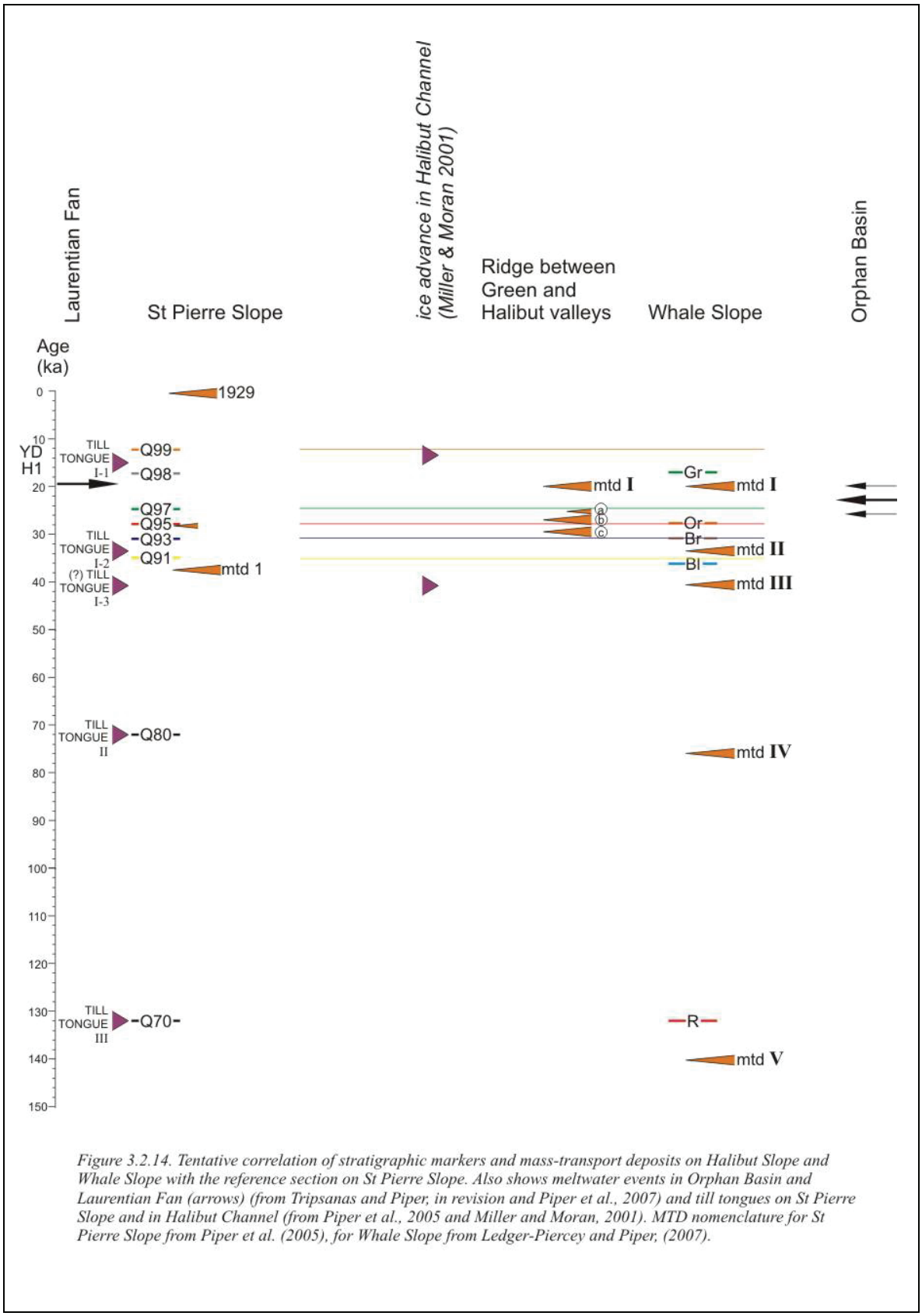


*Figure 3.2.14. Tentative correlation of stratigraphic markers and mass-transport deposits on Halibut Slope and Whale Slope with the reference section on St Pierre Slope. Also shows meltwater events in Orphan Basin and Laurentian Fan (arrows) (from Tripsanas and Piper, in revision and Piper et al., 2007) and till tongues on St Pierre Slope and in Halibut Channel (from Piper et al., 2005 and Miller and Moran, 2001). MTD nomenclature for St Pierre Slope from Piper et al. (2005), for Whale Slope from Ledger-Piercey and Piper, (2007).*

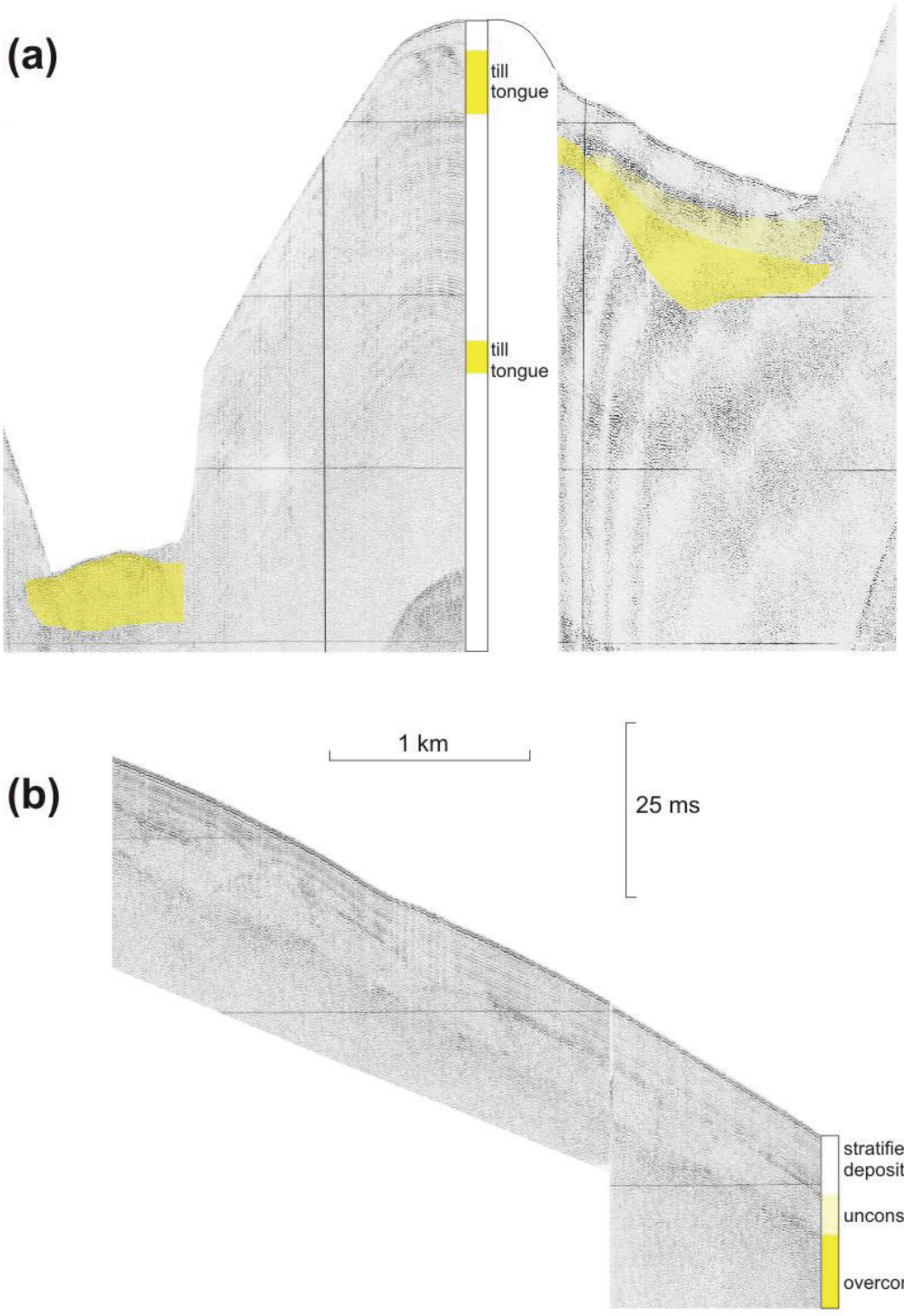


*Figure 3.2.15. Huntec sparker profiles from head of West Halibut Valley showing the presence of glacial till.*

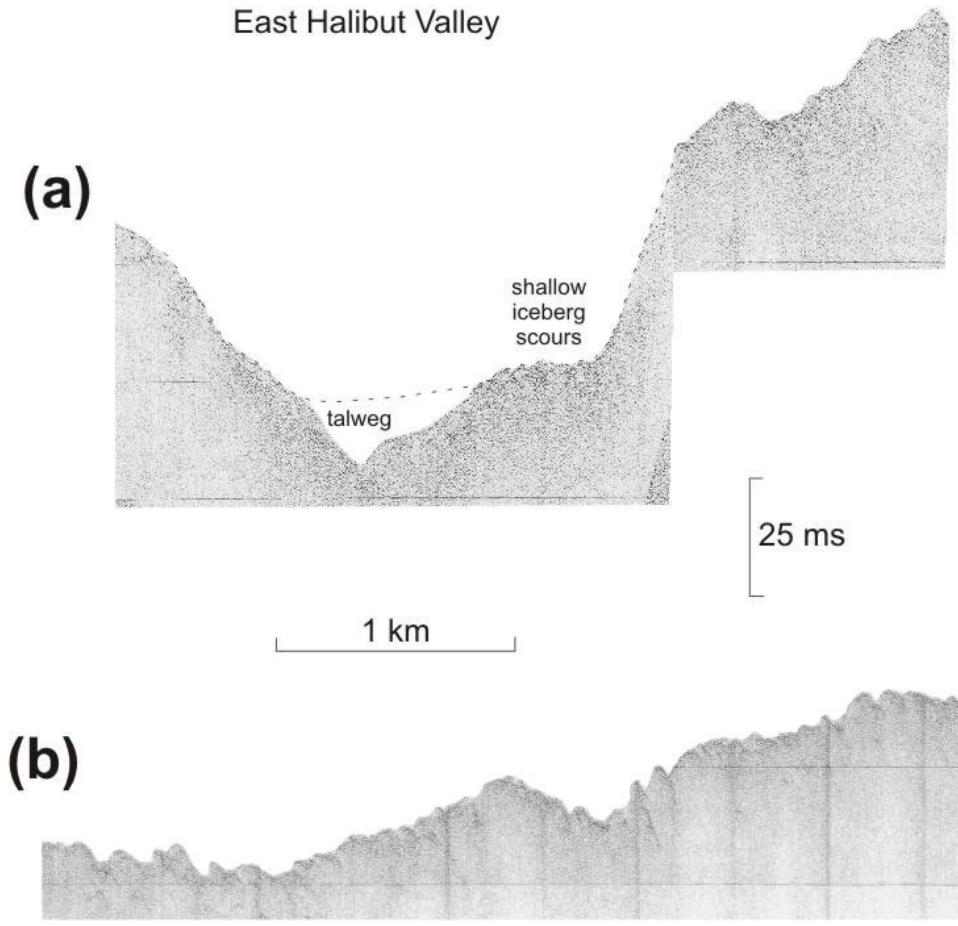


*Figure 3.2.16. Huntec sparker profiles from head of East Halibut Valley. Profiles located in Fig. 3.2.1. (a) Valley head showing U-shaped cross-section with incised talweg and shallow iceberg scours, (b) Part of valley floor in deeper water showing km-scale erosional fluting and abundant deeper iceberg scours, suggesting that till is less overconsolidated.*

(e) The Grand Banks Valley, formed by the confluence of East and West Halibut valleys, transported sandy turbidites to the Laurentian Fan, perhaps as late as the Younger Dryas (Skene and Piper, 2003, 2006). This points to continued supply of sediment, both from a late ice cap on St Pierre Bank that retreated at about 14 ka (cal.) and from storm reworking of sediment on the shallow outer shelf during late Pleistocene low sea level. Sand beds are abundant below the YD marker on West Halibut Valley terraces and on the ridge between Green and East Halibut valleys, areas

(f) Occasional regional failures occurred, in multiple valley systems, likely triggered by rare earthquakes. The highly dissected topography of the Laurentian East block makes recognition of such failures difficult. There appears to have been a regional failure in the eastern part of the block above Q97 that corresponds to the more extensive MTD I on the Whale Slope.

(g) Other failures above Q91 are of very local extent (e.g. a–c in Fig. 3.2.11; the MTD at about the Younger Dryas in core 25 in Green Valley) and their relationship earthquake triggering is unknown.

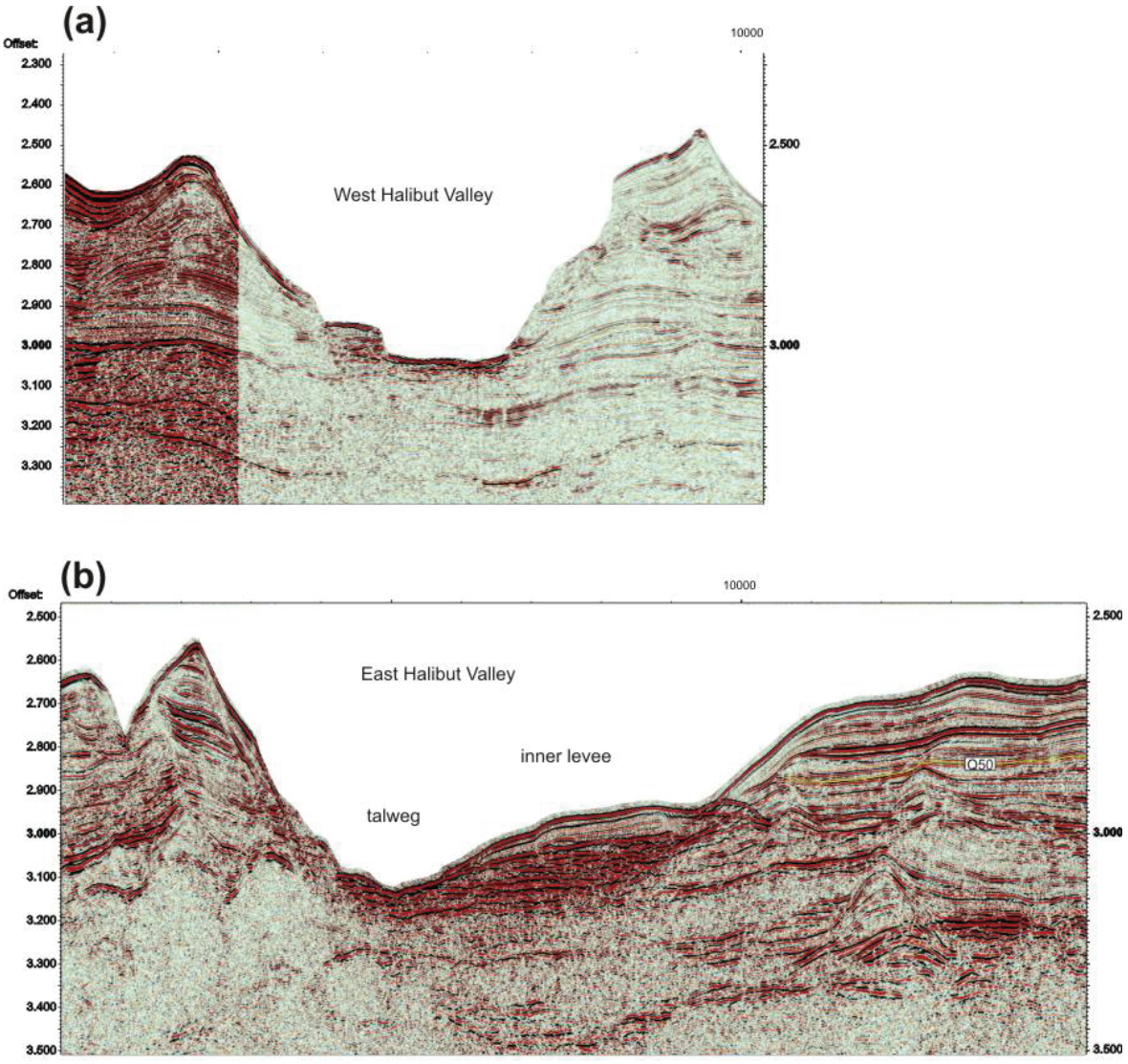


*Fiure. 3.2.17. Sleeve gun profiles across East and West Halibut valleys showing contrasting valley character.*

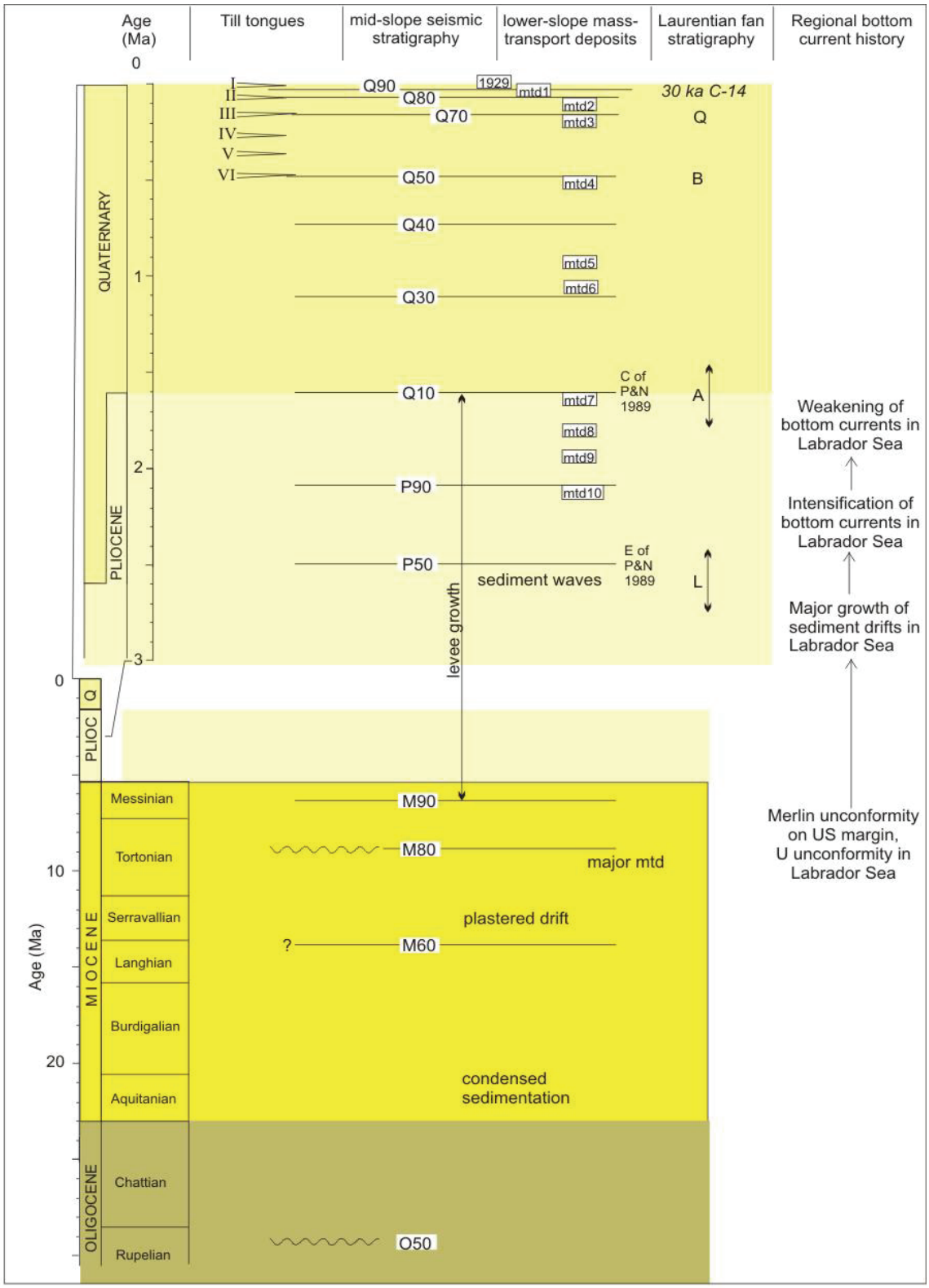


*Figure 3.2.18. Regional stratigraphic markers on St Pierre Slope (from Piper et al.2005, their Fig. 11).*

**Stratigraphic control in the Laurentian East 3-D block**

The following stratigraphic ties have been developed in areas adjacent to the Laurentian East 3-D block and have been correlated with greater or lesser precision into the 3-D block. Little effort was put into tying pre-Neogene horizons. The mid Oligocene unconformity (O50) was brought in from the Hermine E-54 well based on the revised biostratigraphy of G.L.Williams (in Piper et al. 2005) and correlated using the GSC's SPS multichannel lines. A deeper prominent reflection was correlated with the top Cretaceous (K99) in wells on the SW Grand Banks margin and at Hermine E-54.

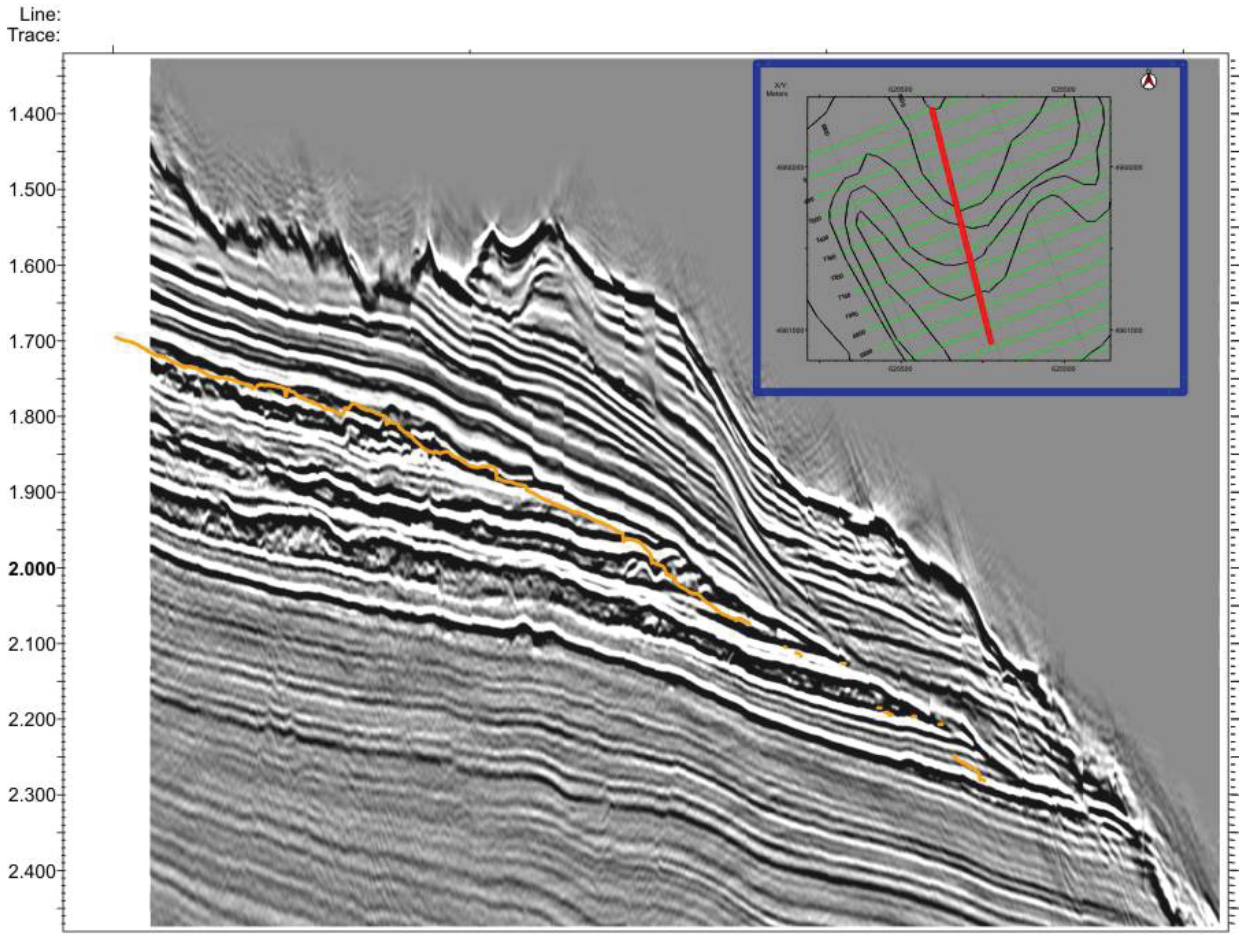


*Figure 3.2.19. Arbitrary line in NW part of block showing direct correlation of the E horizon of Piper & Normark (1989) = P50 of Piper et al. (2005).*

Neogene correlations were attempted with the wells on the SW Grand Banks, but were not successful. The Neogene section in Hermine E-54 is too thin to correlate with confidence, except for a late Miocene pick (M80) that Piper et al. (2005) brought from the Hermine E-54 well to St Pierre Slope. Shallower reflections P50 (mid Pliocene) and Q10 (early Quaternary) were correlated from Laurentian Fan, where they were dated from sparse borehole and outcrop biostratigraphy by Piper and Normark (1989), through TGS Nopec 2-D lines into St Pierre Slope by Piper et al. (2005) (Fig. 3.2.19). Piper et al. (2005) also recognised a mid-Quaternary reflection Q50 as corresponding to the base of the

deepest upper slope till tongue, which is correlated with the earliest major shelf-crossing glaciation at ~0.5 Ma (Piper et al., 1994).

Direct correlation of Neogene reflections from St Pierre Slope was hindered by the deeply incised West and East Halibut valleys and could only be carried into the NW corner of the 3-D cube (Fig. 3.2.19). However, reflections M90 and P50 were jump correlated over much of the study area (Fig. 3.2.20). Reflections Q10 and Q50 were correlated on character to the ridge between West and East Halibut valleys, based on comparison of sediment thickness and levee architecture with St Pierre Slope (Fig. 3.2.20 inset).

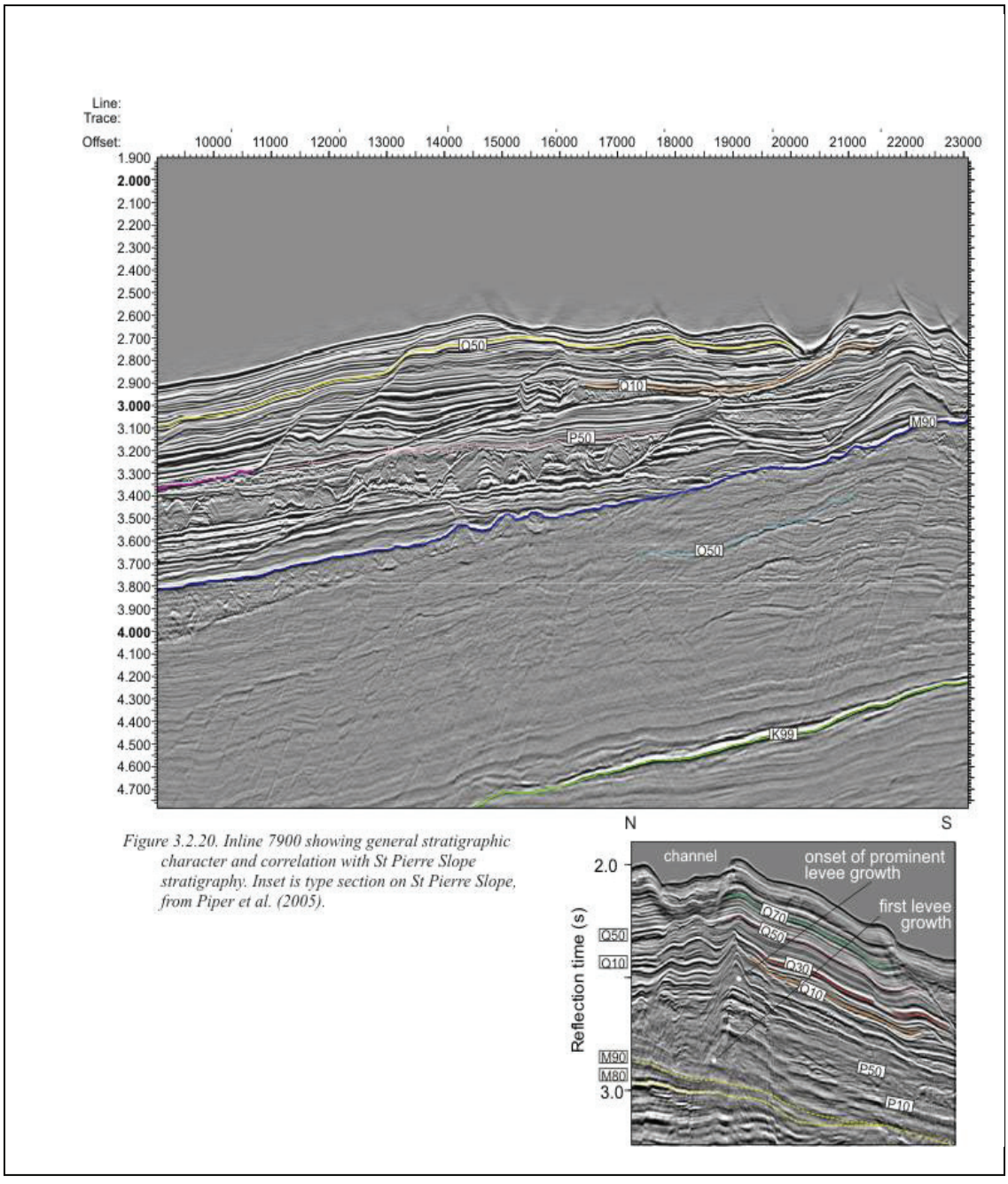


*Figure 3.2.20. Inline 7900 showing general stratigraphic character and correlation with St Pierre Slope stratigraphy. Inset is type section on St Pierre Slope, from Piper et al. (2005).*

**Prediction of shallow sediment character and geohazards in the Laurentian East block**

Integration of the Neogene stratigraphy of the 3-D block with insights from the cores and Huntec data and information from farther west on the Scotian Slope (MacDonald, 2006) allows some suggestions to be made about the general character of sediment within the Laurentian East block.

Above Q50, sedimentation is predominantly pro-glacial. Much of the sediment is derived from proglacial surface muddy plumes derived from an ice stream in Haddock Channel and from more distant ice on the Grand Banks and plume supply in the Labrador Sea. These plumes drift southwestward along the continental slope in the prevailing surface circulation (essentially, the continuation of the Labrador Current). Icebergs would also have been transported in these waters and would have dropped cobbles and boulders. Based on the abundance of ice-rafted detritus in cores 78 and 79 (the only cores to penetrate well into full-glacial sediments), we suggest that the dropstone hazard is similar to that on the Scotian Slope (note the Chevron experience at Newburn, which we consider to have resulted from a soft-sediment "dropstone") and much less severe than in Orphan Basin.

In addition, during glacial times, large amounts of proglacial sediment were supplied through Halibut Channel. Most of this sediment was in surface muddy plumes, but we infer that some was supplied through hyperpycnal flows analogous to those described from Laurentian Fan (Piper et al., 2007) and Orphan Basin (Tripsanas and Piper, in revision). Coarse-grained sediment discharge through East Halibut Valley likely deposited tens of metres of gravel and sand (Fig. 3.2.18) whereas West Halibut Valley was more erosional.

The high rates of proglacial sedimentation and local steep gradients mean that this area is susceptible to failure. Q91, which dates from 36 ka (cal.), is commonly about 100 ms subbottom whereas H1 (17 ka (cal.)) is typically at a depth of 8 m in cores, implying mean sedimentation rates of 3–4 m/ka between Q91 and Q98. Only the extreme base of a few cores penetrated these high sedimentation rate intervals, so that measured geotechnical properties may not be fully representative of the high sedimentation rate interval. These very high sedimentation rates in glacial times were not characteristic of every glacial episode and may have been higher in the last 40 ka than in any other glacial episode except probably MIS 12 at ~ 450 ka, as noted by Piper et al. (2005) and Giosan et al. 2002). In contrast, the comparable last glacial maximum sedimentation rate at wells drilled in the last decade on the Scotian Slope is < 2 m/ka and commonly ~1 m/ka. Clearly the risk of underconsolidation and local failure is greater in Laurentian East than on the central and western Scotian Slope.

On the other hand, large scale widespread failures (such as that in 1929) appear no more frequent in this area than in other parts of the eastern Canadian margin (e.g. as summarized by Piper 2005). Sparse failures are also seen above Q50 in the 3-D cube, but we found them difficult to correlate laterally and close to the limit of resolution. Their frequency is consistent with our suggestion that large-scale widespread failure is rare.

In contrast to St Pierre Slope, we see no evidence for significant fluid escape, either in the form of seismically imaged chimneys nor as gas expansion in cores. No deep-water sidescan data is available to evaluate the possible presence of pockmarks, which are widespread on upper St Pierre Slope.

During deposition of the stratigraphic interval between Q50 and P50, there was glaciation in northern Canada, but probably no significant highland glaciation in Newfoundland prior to Q30 (Piper

et al. 1994). There is thus the potential for rare ice-rafted cobbles and boulders transported through the Labrador Sea. Sea-level lowering was less extreme than above Q50, with fluctuations principally of ~40–60 m rather than ~100–130 m. The prominent transverse troughs were cut after Q50, so that there may have been more widespread shallow outer-shelf between Q50 and P50. At lowstands, deltas from rivers draining Newfoundland would likely have discharged at the shelf edge, depositing slope channels and levees of the type seen on most temperate continental margins. The proportion of levee sedimentation to regional plume sedimentation was higher than in the section above Q50. Above Q50, there was some minor shelf-edge progradation as the result of deposition of glacial till, but below Q50 there may well have headward erosion of canyons, as seen in the section below Q50 in Laurentian Channel (MacLean and Wade, 1992). Such headward erosion may have led to incision of slope valleys and oversteepening of valley walls, leading to large blocky failures.

### ***3.3 Stress History***

The stress state for the sediments of the greater Laurentian Fan region range from underconsolidated to overconsolidated.

*Site 2006048 029*
At site 2006048029 the sediments below 400 cm appear to be underconsolidated. Two consolidation tests using different consolidation systems have OCR values < 0.5 indicating underconsolidation. High liquidity index ($L_i$) values of 2.5 and 2.1 also suggest underconsolidation. Profiles of the miniature shear vane (MV) undrained shear strength and the predicted shear strength values using Eq 1 and the SHANSEP method (Fig. 3.3.1) indicate that the sediment is over consolidated in the upper 200 cm. This overconsolidation in the upper 2 m in marine sediments is generally referred to as apparent overconsoldation. The SHANSEP *S*u values indicate the sediment is underconsolidated below 500 cm while the Mohr-Coulomb *S*u values indicate the sediment is underconsolidated below 300 cm.

*Site 2006048 030*
At site 2006048030 OCR values of 1.4 (315 cm) and 1.3 (460 cm) indicate the sediments are normally to slightly overconsolidated. $L_i$ values of 1.1 and 1.3 suggest the sediment at this depth is normally consolidated. MV and SHANSEP *S*u values (Fig. 3.3.2) indicate the sediment is overconsolidated for the entire core depth. The Eq 1 predicated *S*u indicate the sediment is normally to overconsolidated.

*Site 2006048 031*
At site 2006048031 an OCR value of 1.9 indicate the sediments are overconsolidated at a depth of 712 cm. A $L_i$ value of 1.87 indicates the sediment is underconsolidated. MV, Eq 1 and SHANSEP *S*u values (Fig. 3.3.3) indicate that the sediment is slightly underconsolidated to normally consolidated below an initial 2 meter zone of apparent overconsolidation.

*Site 2006048 036*
At site 2006048036 the sediments appear to be normally to slightly overconsolidated. An OCR value of 1.67 indicating overconsolidation was determined from a consolidation test of sediments at 248 cm. A liquidity index ($L_i$) value of 0.90 also suggests normally consolidated sediments. MV, Eq 1 and SHANSEP *S*u values (Fig. 3.3.4) indicate that the sediment is overconsolidated with the exceptions of

normally consolidated sediments from 160 to 200 cm and from 300 cm to the end of the core at 440 cm.

*Site 2006048 037*

At site 2006048037 the sediments appear to be slightly underconsolidated to overconsolidated. An OCR value of 0.87 and a $L_i$ value of 1.34 indicate the sediments are slightly underconsolidated at 306 cm. MV and SHANSEP *S*u values (Figure 5) indicate the sediment is overconsolidated for the upper 220 cm and then become normally to slightly underconsolidated until the end of the core at 480 cm.

## ***3.4 Strength***

The strength parameters of the sediments were determined from 3 CIU multi-stage triaxial tests from cores 2006048029 and 2006048030 taken on Halibut Slope. Only results from 2006048029 and 2006048031 were deemed applicable to the sediments recovered on the Laurentian Slope. The normalized strength in the normal consolidation stress range (i.e. consolidation pressure > $\sigma'_c$ ) was 0.40. The strength profiles that were calculated using the Mohr-Coulomb equation (Eq2) and the SHANSEP method yielded trends that were consistent with the MV data. The MV strength data increased with depth and the gradients calculated, excluding the upper 2 meters were were 1.8 kPa/m (2006048029), 3.7 kPa/m (2006048030), 2.2 kPa/m (2006048031) 5.2 kPa/m (2006048036), 5.02 kPa/m (2006048037) and 3.0 kPa/m (2006048038). The high gradients for 2006048 31 and 36 may be attributed the limited depth of recovery that ranged from 370 cm to 610 cm. Core 2006048031 (Halibut Slope) has a recovered depth of 900 cm and a Su/m gradient of 2.2 kPa/m. `

Figure 3.4.1. Geotechnical data from 2006048029pc.

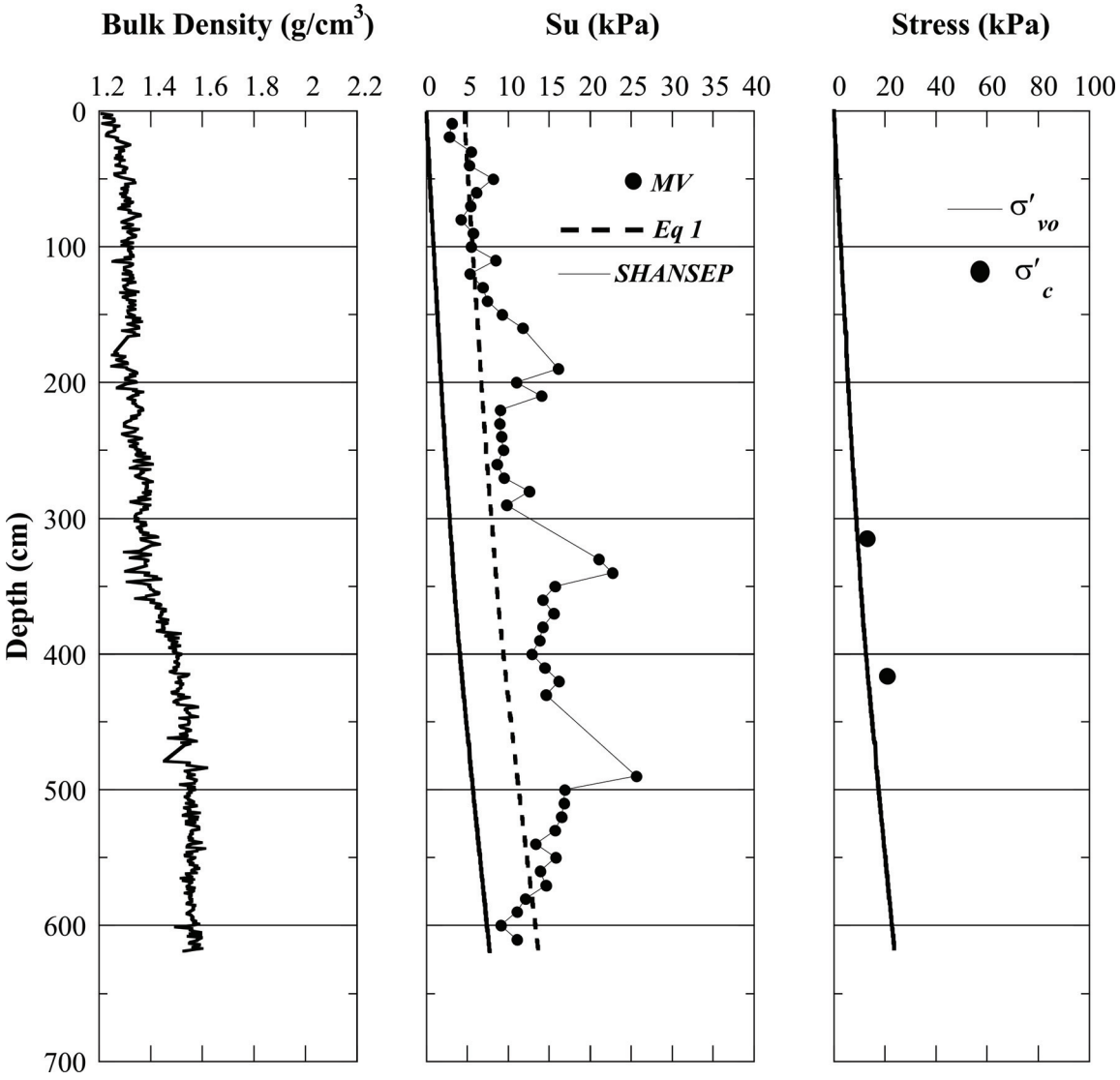


Figure 3.4.2. Geotechnical data from 2006048030frc.

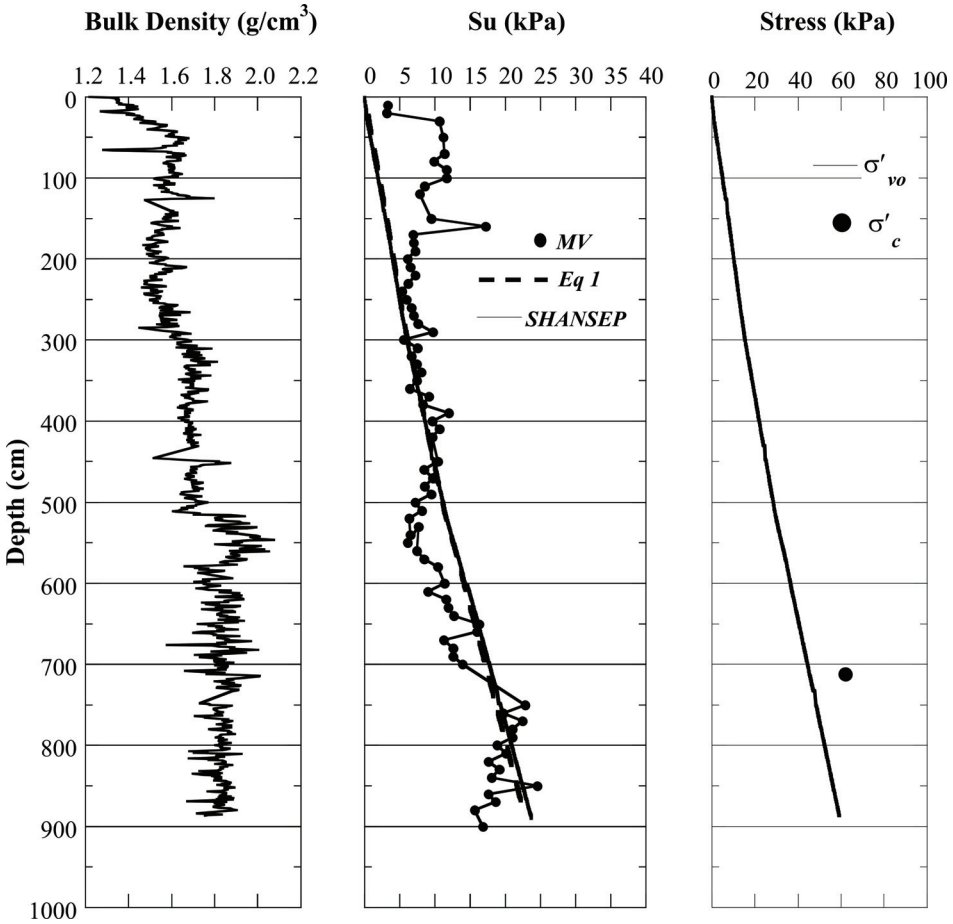


Figure 3.4.3. Geotechnical data from 2006048031pc.

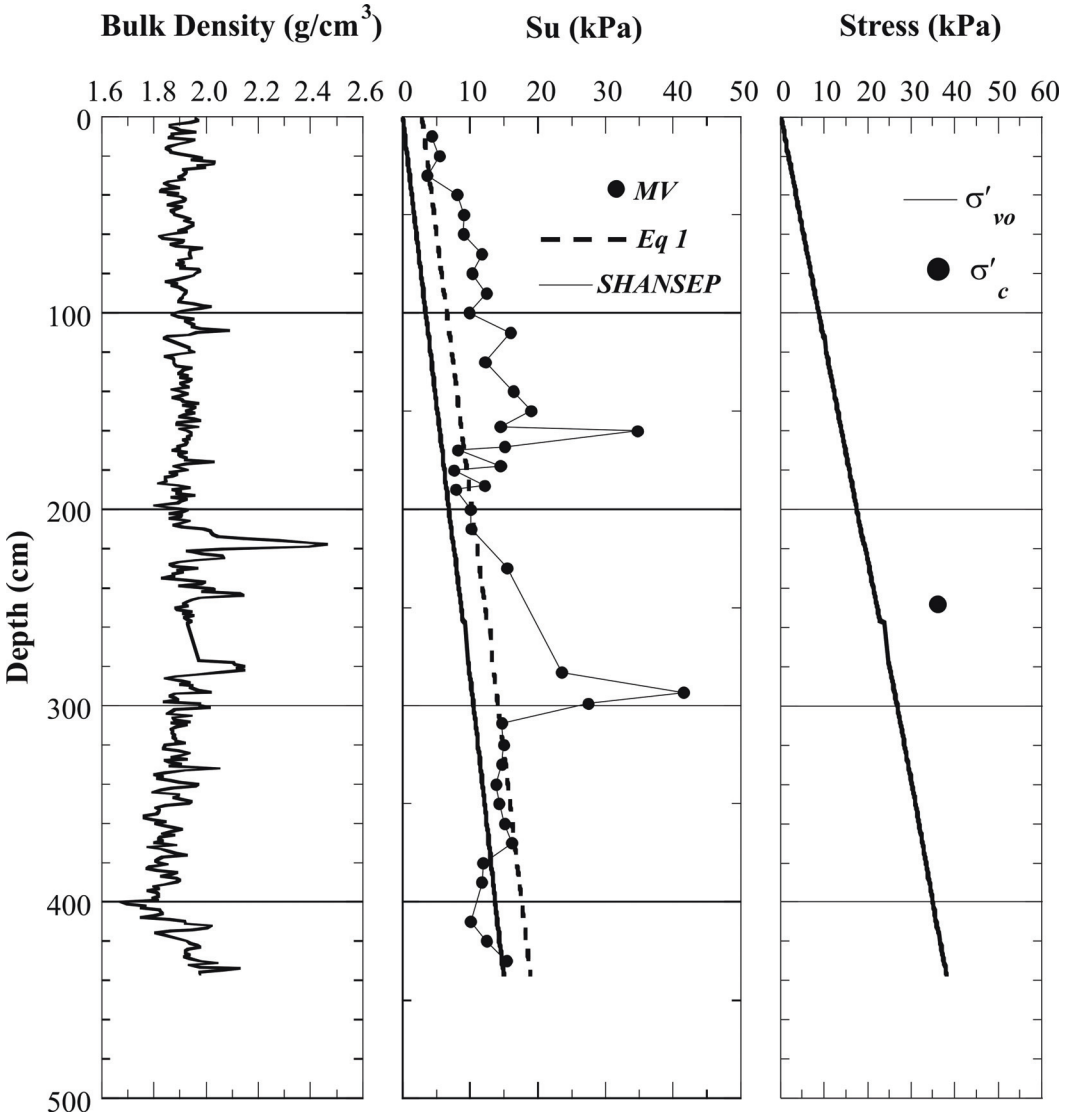


**Figure 3.4.4. Geotechnical data from 2006048036pc.**

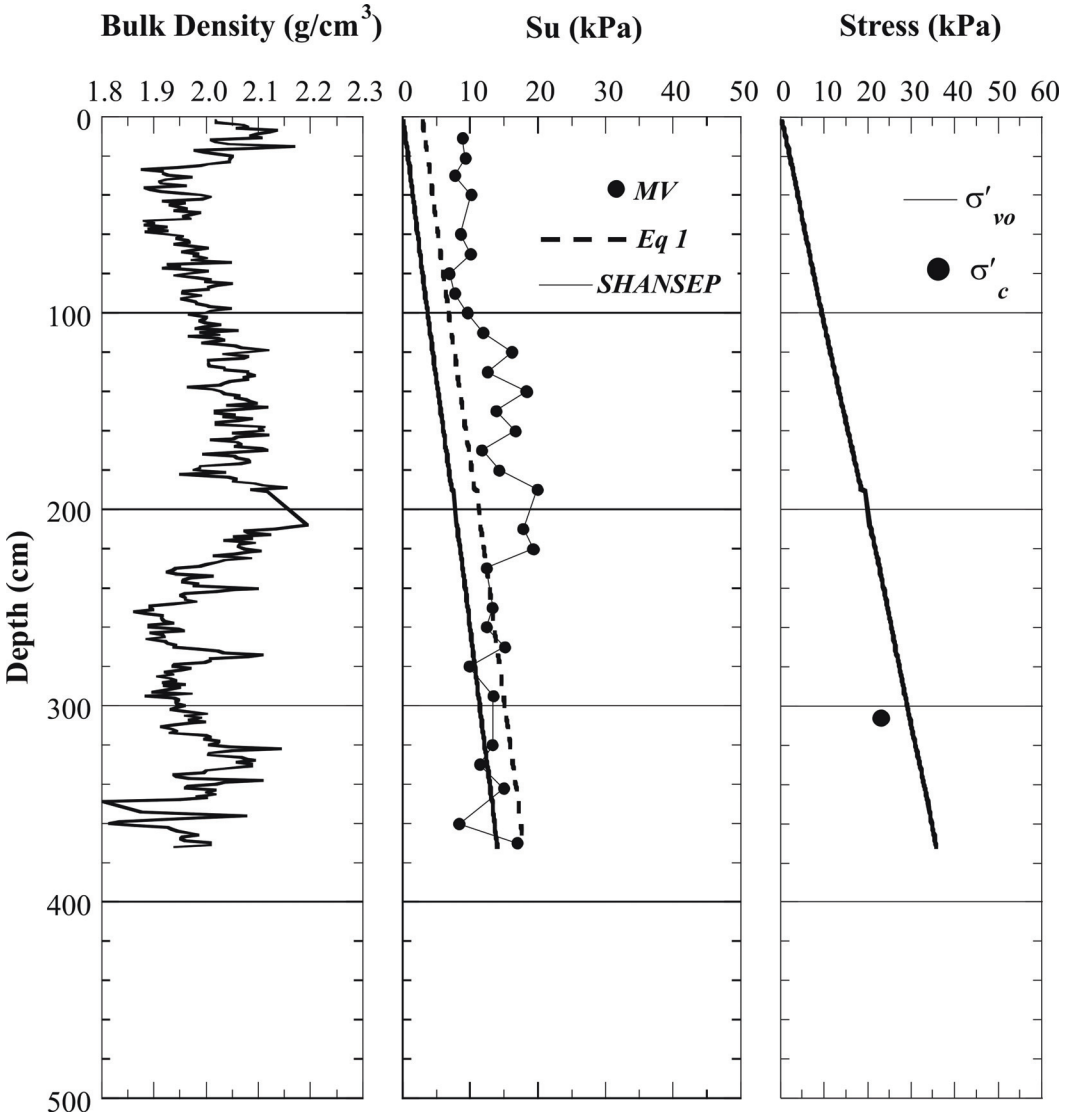


**Figure 3.4.5. Geotechnical data from 2006048037pc.**

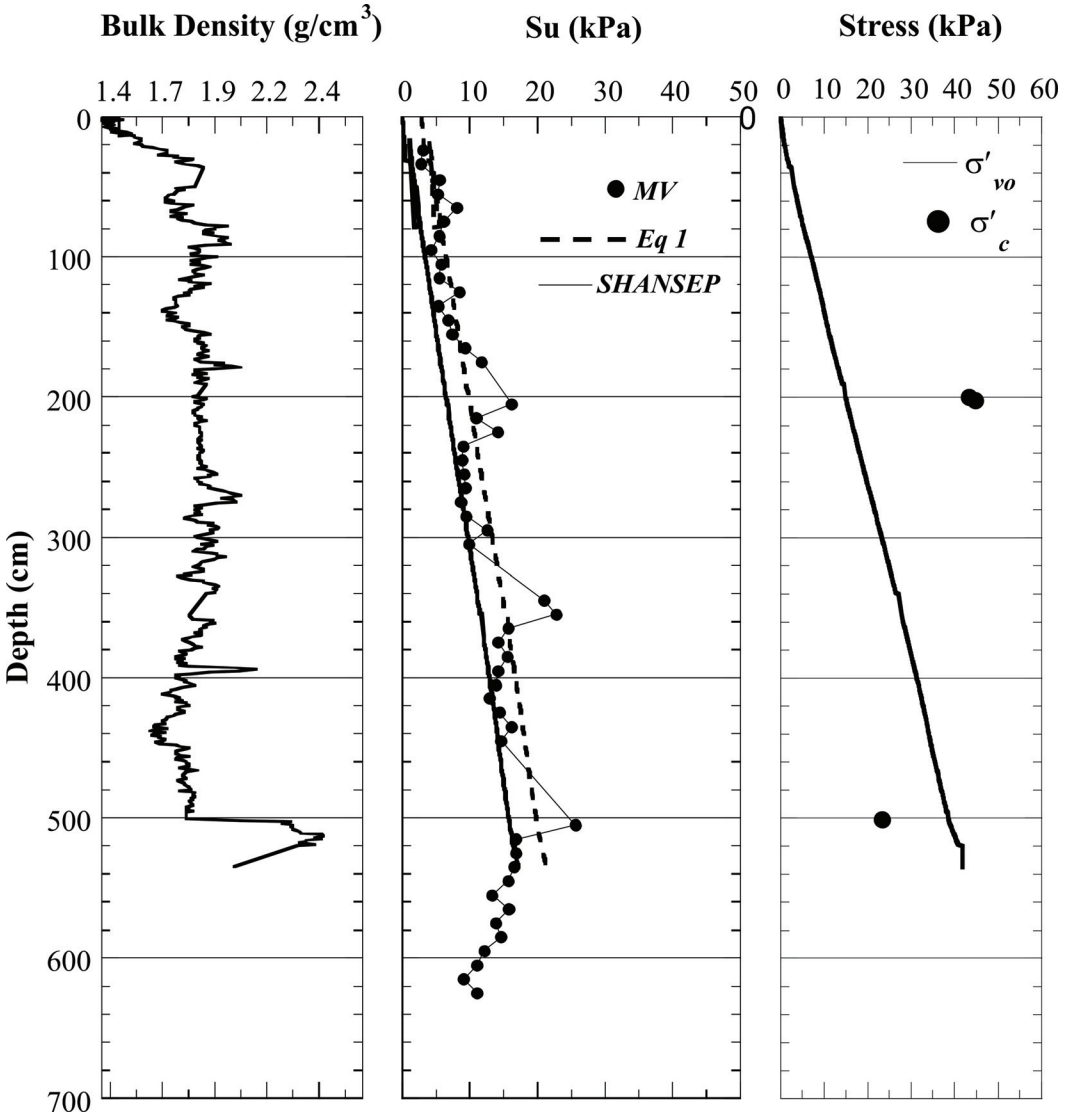


**Figure 3.4.6. Geotechnical data from 2006048038pc.**

## *3.5 Seismic Refraction/wide-angle reflection*

Ocean bottom seismometer experiments were conducted on the St. Pierre Slope and Halibut Channel Slopes (Fig. 3.5.1), in order to derive the shallow velocity structure in these regions. For the St. Pierre Slope, the intent was to investigate the unfailed stratigraphy above the uppermost failure scarp to quantify pre-failure soil conditions. For the Halibut Channel Slope region, the intention was to examine the velocity structure associated with a bottom simulating reflector (BSR) in the area as well as the velocity structure associated with shallow salt diapirs. Interval velocity profiles are shown in Figure 3.5.2. 3-component geophone data also show converted P-S wave signals, from which it is possible to derive shear velocities (Fig. 3.5.3). Shear velocity is particularly sensitive to the sediment's state of consolidation and a good indicator of liquefaction potential.

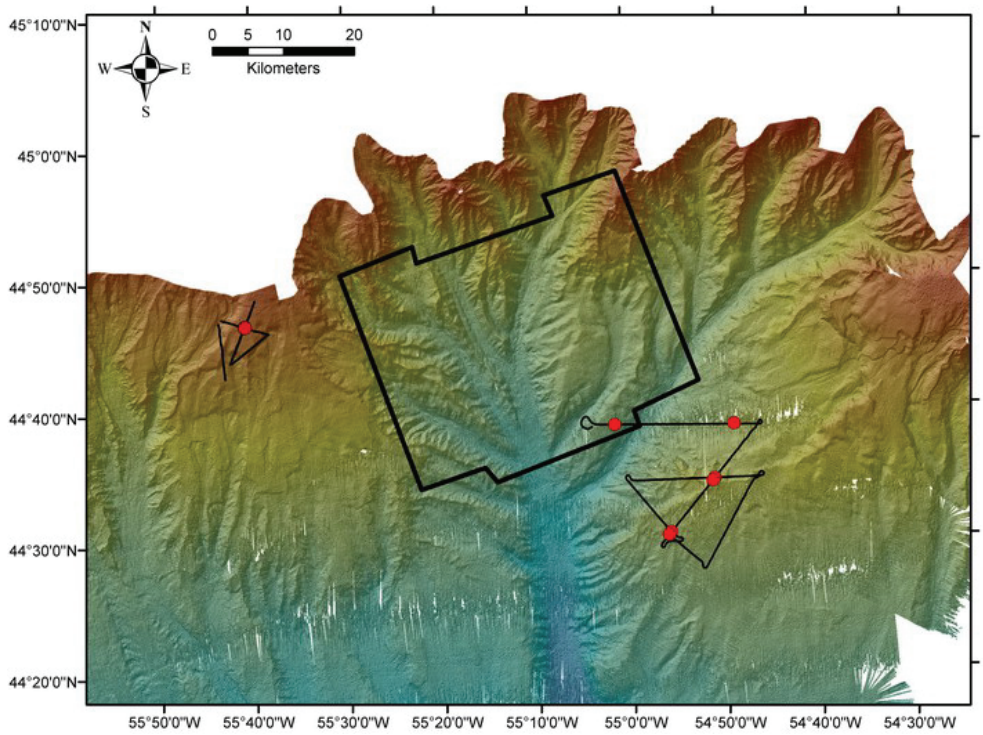


*Figure 3.5.1. Location of ocean bottom seismometer deployments (red dots) and associated seismic track lines. Location of the Laurentian East 3D volume is shown by the black polygon.*

**P-Wave**

Compressional (P) wave velocity results from the various OBS deployments are provided in Figures 3.5.2 and the data comprising these figures is presented in Tables 3.5.1 to 3.5.3. Very shallow (<10 m depth) velocities were made from discrete measurements within cores. These typically show velocities ranging from 1450 to 1600 m/s and show a strong correlation to lithologic change. OBS results show interval velocities over much greater scale. Both sites demonstrate expected velocity increase with depth. By 1000 m below seafloor, velocities are on the order of 2200 m/s. Haddock Channel data show a velocity reversal at 400 to 450 m below seafloor, representing the base of the gas hydrate

stability zone and the presence of free gas trapped beneath hydrate (i.e. the cause of the BSR). No velocity increase is recognized within the hydrate stability zone, suggesting low concentrations of hydrate. Beneath the free gas, velocities resume normal gradients.

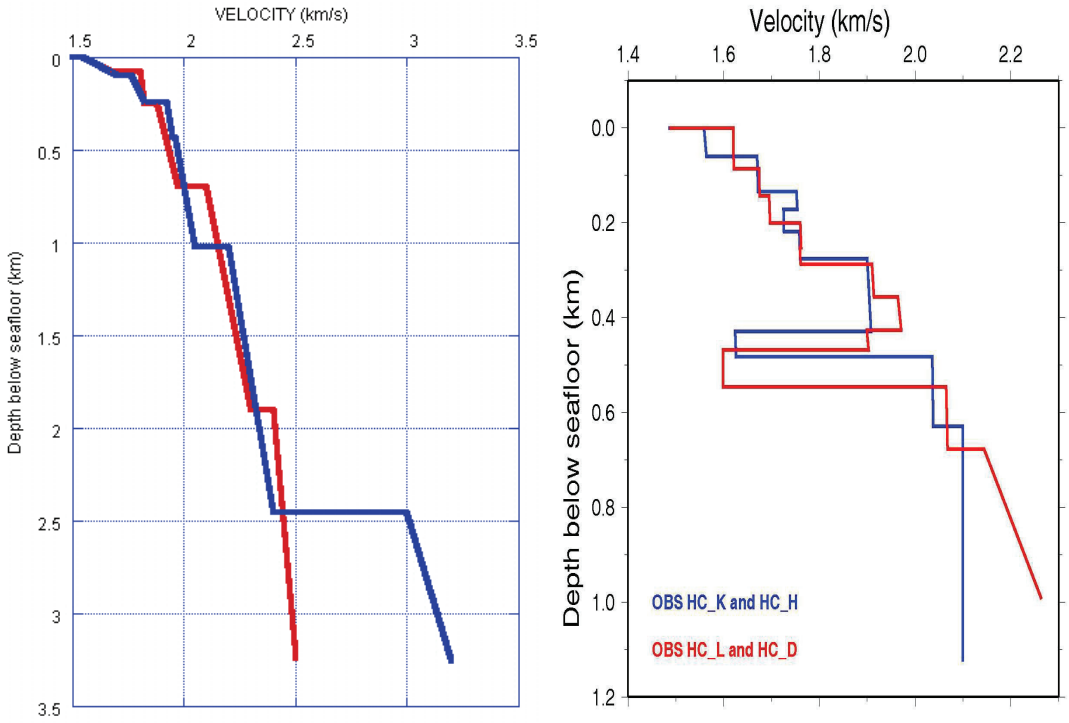


*Figure 3.5.2. Ocean Bottom Seismometer P-wave velocity results from the St. Pierre Slope (left) and Halibut Channel (right). Note the velocity inversion between 0.4 and 0.6 km depth on the Halibut Channel results. This inversion occurs at the depth of the BSR; a result of free gas trapped beneath gas hydrate.*

For long-offset, the velocity depth results are shown in Figure 3.5.3 and Table 3.5.2. These data indicate a velocity increase of up to 5500 m/s by 14 km depth. They also show high velocity anomalies associated with a salt canopy.

**S-Wave**

P to S converted waves are apparent on OBS data, particularly on the horizontal geophone component. Attempts were made, therefore, to derive S-wave velocities as these can be a particular strong indicator of the geotechnical state of the soil. The velocity modeling assumes that a conversion from down-going P-wave (generated by the GI-gun source) to up-going S-wave recorded at the OBS takes place at the seafloor reflection boundary (see Louden and LeBlanc, 2006 for analyses).

The final P-wave velocity model from the 1-D inversion was left unchanged from the

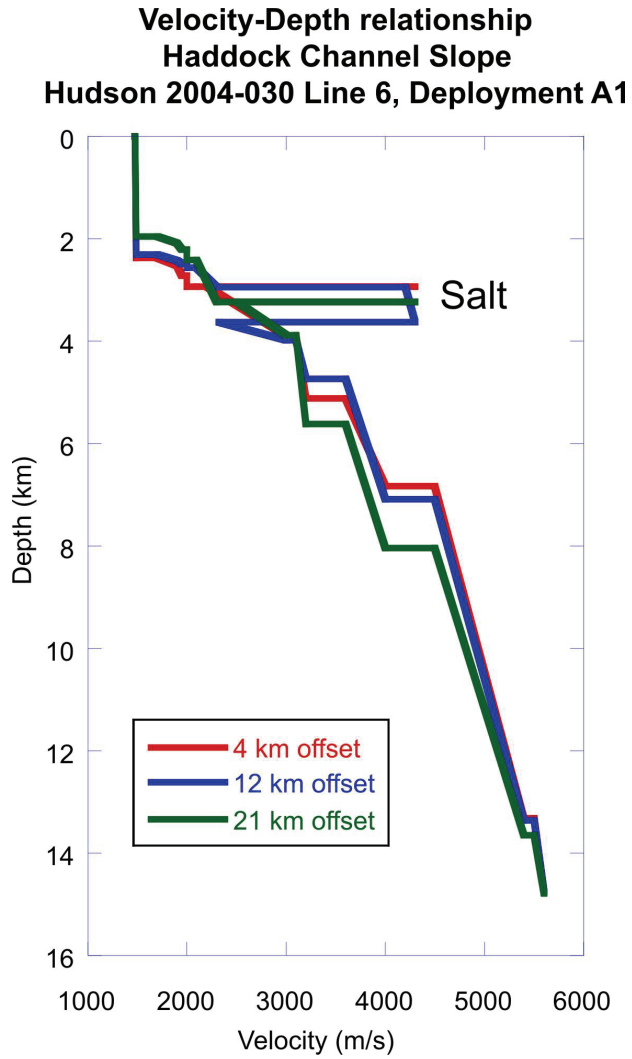


*Figure 3.5.3 Long offset velocity models from OBS refraction data over a salt canopy in the Haddock Channel area of the SW Slope of the Grand Banks.*

forward modeling of P-S converted waves, and only the Poisson's ratio of each layer was modified. This analysis is still quite immature, but the fit of the calculated to observed phases is excellent (Fig. 3.5.4) and the resulting Poisson's ratios are reasonable. However, if the P-wave velocities are incorrect this would also affect the Poisson's ratio and resulting S-wave velocity estimates.

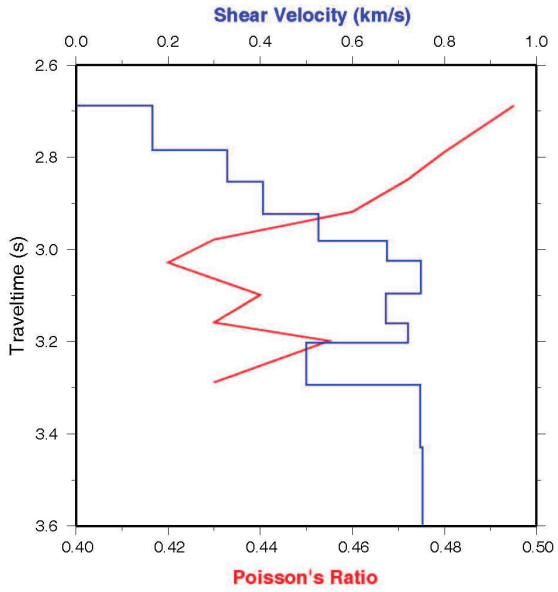


*Figure 3.5.4. Shear wave velocity results and associated Poisson's Ratio, derived from OBS P-S converted waves from the Halibut Channel deployment (2004-030).*

| Depth (km) | Velocity (km/s) | Depth (km) | Velocity (km/s) |
|---|---|---|---|
| 0.000 | 1.485 | 0.000 | 1.487 |
| 1.875 | 1.485 | 2.007 | 1.487 |
| 1.875 | 1.559 | 2.007 | 1.620 |
| 1.935 | 1.564 | 2.093 | 1.621 |
| 1.935 | 1.670 | 2.093 | 1.674 |
| 2.009 | 1.672 | 2.151 | 1.675 |
| 2.009 | 1.752 | 2.151 | 1.695 |
| 2.047 | 1.754 | 2.207 | 1.697 |
| 2.047 | 1.725 | 2.207 | 1.760 |
| 2.093 | 1.726 | 2.259 | 1.762 |
| 2.093 | 1.758 | 2.259 | 1.759 |
| 2.151 | 1.760 | 2.295 | 1.761 |
| 2.151 | 1.900 | 2.295 | 1.910 |
| 2.304 | 1.908 | 2.364 | 1.914 |
| 2.304 | 1.624 | 2.364 | 1.964 |
| 2.358 | 1.626 | 2.433 | 1.971 |
| 2.358 | 2.036 | 2.433 | 1.899 |
| 2.505 | 2.038 | 2.475 | 1.903 |
| 2.505 | 2.100 | 2.475 | 1.599 |
| 3.000 | 2.100 | 2.553 | 1.599 |
| | | 2.553 | 2.065 |
| | | 2.684 | 2.068 |
| | | 2.684 | 2.144 |
| | | 3.000 | 2.264 |
| | | | |

*Table 3.5.1 Velocity depth relationship for Haddock Channel Slope, OBS' L and K (see Louden and LeBlanc, 2006). See Figure 2.3.1 for locations of OBS'.*

| Depth (km) | Velocity (km/s) | Depth (km) | Velocity (km/s) |
|---|---|---|---|
| 0.000 | 1.490 | 0.000 | 1.490 |
| 0.719 | 1.500 | 0.733 | 1.500 |
| 0.719 | 1.550 | 0.733 | 1.550 |
| 0.817 | 1.700 | 0.809 | 1.670 |
| 0.817 | 1.762 | 0.809 | 1.800 |
| 0.962 | 1.820 | 0.986 | 1.820 |
| 0.962 | 1.920 | 0.986 | 1.880 |
| 1.152 | 1.950 | 1.431 | 1.970 |
| 1.152 | 1.960 | 1.431 | 2.100 |
| 1.745 | 2.050 | 2.633 | 2.300 |
| 1.745 | 2.200 | 2.633 | 2.400 |
| 3.175 | 2.400 | 3.976 | 2.500 |
| 3.175 | 3.000 | | |
| 3.977 | 3.200 | | |

*Table 3.5.2 Velocity depth relationship for St. Pierre Slope, Lines Hudsonc 2007020-007/11 and 009 (see Chian, 2008). See Figure 2.3.1 for location of the OBS deployment.*

| Depth (km) | Velocity (km/s) | Deph (km) | Velocity (km/s) | Depth (km) | velocity (km/s) |
|---|---|---|---|---|---|
| 0.0000 | 1.4700 | 0.0000 | 1.4700 | 0.0000 | 1.4700 |
| 0.013000 | 1.4800 | 0.013000 | 1.4800 | 0.013000 | 1.4800 |
| 0.013000 | 1.4800 | 0.013000 | 1.4800 | 0.013000 | 1.4800 |
| 2.3740 | 1.4900 | 2.3110 | 1.4900 | 1.9540 | 1.4900 |
| 2.3740 | 1.7000 | 2.3110 | 1.7000 | 1.9540 | 1.7000 |
| 2.5210 | 1.9000 | 2.4250 | 1.9000 | 2.0820 | 1.9000 |
| 2.5210 | 1.9000 | 2.4250 | 1.9000 | 2.0820 | 1.9000 |
| 2.7280 | 1.9500 | 2.4870 | 1.9500 | 2.2140 | 1.9500 |
| 2.7280 | 2.0000 | 2.4870 | 2.0000 | 2.2140 | 2.0000 |
| 2.9400 | 2.0000 | 2.5620 | 2.0000 | 2.4200 | 2.0000 |
| 2.9400 | 2.1000 | 2.5620 | 2.1000 | 2.4200 | 2.1000 |
| 2.9400 | 2.3000 | 2.9490 | 2.3000 | 3.2300 | 2.3000 |
| 2.9400 | 4.2000 | 2.9490 | 4.2000 | 3.2300 | 4.2000 |
| 2.9400 | 4.3000 | 3.6330 | 4.3000 | 3.2300 | 4.3000 |
| 2.9400 | 2.2000 | 3.6330 | 2.3230 | 3.2300 | 2.5000 |
| 3.8930 | 3.0000 | 3.9830 | 3.0000 | 3.8870 | 3.0000 |
| 3.8930 | 3.1000 | 3.9830 | 3.1000 | 3.8870 | 3.1000 |
| 5.1170 | 3.2000 | 4.7370 | 3.2000 | 5.6200 | 3.2000 |
| 5.1170 | 3.6000 | 4.7370 | 3.6000 | 5.6200 | 3.6000 |
| 6.8300 | 4.0000 | 7.0820 | 4.0000 | 8.0430 | 4.0000 |
| 6.8300 | 4.5000 | 7.0820 | 4.5000 | 8.0430 | 4.5000 |
| 13.320 | 5.4000 | 13.360 | 5.4000 | 13.651 | 5.4000 |
| 13.320 | 5.5000 | 13.360 | 5.5000 | 13.651 | 5.5000 |
| 14.769 | 5.6000 | 14.767 | 5.6000 | 14.783 | 5.6000 |
| | | | | | |

*Table 3.5.3 Velocity depth relationship for Haddock Channel Slope at 4, 12 and 21 km offset (see Chian, 2005). See Figure 2.3.1 for location of the OBS deployment.*

# 4 References


Adams J. and Halchuk S., 2003. Fourth generation seismic hazard maps of Canada: Values for over 650 Canadian localities intended for the 2005 National Building Code of Canada. Geological Survey of Canada Open File 4459: 1-155.

Becker D.E. et al. 1987. Work as a criterion for determining *in situ* and yield stresses in clays. Canadian Geotechnical Journal. Vol. 24, p.549-564.

Brake, V., 2009. Evolution of an Oligocene Canyon System on the Eastern Scotian Slope. Unpublished MSc thesis, Dept. Earth Sciences, Dalhousie University, Halifax, Nova Scotia, 139 pp.

Brake, V., Mosher, D.C., and Wach, G., 2008a. Oligocene canyon and fan development: the respective roles of sea level and sediment delivery in evolution of the eastern Scotian margin. Extended

Abstract, Proceedings of the Canadian Society of Petroleum Geologists joint annual convention, May 12-15, 2008, Calgary, Alta.

Brake, V., Mosher, D., and Wach, G. 2008b. Oligocene canyon development: Implications for sediment delivery on the eastern Scotian Margin. In: (Brown, D. and Watson, N., eds) Extended Abstract Proceedings and POSTER, Central Atlantic Conjugate Margins Conference, Halifax, Nova Scotia, August 13-15, 2008, p. 366-370.

Chian, D. 2007. Final Report for Hud2007020 Ocean bottom seismomenter data analysis. Unpublished contract report to D.C. Mosher, Natural Resources Canada, Geological Survey of Canada – Atlantic, Dartmouth, NS. Public Works and Government Services Canada Contract No HAL-7-50545(217).

Deptuck, M.E., 2003. Post-rift geology of the Jeanne d'Arc Basin, with a focus on the architecture and evolution of early Paleogene submarine fans, and insights from modern deep-water systems. Ph.D. thesis, Dalhousie University.

Dyke, A.S. and Prest, V.K., 1987. Late Wisconsinan and Holocene history of the Laurentide ice sheet. Géographie physique et Quaternaire, v. 41, p. 237-263.

Giosan, L., Flood, R.D., Gruetzner, J. and Mudie, P.J., 2002. Paleoceanographic significance of sediment color on western North Atlantic drifts; II, Late Pliocene-Pleistocene sedimentation. Marine Geology, v. 189, p. 43-61.

Gradstein, F M; Jansa, L F; Srivastava, S P; Williamson, M A; Bonham Carter, G; Stam, B; 1990. Chapter 8: Aspects of North Atlantic Paleo- Oceanography. in, Geology of the Continental Margin of Eastern Canada; Keen, M J (ed.); Williams, G L (ed.); Geological Survey of Canada, Geology of Canada Series no. 2, 1990; pages 351-389

Grant, D.R., 1989. Chapter 5: Quaternary Geology of the Atlantic Appalachian Region of Canada. in, Quaternary Geology of Canada and Greenland; Fulton, R J (ed.); Geological Survey of Canada, Geology of Canada Series no. 1, 1989; pages 393-433.

Hinz, K., Schluter, H.-U., Grant, A.C., Srivastava, S.P., Umpleby, D. and Woodside, J. 1979. Geophysical transects of the Labrador Sea. Labrador to southwest Greenland. Tectonophysics, v. 59, p. 151-184.

Holtz, R.D. and Kovacs, W.D., 1981. An Introduction to Geotechnical Engineering. Prentice-Hall, Inc., Englewood Cliffs, N.J. pp.294-299

Hughes Clarke, J.E., 1990, Late stage slope failure in the wake of the 1929 Grand Banks earthquake. Geo-Marine Letters, v. 10, p. 69-80.

Hughes Clarke, J.E., Shor, A.N., Piper, D.J.W. and Mayer, L.A. 1990. Large-scale current-induced erosion and deposition in the path of the 1929 Grand Banks turbidity current. Sedimentology, 37, p. 613-629.

Jenner, K.A., Piper, D.J.W., Campbell, D.C. and Mosher, D.C., 2006. Lithofacies and origin of late Quaternary mass transport deposits in submarine canyons, central Scotian Slope, Canada. Sedimentology, v. 53., 20 pp.

Ledger-Piercey, S. and Piper, D.J.W., 2007. Late Quaternary geological history of the SW Grand Banks Slope and Rise off Green Bank and Whale Bank: implications for geohazard assessment. Geological Survey of Canada, Open File 5663, 84 pp.

Louden, K.E. and LeBlanc, C., 2006. Ocean bottom seismometer wide angle reflection and refraction processing for gas hydrate characterization. Unpublished contract report to D.C. Mosher, Natural Resources Canada, Geological Survey of Canada, Atlantic, Dartmouth, Nova Scotia. Public Works and Government Services Canada Contract No 23420-050956/001/HAL, 36 pp.

MacDonald, A.W.A., 2006. Cenozoic seismic stratigraphy of the central Nova Scotian continental margin: the interplay of erosion, deposition and salt tectonics. M.Sc. thesis, Saint Mary's University, 152 p.

MacLean, B.C. and Wade, J.A. 1992. Petroleum geology of the continental margin south of the islands of St Pierre and Miquelon, offshore eastern Canada. Bulletin of Canadian Petroleum Geology, v. 40, p. 222-253.

Mazzotti, S., and Adams, J., 2005, Rates and uncertainties on seismic moment and deformation in eastern Canada: Journal of Geophysical Research, v. 110, B09301, doi:10.1029/2004JB003510, 16 p.

McCall, C.W. 2006. A geological and geophysical study of the 1929 Grand Banks slide. M.Sc. thesis, Saint Mary's University, 230 p.

Miller, A. A. L. Fader, G. B. J., and Moran, K., 2001. Late Wisconsinan ice advances, ice extent, and glacial regimes interpreted from seismic data, sediment physical properties, and Foraminifera: Halibut Channel, Grand Banks of Newfoundland. Special Papers, Geological Society of America, Special Paper 351, 51-108.

Mosher, D.C., 2005. Hudson 2004-030, Cruise Report. July 10-20. GSC Open File 4824., 68 pp.

Mosher, D.C., Bigg, S. and LaPierre, A. 2006. 3D seismic versus multibeam sonar seafloor surface renderings for geohazard assessment: Case examples from the central Scotian Slope. The Leading Edge, V. 25, p. 1484-1494.

Mosher, D.C., and Piper, D.J.W., 2007a. Analysis of multibeam seafloor imagery of the Laurentian Fan and the 1929 Grand Banks landslide area. In: Lykousis, V., Dimitris, S., and Locat, J. (eds), Submarine Mass Movements and Their Consequences, III. Springer, The Netherlands, p. 77-88.

Mosher, D.C. and Piper, D.J.W., 2007b. Multibeam seafloor imagery of the Laurentian Fan and the 1929 Grand Banks Landslide Area. GSC Open File 5638. POSTER.

Mosher, D.C., Piper, D.J.W. , Campbell, D.C. and Jenner, K. 2004. Near surface geology and sediment-failure geohazards of the central Scotian Slope. American Association of Petroleum Geologists Bulletin, v. 88, p. 703-723.

Mosher, D.C., Piper, D.J.W., Vilks, G., Aksu, A.E., and Fader, G.B., 1989. Evidence for Wisconsinan glaciations in the Verrill Canyon area, Scotian Slope. Quaternary Research, 31: 27-40.

Mosher, D.C. and West, M.T.N., 2007. CCGS Hudson 2007020 Cruise Report: Laurentian Fan and eastern Scotian Slope, Argentia to Halifax; Geological Survey of Canada, Open File 5668, 1 DVD.

Mulder, T., Berry, J.A. and Piper, D.J.W., 1997. Links between geomorphology and geotechnical characteristics of large debris flow deposits in the Albatross area on the Scotian slope (E. Canada). Marine Georesources and Geotechnology, v. 15, p. 253-281.

Pacheco Silva, F. 1970. A new graphical construction for determination of the pre- consolidation stress of a soil sample. *In* Proceedings of the 4th Brazilian Conference on Soil Mechanics and Foundation Engineering, Rio de Janeiro, Brazil. Vol. 2, p. 225–232.

Piper, D.J.W.,1988. Glaciomarine sediments on the continental slope off eastern Canada. Geoscience Canada, Vol. 15, p. 23-28.

Piper, D.J.W., 2005. Late Cenozoic evolution of the continental margin of eastern Canada. Norwegian Journal of Geology vol. 85, p. 231-244

Piper, D.J.W. and Brunt, R.A., 2006. High-resolution seismic transects of the upper continental slope off southeastern Canada. Geological Survey of Canada, Open File 5310, 77 pp.

Piper, D.J.W. and Campbell, D.C., 2005. Quaternary geology of Flemish Pass and its application to geohazard evaluation for hydrocarbon development. in, Petroleum resources and reservoirs of the Grand Banks, eastern Canadian margin; Hiscott, R.N. and Pulham, A.J. (eds.), Geological Association of Canada, Special Paper 43, p. 29-43.

Piper, D.J.W. and Gould, K. 2004. Late Quaternary geological history of the continental slope, South Whale Basin, and implications for hydrocarbon development. Current Research 2004-D1, 13 pp.

Piper, D.J.W. and Ingram, S., 2003. Major Quaternary sediment failures on the east Scotian Rise, eastern Canada. Geological Survey of Canada, Current Research, no. 2003-D1, 7 p.

Piper, D.J.W. and King, E.L. 2006. Cruise report Hudson 2006048: Geoscience constraints to offshore development off Newfoundland. Unpublished cruise report, Geological Survey of Canada – Atlantic, Dartmouth, NS. 58 pp.

Piper, D.J.W. and MacDonald, A., 2002. Timing and position of late Wisconsinan ice-margins on the upper slope seaward of Laurentian Channel. Geographie Physique et Quaternaire, 55, p. 131-140.

Piper, D.J.W., MacDonald, A.W.A., Ingram, S., Williams, G.L. and McCall, C., 2005. Late Cenozoic architecture of the St Pierre Slope. Canadian Journal of Earth Sciences, v. 42, p. 1987-2000

Piper, D.J.W., Mosher, D.C., and Newton, S., 2002. Ice-margin seismic stratigraphy of the central Scotian Slope eastern Canada, Geological Survey of Canada Current Research, 2002-E16, 10 pp.

Piper, D.J.W., Mudie, P.J., Aksu, A.E. and Skene, K.I., 1994. A 1 Ma record of sediment flux south of the Grand Banks used to infer the development of glaciation in southeastern Canada. Quaternary Science Reviews vol. 13, p. 23-37.

Piper, D.J.W. and Normark, W.R., 1989. Late Cenozoic sea-level changes and the onset of glaciation: impact on continental slope progradation off eastern Canada. Marine and Petroleum Geology, Vol. 6, p. 336-347.

Piper, D.J.W., Shaw, J. and Skene, K.I., 2007. Stratigraphic and sedimentological evidence for late Wisconsinan sub-glacial outburst floors to Laurentian Fan. Palaeogeography, Palaeoclimatorlogy, Palaeoecology, Vol. 246, p. 101-119, doi: 10.1016/ j.palaeo.2006.10.029.

Piper, D.J.W., MacDonald, A.W.A., Ingram, S., Williams, G.L. and McCall, C., 2005. Late Cenozoic architecture of the St Pierre Slope. Canadian Journal of Earth Sciences, v. 42, p. 1987-2000.

Piper, D.J.W., Shaw, J. and Skene, K.I. 2007. Stratigraphic and sedimentological evidence for late Wisconsinan sub-glacial outburst floods to Laurentian Fan. Palaeogeog. Palaeoclim. Palaeoecol., 246, 101-119.

Roberts J.A and Cramp, A.,1996. Sediment stability on the western Flaks of the Canary Islands, Marine Geology, v. 134, pp. 13-30.

Shaw, J., Piper, D.J.W., Fader, G.B., King, E.L., Todd, B.J., Bell, T., Batterson, M.J., and Liverman, D.J.E., 2006. A conceptual model of the deglaciation of Atlantic Canada. Quaternary Science Reviews, Vol. 25, p. 2055-2081.

Shor, A.N., Piper, D.J.W., Hughes Clarke, J.E., and Mayer, L.A., 1990. Giant flute - like scour and other erosional features formed by the 1929 Grand Banks Turbidity Current. Sedimentology, Vol. 37, p. 631-645.

Skempton, A.W., 1970. The consolidation of clays by gravitational compaction. Quarterly Journal of the Geological Society of London, Vol. 125, p. 373-411.

Skene, K.I. and Piper, D.J.W. 2003, Late Quaternary stratigraphy of Laurentian Fan: a record of events off the eastern Canadian continental margin during the last deglacial period; Quaternary International, Vol. 99-100, p. 135-152.

Skene, K.I. and Piper, D.J.W., 2006. Late Cenozoic evolution of Laurentian Fan: development of a glacially-fed submarine fan, Marine Geology, vol. 227, p.67-92.

Sonnichsen, G.V. and King, E.L. 2005. Grand Bank seabed and shallow subsurface geology in relation to subsea engineering design. in, Petroleum resources and reservoirs of the Grand Banks, eastern Canadian margin. Hiscott, R.N. and Pulham, A.J. (eds.); Geological Association of Canada, Special Paper 43, pp. 11-27

Stow, D.A.V., 1981. Laurentian Fan: Morphology, sediments, processes and growth pattern. American Association of Petroleum Geologists Bulletin, Vol. 65, p. 375-393.

Tripsanas, E.K. and Piper, D.J.W., 2008. Late Quaternary stratigraphy and sedimentology of Orphan Basin: implications for meltwater dispersal in the southern Labrador Sea. Palaeogeography, Palaeoclimatology, Palaeoecology, v. 260, p. 521–539.

Tripsanas, E.K. and Piper, D.J.W., 2008. Glaciogenic debris-flow deposits of Orphan Basin, offshore eastern Canada: Sedimentological and rheological properties, origin, and relationship to meltwater discharge. Journal of Sedimentary Research vol. 78, pp. 724-744.

Tripsanas, E.K., Piper, D.J.W. and Jarrett, K.A. 2007. Logs of piston cores and interpreted ultra-high-resolution seismic profiles, Orphan Basin Geological Survey of Canada, Open File 5299, 2007; 339 pages 1 DVD

Uchupi, E. and Austin, J.A.Jr., 1979. The stratigraphy and structure of the Laurentian Cone region. Canadian Journal of Earth Sciences, Vol. 16, p.1726-1752.

Wade, J.A., MacLean, B.C. and Williams, G L., 1995. Mesozoic and Cenozoic stratigraphy, eastern Scotian Shelf: new interpretations. Canadian Journal of Earth Sciences vol 32, pp.1462-1473

Wielens, H., Jauer, C. and Williams, G.L., 2004. Data synthesis for the Carson Basin, offshore Newfoundland: results of 4-D petroleum system modeling. Geological Survey of Canada, Open File 4739, 1 sheet 1 CD-ROM

# APPENDIX A Consolidation Test Results

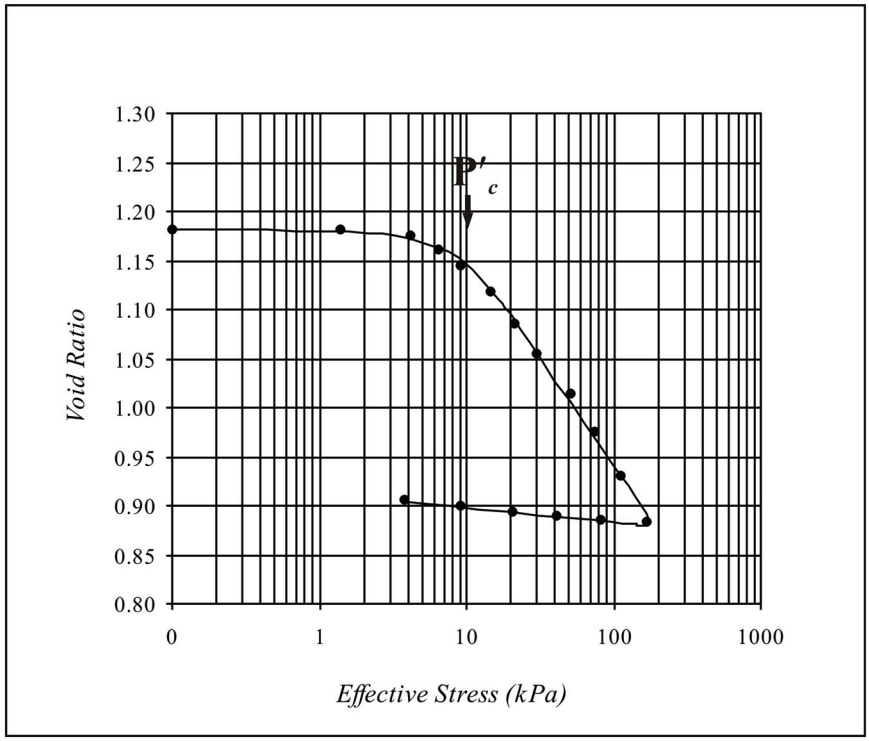


**Consolidation plot (e-log p') for sample 2006048 029pc (463 cm).**

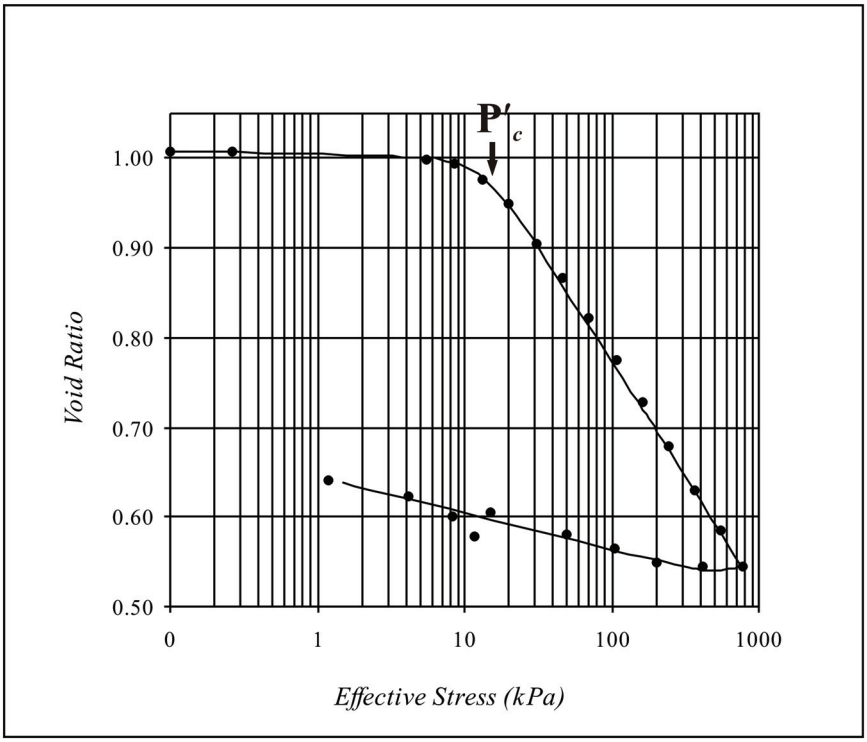


**Consolidation plot (e-log p') for sample 2006048 029pc (474 cm).**

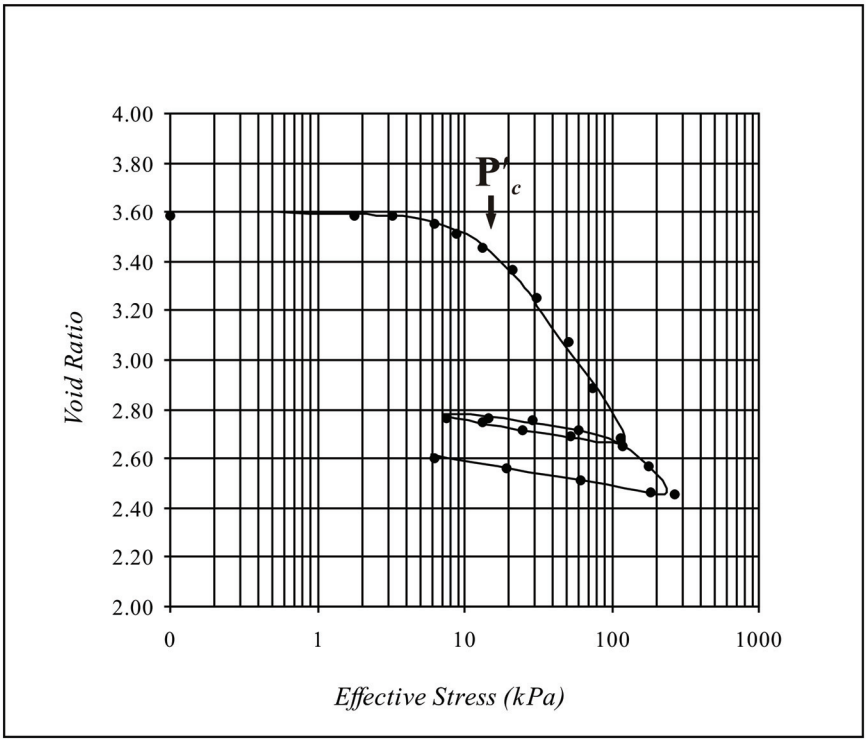


**Consolidation plot (e-log p') for sample 2006048 030frc (315 cm).**

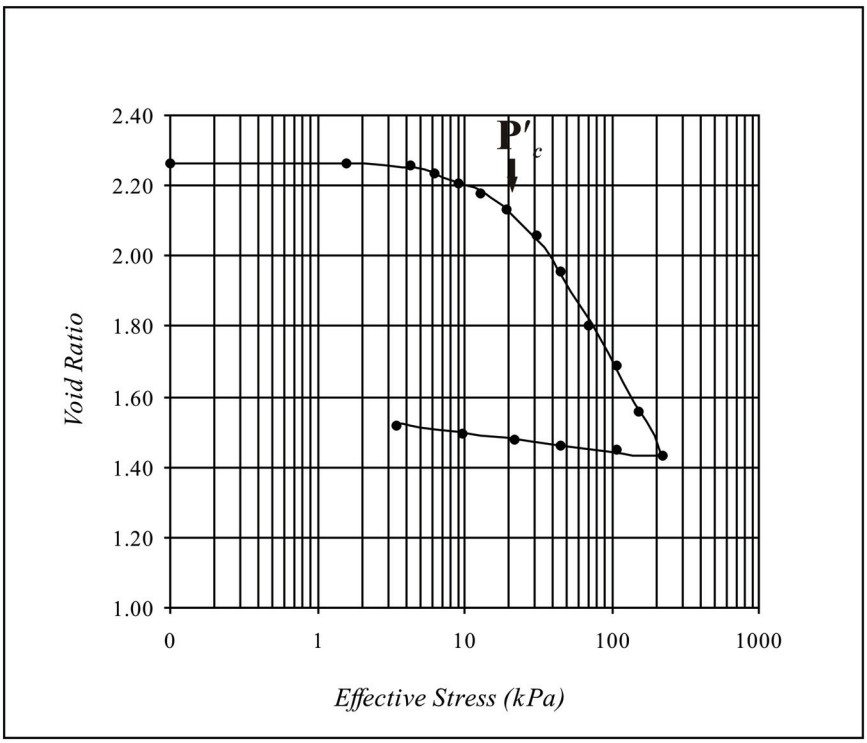


**Consolidation plot (e-log p') for sample 2006048 030frc (460 cm).**

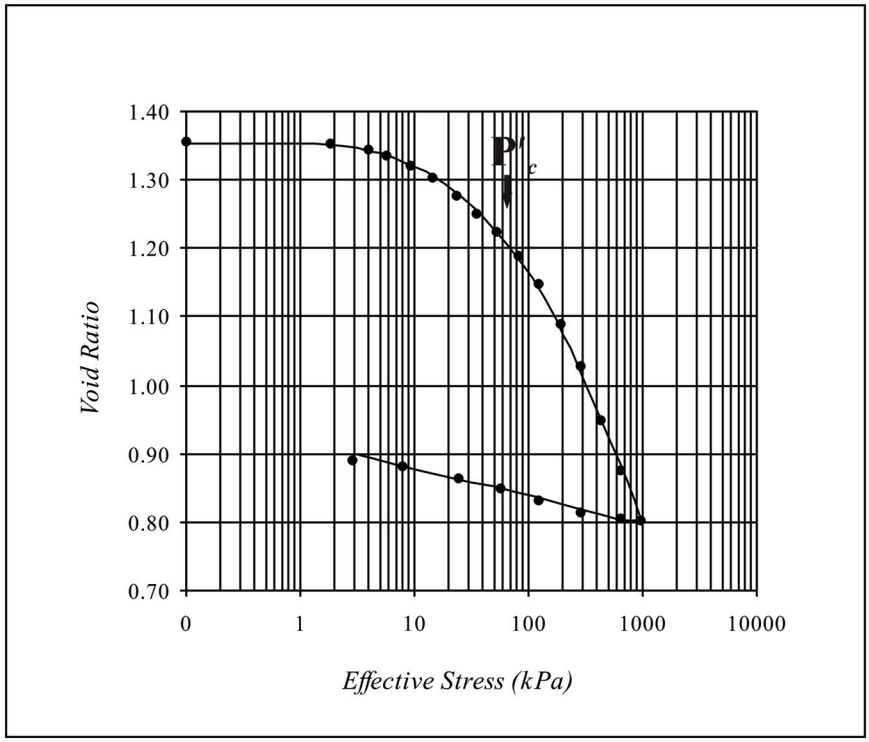


**Consolidation plot (e-log p') for sample 2006048 031 pc (712 cm).**

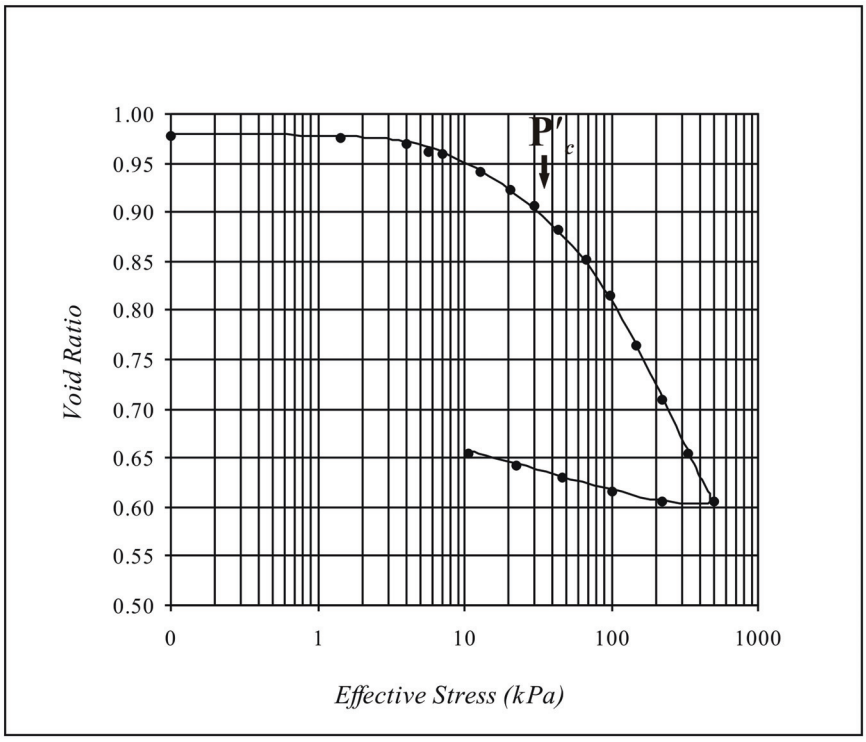


**Consolidation plot (e-log p') for sample 2006048 036pc (248 cm).**

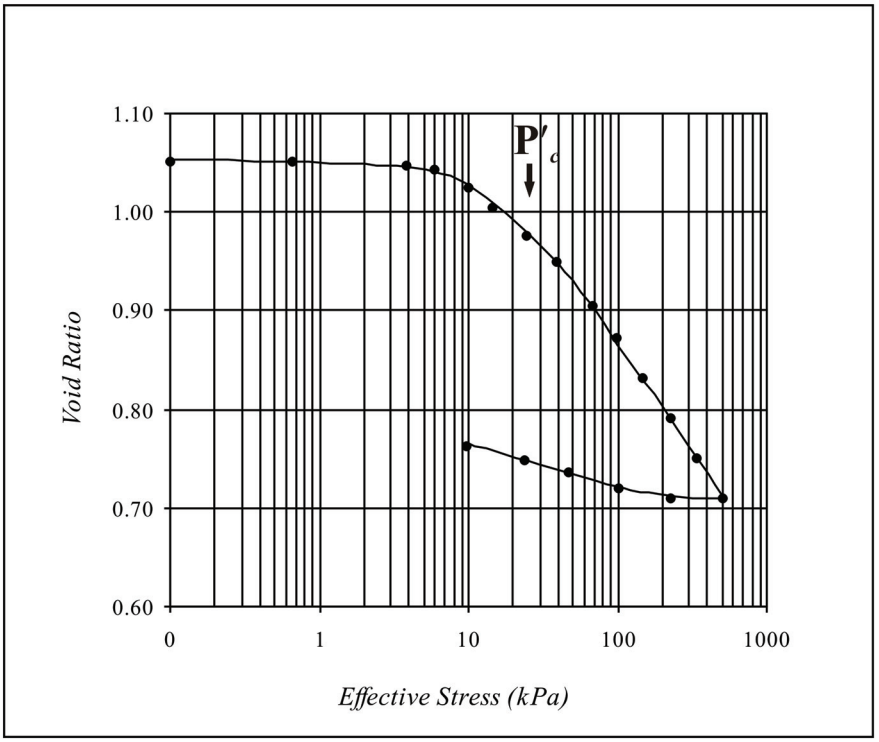


**Consolidation plot (e-log p') for sample 2006048 037pc (306 cm).**

# APPENDIX B Triaxial Test Results

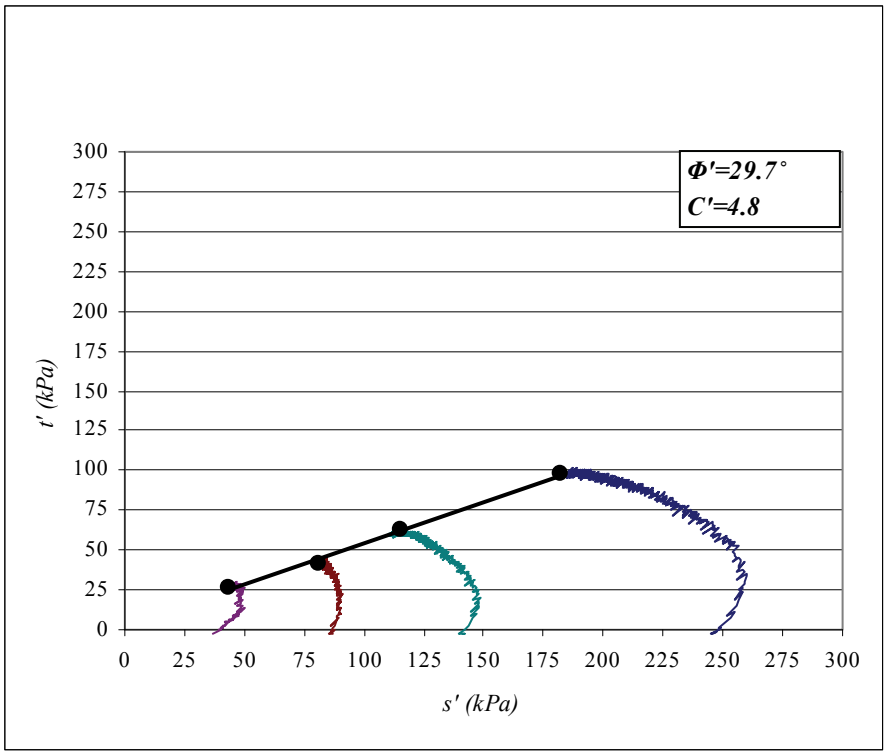


**Figure 5. Stress paths and strength envelope for sample 2006048 030frc.**

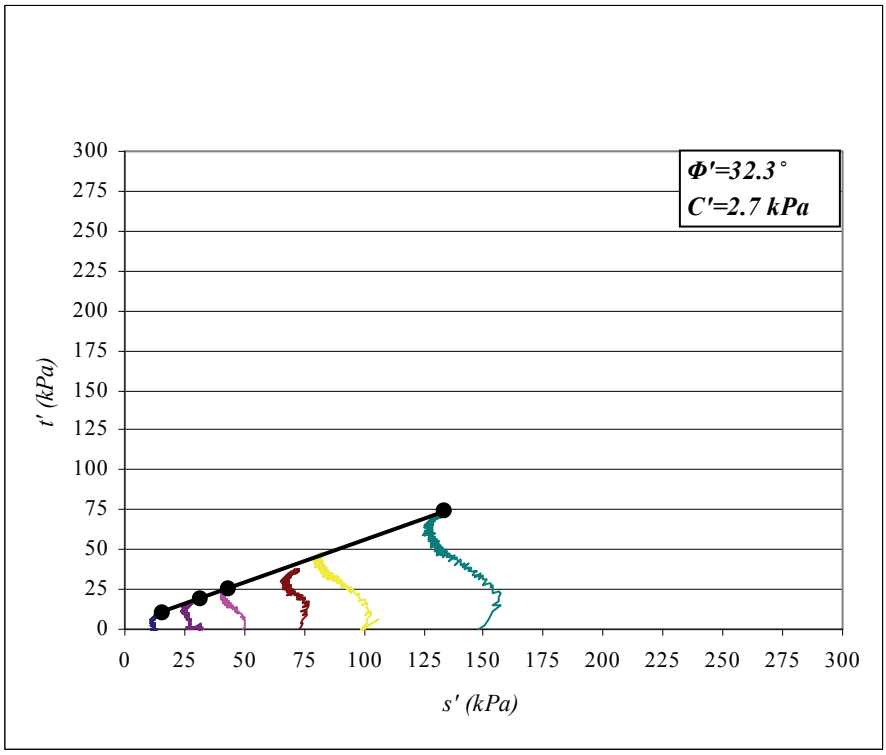

**Stress paths and strength envelope for sample 2006048 029pc**

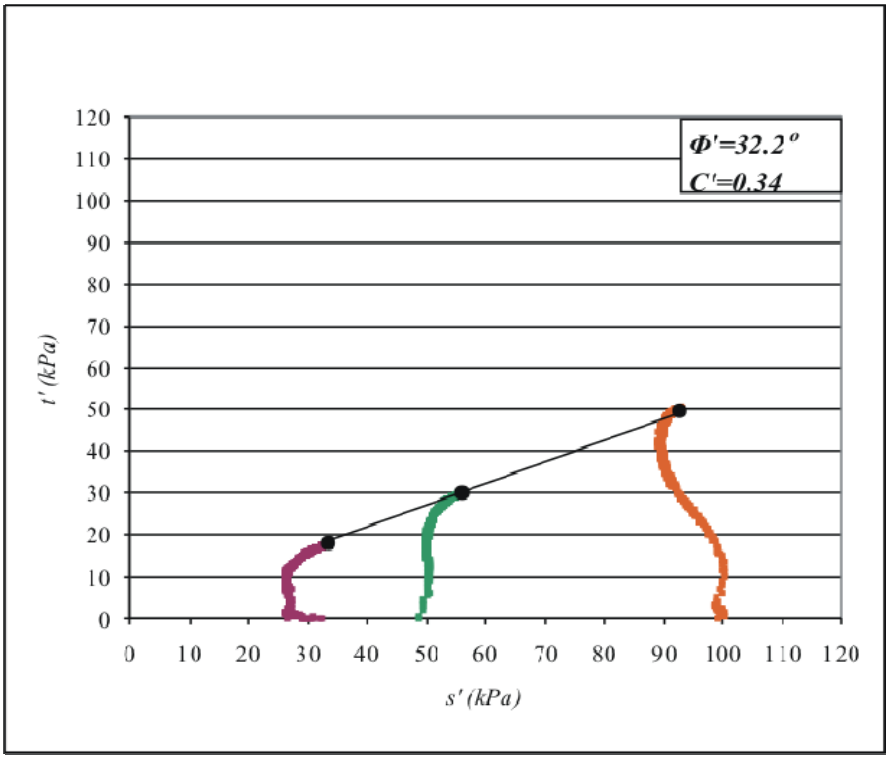


**Figure 6. Stress paths and strength envelope for sample 2006048 031pc**

# APPENDIX C Bender Element Test Results

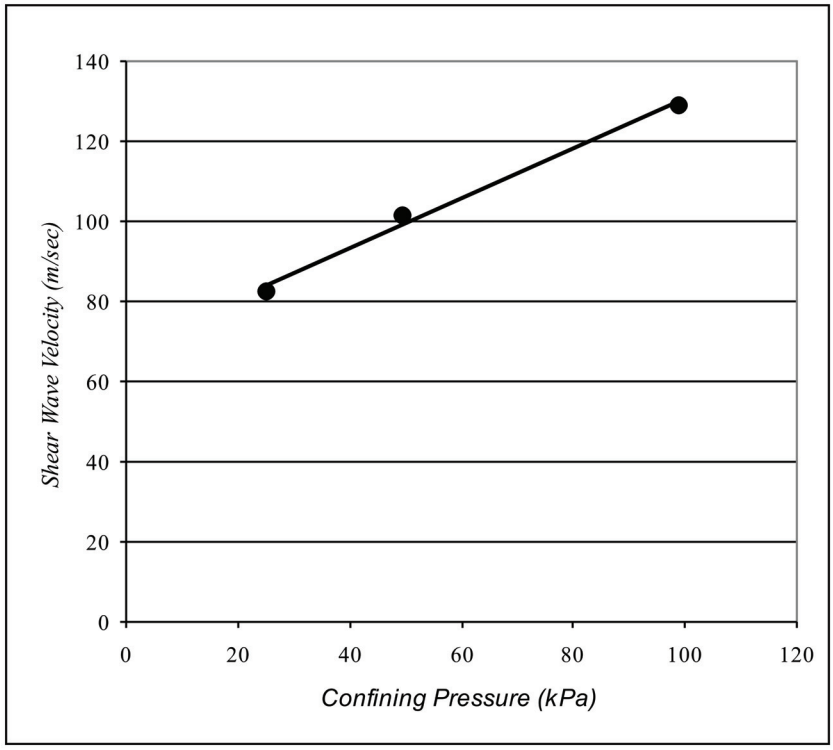


**Figure 1. Shear Wave velocity data from 2006048031pc.**

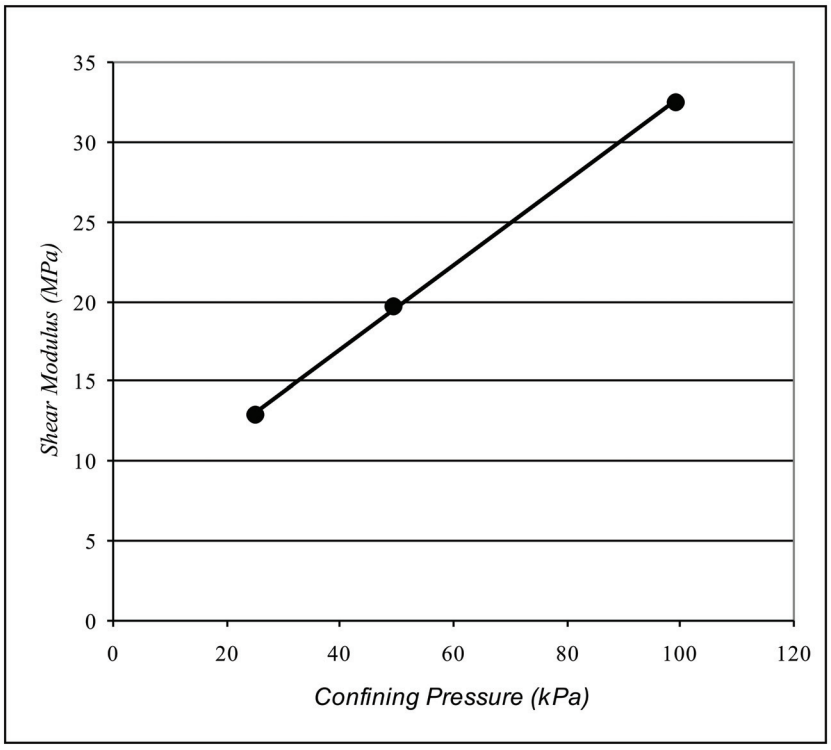


**Figure 2. Shear Modulus data from 2006048031pc.**